Structural Analysis of Laminated Composites using Function-Behavior-Structure Model and Virtual Material Method

by

Goldy Kumar

A dissertation submitted in partial fulfillment of
the requirements for the degree of

Doctor of Philosophy

(Mechanical Engineering)

at the

University of Wisconsin- Madison

2017

Date of final oral examination: 16th May 2017

The dissertation is approved by the following members of the Final Oral Committee:
Dr. Vadim Shapiro, Professor, Mechanical Engineering and Computer Sciences
Dr. Robert E. Rowlands, Professor, Mechanical Engineering and Materials Science
Dr. Krishnan Suresh, Professor, Mechanical Engineering
Dr. Xiaoping Qian, Associate Professor, Mechanical Engineering
Dr. Natalie M. Rudolph, Assistant Professor, Mechanical Engineering

Acknowledgment

First and foremost, I express my sincere gratitude to my advisor, Professor Vadim Shapiro. I feel very fortunate to have worked with you and be a part of the Spatial Automation Lab. Your knowledge of the subject, insights, creative approach to research, and enthusiasm are unparalleled. This thesis was not possible without your guidance, feedbacks, and constructive criticisms. More importantly, thank you for not only being patient, but also challenging me to venture out of my comfort zone, and, at the same time, allowing me to pursue my research interests.

Beside my advisor, I am also grateful to Professor Krishnan Suresh, Professor Robert Rowlands, Professor Xiaoping Qian, and Professor Natalie Rudolph for serving on my defense committee and providing vital comments. I would like to specially thank Professor Suresh for always be willing to provide his feedback and guiding me, every time I walked into his office. I am also indebted to Michael Freytag for allowing me to use Scan&Solve for my research and helping me whenever needed. This thesis will also not be possible without the advice and fun discussions, both academic and non-academic, with Xingchen, Vaidy, Shiguang, Sai, Brian, and Mik. In particular, thank you Xingchen and Vaidy for your motivation and being great lab mates throughout my stay.

I was lucky enough to call Madison home and make several lifelong friends during my Ph.D. Thank you Dev for being a great roommate, my partner in crime, and, above all, a trustworthy friend. I am also grateful to Ankur and Sameer for being wonderful and generous friends. Thank you Tom, Bonnie, Ginny, and Marrissa for being my 'family' away from home. To all my other friends (too many to list here), it would not have been possible without your support and encouragement.

Finally, words cannot describe how grateful I am to my family for their unconditional love and support. I specially thank my parents for all their hard work and blessings, without which I would not be who I am. Thank you for supporting my decision to move abroad, even though it was hard for you. To my sister Juhi and brother Saurav, thank you for sharing your positiveness and brightening my days. I also thank my uncle Pranab for his guidance and encouragement throughout my career. And, last but not least, I thank my partner Meg for all her love and support, specially during the final, most difficult phase of my Ph.D. Thank you all!

ABSTRACT

Layered composite structures are not only mechanically superior to conventional structures, but they also provide material customizability and ability to manufacture assembly-free unitized structures. However, structural analysis of composite structures still remains challenging. Currently, the analysis is done using finite element method on a simplified mixed-dimensional analysis model for composite structures. The simplification is done using behavior models, such as 2D plate and 1D beam models, which is necessary as meshing hundreds of material layers individually is extremely expensive. There are two major challenges to this approach- (i) lack of a systematic method for identification and documentation of the different behavior models in a composite structure and the exact regions in the structure where the behavior models are applicable and (ii) FEA using mixed dimensional analysis models require dimension reduction, different types of finite elements, and compatibility between different elements. These FEA pre-processing steps are time-consuming, require manual intervention and are often error-prone.

I propose a new framework for an automatic and efficient analysis of laminated composite structures. The framework is based on two novel contributions- i) a formal *Function-Behavior-Structure*(FBS) framework for structural engineering and ii) the *virtual material method*. The popular, but informal, FBS framework provides a general language and tools for design activities. I provide a formalism to the FBS framework in the context of engineering structures and use it to represent and record the functional components and the corresponding behaviors in a composite structure. This allows for the systematic identification and organization of behaviors and their regions in a structure. The formalism is based on *physical solid modeling*, an extension of the traditional solid modeling to include physics and behavior. In the virtual material method, I replace an original layup of materials in a composite structure, that can have hundreds of plies, by an equivalent but much simpler layup, called virtual material. The two layups are equivalent for a given behavior model. In essence, instead of using behavior models to obtain a simplified mixed dimensional analysis model, I propose to use them to obtain a new type of analysis model which is three-dimensional but has considerably simple material layups as compared to the original composite structure. Virtual material method, therefore, makes 3D FEA of composite structures practical and, as a result, eliminates the heuristic and expensive pre-processing steps.

To demonstrate the effectiveness of the proposed framework, I implemented the FBS framework and the virtual material method in a 3D meshfree finite element system. The system allows a structured documentation of function and behavior information for composite structures and automatically computes virtual materials wherever applicable. The 3D meshfree nature of the system not only eliminates the pre-processing steps but also the errors encountered in 3D conforming meshing. I validated the accuracy of the virtual material method by analyzing several benchmark problems found in the literature. Finally, I also analyzed some complex composite structures, including an airplane fuselage section, to demonstrate how practical composite structures can be analyzed using my system.

Contents

List of Figures

List of Tables

Chapter 1

Introduction

1.1 Motivation

Laminated composite structures are widely used in a variety of industries, including aerospace, automobile, medical, and sports [1–3]. Laminated composites are lightweight and stiff with customizable material properties, resulting in structures which can be superior to those made of homogeneous materials [2–4]. High stiffness-to-weight ratio is achieved using fiber-reinforced plies, which are fused together under high temperature and pressure to form complex, monolithic laminate parts. The fiber reinforcements, laid using techniques ranging from manual to fully automatic, are generally parallel and unidirectional, therefore, resulting in plies with anisotropic material properties. Global stiffness properties of laminated parts are customizable by varying the fiber angle within each ply, controlling the number of plies, and adding extra materials between plies, such as honeycomb cores.

Laminated composite artifacts[1], as a result, have a complex *manufacturing structure*; that is, they consist of a large number of manufacturing elements such as plies, cores, and fillers, which are systematically placed during manufacturing. The complexity of the manufacturing structure is demonstrated with the help of an example composite artifact in Figure 1.1— (i) Lam1 is a flat laminate with an embedded core, three dropped plies, and a cutout, (ii) Lam2 is a curved laminate, and (iii) Laminates in S1, S2, and S3 form a Hat-stiffener, T-stiffener, and Flat-stiffener respectively. Laminates Lam1 and Lam2 are joined using lap joint LJ1. Finally, ply drop-off PD1

[1]From now on, I will refer to engineering structures, which include composite structures, as *artifacts* to avoid confusion with structure as used in function-behavior-structure.

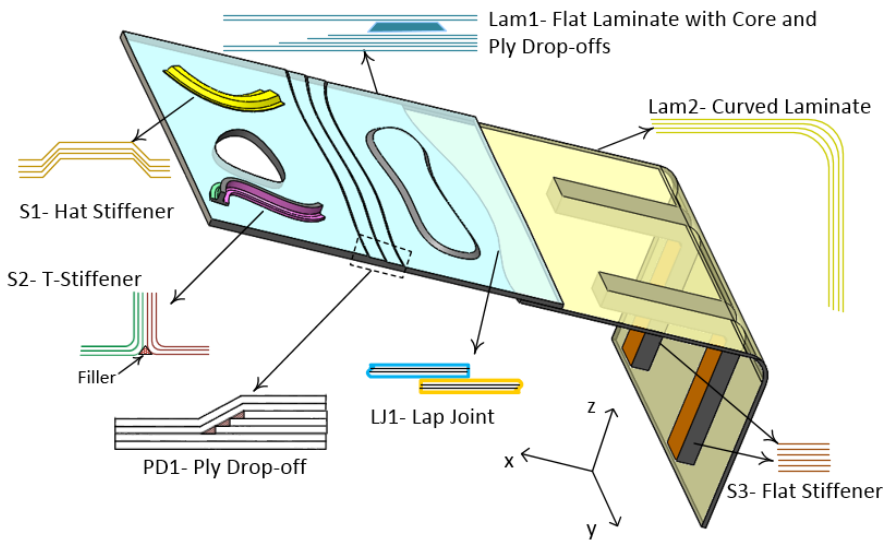

Figure 1.1: Figure shows a composite artifact with multiple laminates

leads to a tapered region in the composite artifact. Due to the layered nature of laminated composite artifacts, features such as ply drop-offs, embedded cores, and T-stiffeners with fillers are unique to them. Moreover, artifacts which were traditionally manufactured as assemblies of several structural components using fasteners can be manufactured as laminated composite artifacts that are free of assembly [2, 5]. Such composite artifacts are sometimes also referred to as *unitized* or *integrated* artifacts to indicate their assembly-free nature. Figure 1.2b shows a unitized airplane door [6]. Unitized artifacts have the advantage of having lower weight (no fasteners required) and lower manufacturing cost (surface finish and precision for mating of parts are not an issue) in comparison to assembled artifacts.

Increased complexity of manufacturing structures provide more freedom to customize mechanical properties of composite artifacts, but the cost of their structural analysis also increases tremendously—finite element analysis by meshing hundreds of thin plies independently is practically infeasible. From a design perspective, however, these artifacts usually have a simple *functional structure*. They are designed as a combination of functional elements (generally referred to as structural elements in structural engineering) such as plates, beams, shells, and so on [7–9], which are chosen by designers for their known mechanical behaviors. The knowledge of functional elements can speed up the structural analysis of composite artifacts, as simplifying assumptions can be made about behaviors of 1D (beams, bars, shafts, etc.) and 2D (plates, shells, membranes, etc.) functional

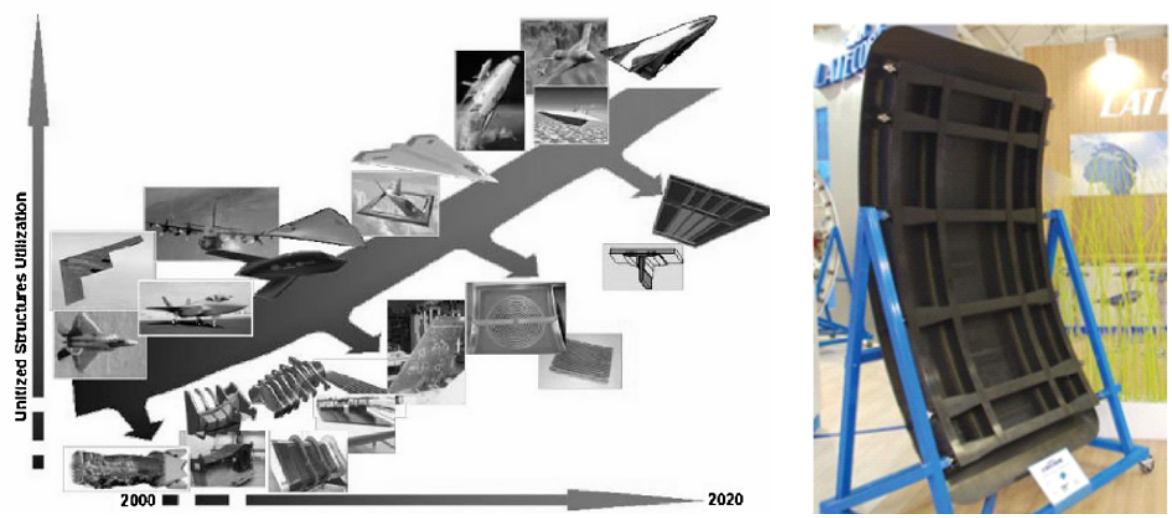

(a) Trend of Unitized Structure Utilization [5].

(b) A unitized airplane door.

Figure 1.2: Unitized Composite Artifacts: trends and examples

elements, which greatly reduce the number of degrees of freedom required during finite element analysis [10–12]. Different theories, or *behavior models*, such as Classical Lamination Plate Theory (CLPT), First-order Shear Deformation Theory (FSDT), etc. [4, 13, 14] are available to model the beam and plate behaviors.

Even though using simplified behavior models reduces the cost of structural analysis of composite artifacts, there are several challenges which forbid efficient and automatic analysis of practical composite artifacts. The following subsections present the challenges with the help of examples.

1.1.1 Lack of Function and Behavior Representation

As discussed above, knowledge of the function elements and associated behaviors in composite artifacts is necessary for their design and analysis. The functional structures of composite artifacts, however, are not usually provided with their CAD models. Currently, CAD models are based on the manufacturing structure and are limited to information such as tooling surfaces, plies, ply stack-up order, and other ply-related information [15, 16]. Designers and analysts, therefore, manually and heuristically identify the functional elements in the composite artifact. The process, as a result, is not only subjective, but also challenging for the following reasons:

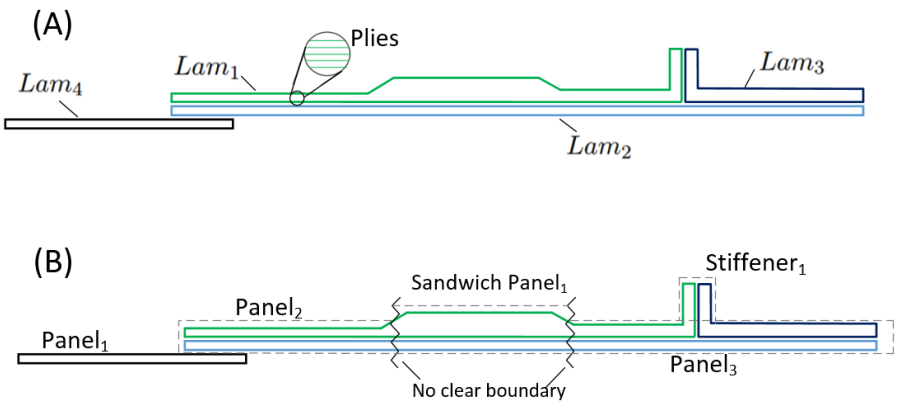

Figure 1.3: Cross-section of a unitized composite artifact to illustrate the lack of correspondence between elements of (A) manufacturing structure and (B) functional structure.

Lack of Correspondence between Functional and Manufacturing Structures As mentioned earlier, composite artifacts are increasingly being manufactured as unitized artifacts, wherein multiple functional elements are realized as one monolithic part. One functional element smoothly transitions into another in a part, with no 1:1 correspondence between elements of functional and manufacturing structures, which makes it difficult to isolate the functional elements. For illustration, the composite artifact in Figure 1.3 consists of five functional elements— three plates (panels), one thick plate (sandwich panel), and a beam (stiffener)— with no explicit boundary between the Sandwich Panel and Panels 2 and 3, nor between Stiffener 1 and Panel 3 (Figure 1.3B). An explicit boundary is absent because plies, which are manufacturing elements, are shared between multiple functional elements. For example, plies of laminate Lam_1 are shared between four functional elements– Panels 2 and 3, Sandwich Panel 1, and Stiffener 1.

Emergent Behaviors Emergent behaviors are behaviors that appear in a functional element after it is composed/joined to other functional elements. Emergent behaviors are usually found in regions around a joint between 1D and 2D functional elements. The simplifying assumptions for behaviors of 1D and 2D functional elements are not applicable in such regions due to St. Venant's Principle [17, 18]. As a result, the *actual* behaviors in an artifact are usually different from the *expected* behaviors, as illustrated in Figure 1.4. Therefore, just the knowledge of functional elements in an artifact is not enough to predict regions of simplified behaviors.

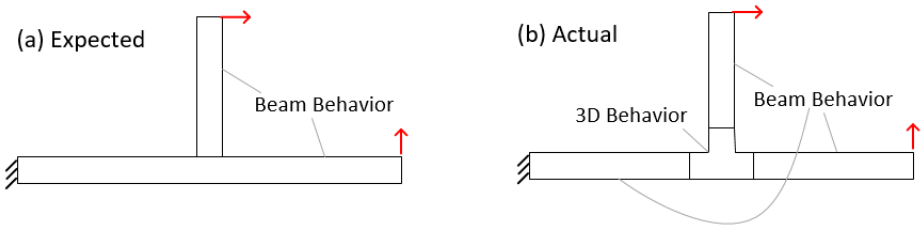

Figure 1.4: Emergent behaviors in artifacts.

Lack of a method to track function and behavior information Even when the complexity of a functional structure is orders of magnitude lower than that of the manufacturing structure, there could still be a considerable amount of function and behavior information to track during the design and analysis of composite artifacts. The information includes the functional elements, how the elements are connected, the behavior of functional elements as intended/expected, emergent behaviors after the elements are assembled, and so on. A general and mathematical framework is needed to document this information, as well as to support the transformations that the information undergoes during the design and analysis of composite artifacts.

1.1.2 Challenges in Finite Element Analysis of Composite Artifacts

The second set of challenges is faced during the pre-processing step of the finite element analysis (FEA) of composite artifacts. For carrying out the FEA of a composite artifact, a mixed-dimensional simplified *analysis model* for the composite artifact is required: regions in the artifact with 1D behavior are modeled as curves, regions with 2D behavior as surfaces, and regions with 3D behavior are left as they are. Obtaining surface and line models requires a dimension reduction of the 3D model of the composite artifact. Once the mixed-dimensional model of a composite artifact is obtained, the model is discretized using elements of appropriate dimension. The different behavior models are incorporated in the basis functions of the elements [13]. Therefore, the basis functions of a 2D element modeled using FSDT has additional degrees of freedom for transverse shear deformation in comparison to the ones modeled using CLPT.

There are several problems with the above approach. Firstly, dimension reduction of a 3D model into a surface or a curve is a heuristic step and sometimes requires manual simplification of

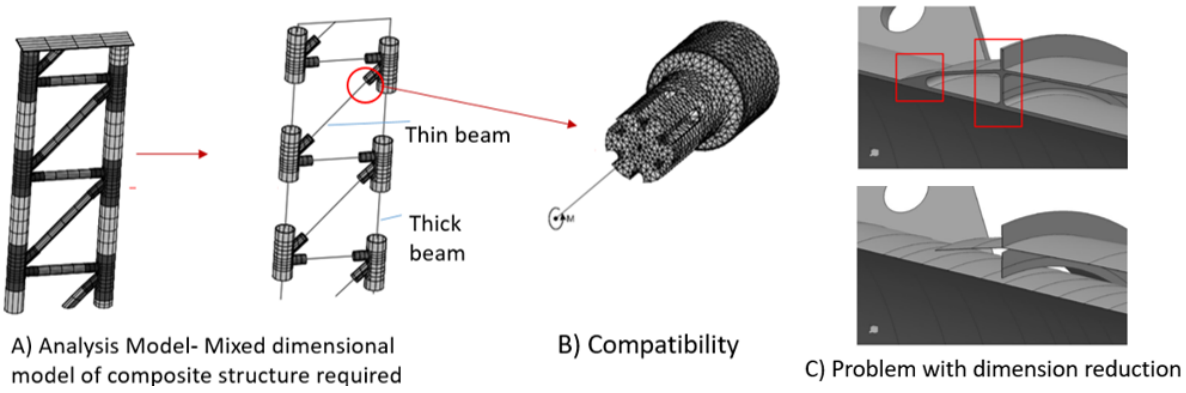

Figure 1.5: Pre-processing steps and challenges in multi-dimensional FEA.

the geometry of the 3D model [19]. For example, dimension reduction sometimes lead to loss of connectivity, as illustrated in Figure 1.5C. But, more importantly, this approach necessitates several different types of finite elements- one for each behavior model used in the artifact. For example, for the artifact in Figure 1.5A, we need 3D finite elements, thick beam elements, and thin beam elements. Different element types have different degrees of freedom, causing compatibility issues among other problems, as illustrated in Figure 1.5B. Compatibility is ensured either by constraining the degrees of freedom of elements at the interface or by using a transition element for the interface region [19–21]. The above pre-processing steps during FEA of composite artifacts bog down the analysis process and more often require manual intervention, preventing automation of the structural analysis of composite artifacts.

1.2 Overview of The Proposed Approach

The primary objective is to have an automated and efficient way to analyze practical composite artifacts. I propose a new framework to address the problems preventing the realization of this objective. In the framework, I

1. represent the functional knowledge behind the engineering artifacts using a well known function-behavior-structure framework for design. My implementation distinguishes the manufacturing and functional structures of the artifact and supports notions of expected and emergent behaviors. The functions and behaviors for a structure are obtained from the designer and stored in the CAD model, which is based on the manufacturing structure.

2. use the concept of behavior equivalence to obtain a *virtual material model* for the composite artifacts. Layups in the virtual material models are much simpler than the original layups, but the two layups are equivalent with respect to a behavior.

3. carry out the finite element analysis using a 'new type' of simplified analysis model that is obtained using the virtual material method. This new analysis model is three-dimensional and requires only 3D finite elements, eliminating the need for dimension reduction, multiple types for elements, and compatibility maintenance between elements.

The proposed framework hinges on two key contributions— a formalized *function-behavior-structure* model for design of engineering artifacts and the *virtual material method*, which are briefly discussed below.

1.2.1 Formal FBS Framework to Track Design Knowledge

The proposed framework to track design knowledge is based on the well-known function-behavior-structure (FBS) [22–25] framework for design, which is a general, but informal, framework to support the engineering design process. I make the FBS framework concrete for structural engineering by giving mathematical definitions to structure, behavior, and function. The definitions are based on the proposed extension of solid modeling to *physical solid modeling*, wherein physical solids have (1) states based on some physics and (2) physical behaviors as mappings between boundary value problems. In the thesis, I only consider linear elasticity physics, for which the physical solid is an *elastic solid*. The formal FBS framework leads to a systematic formulation of computational problems in structural design and analysis, including that for composite artifacts, which is the primary focus. Briefly, within the framework (summarized in Figure 1.6),

1. Manufacturing structure S^M captures the organization of manufacturing elements in an artifact.

2. Functional structure S^F stores the functional/structural elements in the artifact and how they are joined to each other.

3. Expected behavior B^e is the behavior of the artifact as intended by the designer. B^e is obtained from the known behavior of the functional elements, such as plate and beam behaviors.

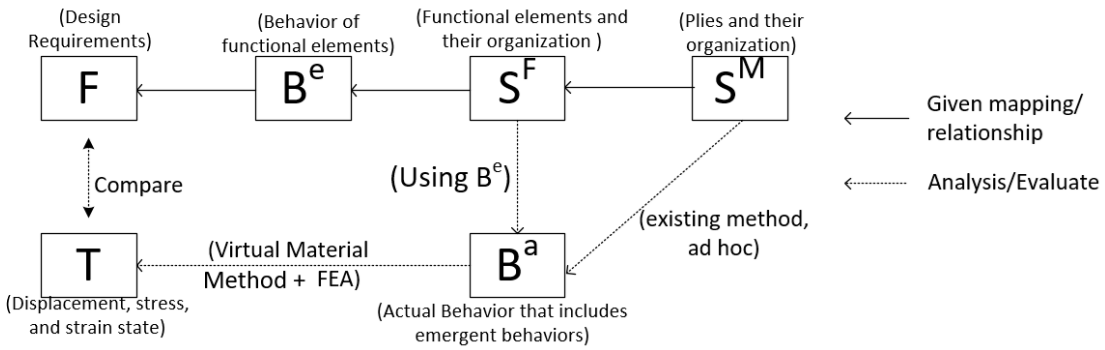

Figure 1.6: Summary of the proposed framework.

4. Actual behavior B^a of the artifact is obtained from the expected behavior after it is modified to include the emergent behaviors that arise when functional elements are joined.

5. Function F is a set of design requirements for the artifact, such as maximum stress or displacement at a point, to ensure that the artifact will perform without failing.

6. Numerical analysis of the artifact is carried out using the actual behavior B^a to obtain the state of the artifact (stress, strain, and displacement fields). The states are compared to F to ensure that the design requirements are satisfied.

I implement the above framework for composite artifacts with the most commonly used functional elements and joining methods. The framework, however, can be easily extended to include other types of elements and joints. The main assumption is that the artifact was designed as an assembly of functional elements, wherein a pair of elements is either perfectly bonded through adhesive joints or the elements are manufactured as one unitized/monolithic part.

1.2.2 Analysis Model for Composite Artifacts Based on Virtual Material Method

Finite element analysis of composite artifacts can be automated using general 3D finite elements, which are valid everywhere in the artifact and, therefore, eliminate the inefficient and manual preprocessing steps. However, as mentioned earlier, using 3D elements is prohibitively expensive due to the presence of numerous thin layers of plies in composite artifacts. To reduce the cost of 3D FEA of composite artifacts, I propose the concept of *virtual material* as a replacement for the original layup in a composite artifact. The concept of virtual material is summarized in Figure 1.7.

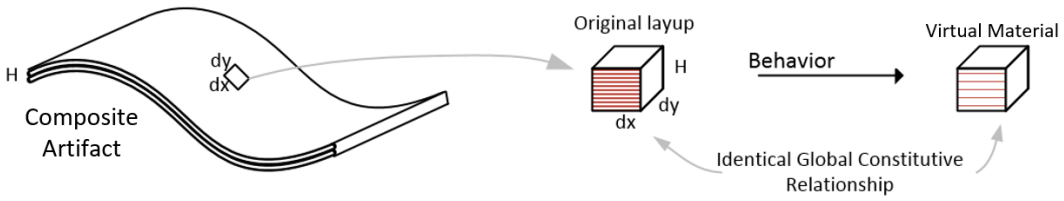

Figure 1.7: Virtual Material for a given layup and behavior.

Instead of using simplified behaviors of functional elements to obtain a mixed-dimensional analysis model for a composite artifact, I propose to use them to simplify the original layup of the composite artifact. The new layup will be equivalent to the original layup for a given behavior and, at the same time, will be simple enough to make the 3D FEA of composite artifacts efficient and practical. Virtual materials are simple due to the fact that the macro behavior of a typical composite artifact is much simpler than its material complexity. The behaviors used to compute the virtual materials will be obtained from the FBS information behind the composite artifact, resulting in a structured and non-heuristic method for efficient finite element analysis of composite artifacts. The numerical computational cost of 3D FEA is still higher than that of lower dimensional FEA, but, if the cost of all heuristic and manual pre-processing steps are included, 3D FEA of composite artifacts using virtual material is considerably more attractive.

1.3 Contributions Summary

I propose a new framework for the efficient and automatic analysis of laminated composite artifacts, which has resulted in the following major research contributions:

1. I proposed physical solid modeling as an extension of traditional solid modeling to include physics. Using the notion of elastic solid and behavior, I was then able formalize the widely used, but informal, function-behavior-structure framework for design and analysis of engineering artifacts.

2. I applied the formal FBS framework to composite artifacts and showed how the manufacturing data and intent (function and behavior) behind the artifacts can be documented and tracked. A deterministic approach to finding the emergent behaviors for the most commonly used composite artifacts is also proposed. This can be extended to other new types of ar-

tifacts (including those which are 3D printed) that have considerably higher manufacturing complexity than their functional complexity.

3. I also proposed a new type of simplified analysis model for the efficient FEA of composite artifacts using, what I refer to as, the "virtual material method". This method is based on the notion of behavior equivalence, as defined in the FBS framework. Virtual-material-based analysis models eliminate several pre-processing steps and save considerable manual effort.

4. Finally, I implemented a prototype system to show how practical composite artifacts can be analyzed using the FBS and the virtual material method in a 3D meshfree finite element system, thereby utilizing all the advantages that meshfree systems offer over mesh-based FEA systems.

1.4 Outline

The thesis has been divided into following chapters:

1. Background and past work related to the contributions are presented in Chapter 2. The chapter consists of three sections, which are as follow. In the first section, a background of composites and artifacts made of composites is presented. I review the terminologies, the common manufacturing and functional features, and the different representation methods for composite artifacts. In the next section, I survey the past work for analyzing composite artifacts. Firstly, I review behaviors of different functional features in composite artifacts and how they are modeled. Finally, I discuss how behavior models are used during analysis of practical composite artifacts that have several of these functional features. In the final section, I present the existing work related to modeling intent in design. Primarily, I discuss the informal definitions of function, behavior, and structure using the example of a chair artifact. I also touch upon other models for intent in engineering.

2. In Chapter 3, I present the formal definitions for the function-behavior-structure terminologies in the context of structural engineering. I use physical solid modeling as the basis for the FBS definitions, which I define for linear elasticity.

3. In Chapter 4, I present applications of the FBS framework from Chapter 3 for composite artifacts. Specifically, I discuss how the structures of an artifact from different views can be used to organize manufacturing and functional information, as well as how behavior equivalence can be used for efficient 3D analysis of composite artifacts.

4. Chapter 5 dives into the details of the virtual material method based on the behavior equivalence concept. I derive virtual materials for laminated composite panels with thin and thick plate behaviors. I also demonstrate how composite beams can be analyzed using virtual materials. Several benchmark problems are analyzed to establish the effectiveness of the virtual material method.

5. I describe the meshfree-based finite element system to analyze practical composite artifacts in Chapter 6. The system uses the proposed analysis model using the virtual material method. I demonstrate the working of the system by analyzing a section of a fuselage that consists of several panel and stiffener functional elements.

6. I conclude the thesis by discussing the overall limitations, possible extensions, and open issues in Chapter 7.

Chapter 2

Background and Related Work

This chapter is divided into three sections. The first section gives a quick background of terminologies and features of composite artifacts. The survey of methods to analyze composite artifacts in the second section. Finally, I briefly discuss the informal function-behavior-structure framework for design.

2.1 Composite Artifact Background

I first discuss the concepts and terminologies related to composite materials and composite artifacts. Several terminologies have been formulated in order to systematically document artifacts made of composites. Many of the manufacturing-related terminologies discussed here are from the ASME Standard on Composite Part Drawing [26]. I also go over methods currently used to represent and analyze composite artifacts on computers.

2.1.1 Common Manufacturing Terminologies

Composite material, informally, is a combination of two or more constituent materials and has properties superior to the properties of the constituent materials. In the current work, I consider advanced composites, which are made of continuous and parallel fibers embedded in resin. Advanced composites are particularly popular in engineering applications because of their high stiffness and load carrying capacity in comparison to traditional materials such as steel and aluminum. Composites with aligned fibers are strong in the fiber, or the reinforcement, direction, but they are weaker

in directions perpendicular to the fiber direction. Usually, therefore, multiple layers of composite materials with different fiber direction in each layer are combined to form, so-called, *Laminates* [27]. Fibers can also be weaved, stitched, or braided together to provide lateral strength to the composite material.

In general, manufacturing elements in composite artifacts have hierarchical organizational structure [15, 28] as illustrated using the UML diagram in Figure 2.1. The starting items are plies, cores, and embedding. Plies consist of resin reinforced by parallel fibers and are an extremely thin plate/shell-like solids, usually with uniform thickness. In comparison to plies, cores are relatively thicker and have internal structures such as honeycomb and foam. Embedding such as fillers, sensors, cooling pipes, etc., can also be placed between plies [29]. I only consider unavoidable fillers (resin pockets) in the current work, which are found in regions that cannot be reached by plies. Although these starting materials usually have internal structures, they are considered to have homogeneous material properties for the purpose of design and analysis. Several of the starting items are stacked on a tooling surface to form a laminate. One or more laminates are cured together to result in one monolithic part called *laminated composite component*. A component that contains a core item is usually referred to as a *sandwich structure*. Finally, a composite artifact is obtained by joining multiple laminated components using bonded or mechanical joints. In summary, practical composite artifacts can consist of hundreds of these starting items organized in the hierarchy discussed above.

2.1.2 Common Functional Elements

In this section, I discuss common functional elements in composite artifacts, which are important from both design and analysis points of view.

Laminated Panels Laminated panels are thin-walled structural elements in composite artifacts. Panels act as plates or shells, and are the most common functional elements in composite artifacts, to which other elements are attached. An example of a panel is component Lam_2 in Figure 1.1.

Sandwich panels A sandwich panel consists of a low-density flexible core bonded to high-density stiff facings (Figure 2.2A). Facings are generally made of fiber-reinforced plies and carry most

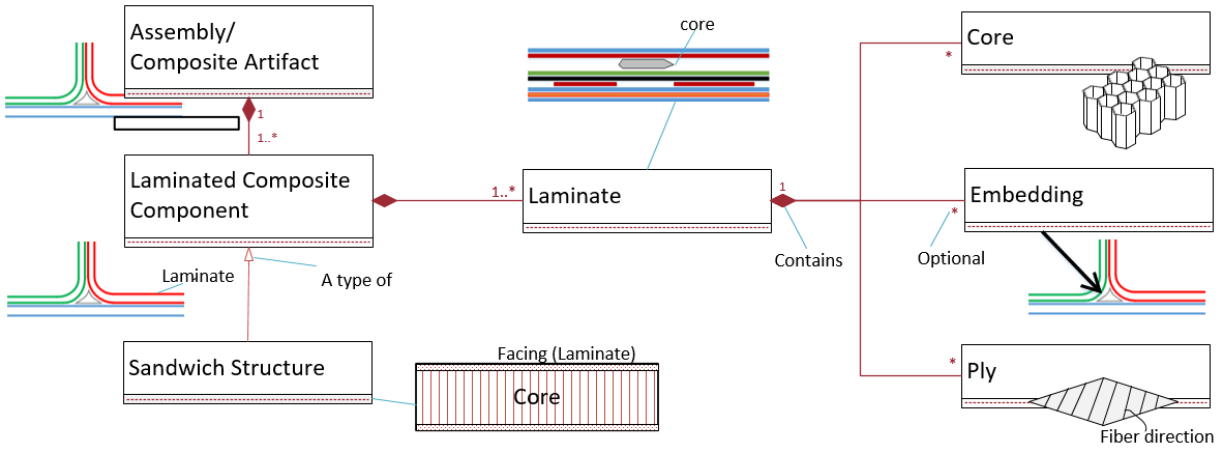

Figure 2.1: UML diagram showing the organizational hierarchy of manufacturing elements for composite artifacts.

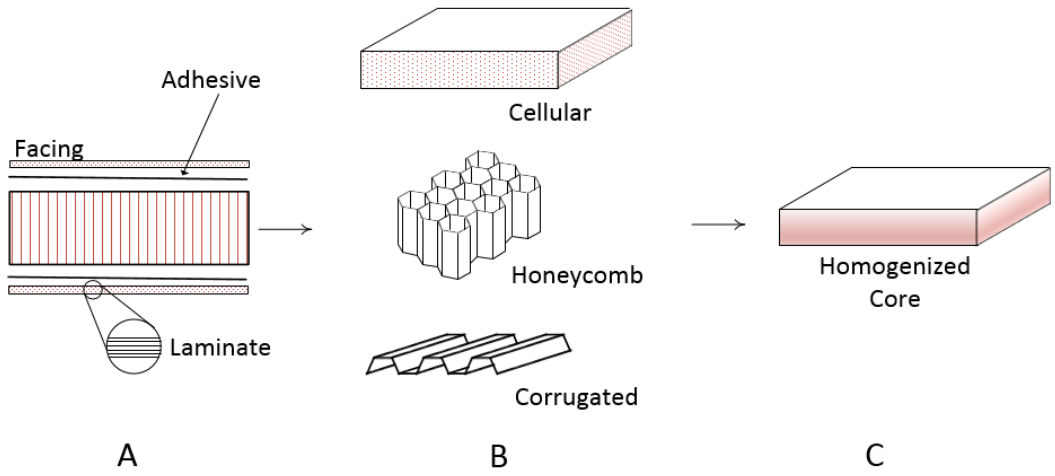

Figure 2.2: A) Front view of a sandwich panel. B) Three different types of cores. C) A core after homogenization.

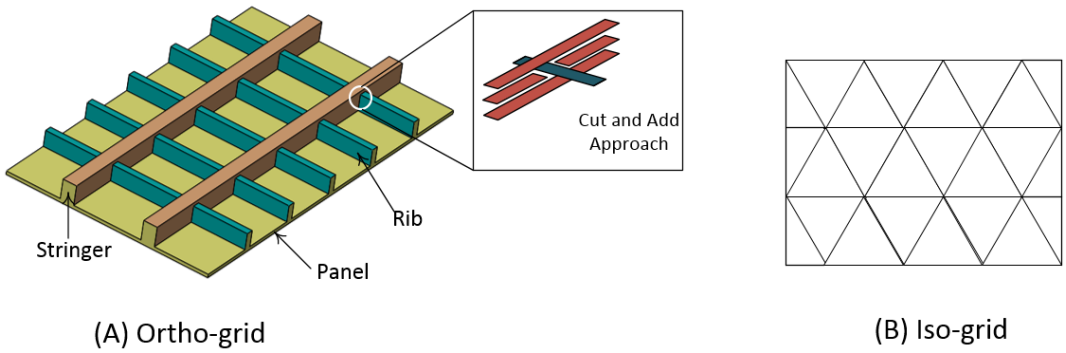

Figure 2.3: Two types of grids A) Ortho-grid and B) Iso-grid. Inset shows how intersection is restricted from having a build-up using the cut and add approach .

of the in-plane load in the panel. Core, on the other hand, carries transverse loads, as well as increases the bending stiffness of the panel by increasing the distance between the facings. Sandwich panels, because of the significant transverse stresses, are usually modeled as thick plates and shells.

Stiffened panels A stiffened panel consists of a flat or curved laminated panel reinforced by stiffeners [30]. For example, stringers and ribs are stiffeners for the panel in Figure 2.3A. Adding stiffeners to a panel increases the panel's stiffness for bending and controls local buckling, while keeping the artifact light. Stiffened panels are extensively used in civil, aerospace, and marine artifacts [31].

Stiffeners, depending on the type of artifact they are used for and their axial direction, are referred to by different names such as ribs, stringers, longerons, frames, and rings. Figure 2.3A illustrates a grid of stiffeners in which the longitudinal stiffeners are called stringers, while the transverse ones are ribs. Stiffeners form a grid when placed in a uniform pattern, such as ortho-grid and iso-grid as shown in Figures 2.3A and B respectively.

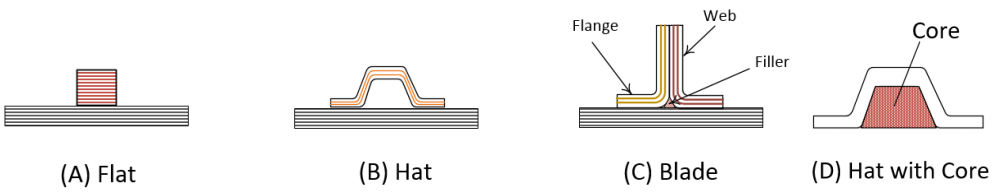

Figure 2.4: Examples of different types of stiffeners based on their cross-sections.

Stiffeners may have different cross-sections, each cross-section having its own advantages and disadvantages. Some example stiffener cross-sections are shown in Figure 2.4. Flanges are the horizontal elements of the stiffener, while webs are the vertical elements. Also, the hat stiffener is a closed-configuration stiffener due to the gap between the stiffener and the panel. The flat and blade stiffeners are open-configuration stiffeners. Closed-configuration stiffeners show higher stiffness to torsion, but are harder to manufacture as they need internal support. Cores can also be inserted in stiffeners, as shown in Figure 2.4D, for even higher bending stiffness.

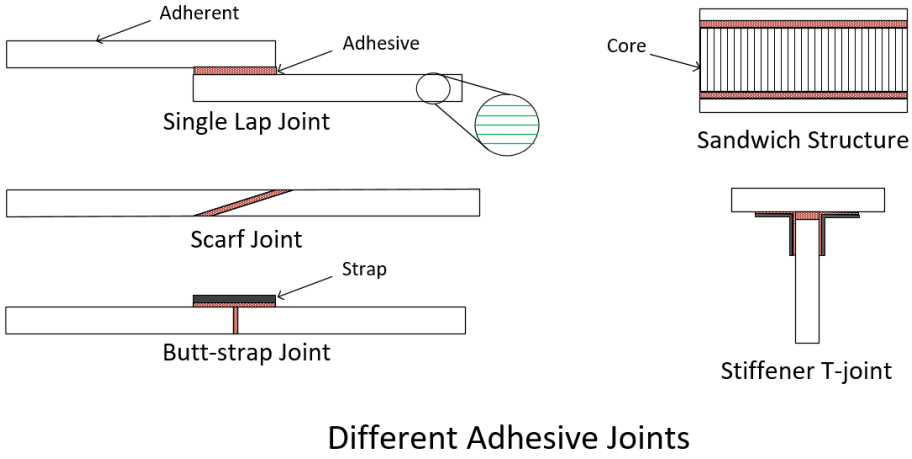

Figure 2.5: Different types of bonded joints in composites using adhesives.

Bonded Joints Theoretically, a composite artifact can be created as one monolithic artifact free from any assembling. However, due to manufacturability and serviceability constraints, composite artifacts might still be manufactured as separate components. Joints are used to assemble and transfer loads between the components [7].

Joining using mechanical fasteners is generally avoided in composite artifacts, as drilling holes and cutouts breaks the fibers and makes the artifact weaker. Adhesive joints, which allow for a gradual transfer of load between two components over a region, are more popular [32]. Adhesive joints are easier to fabricate, and also provide design flexibility, as several joint configurations are available (Figure 2.5).

Ply drop-offs Regions in composite artifacts under high load can be stiffen by adding extra plies. These extra plies are dropped gradually when not needed as a cost-saving measure. This leads

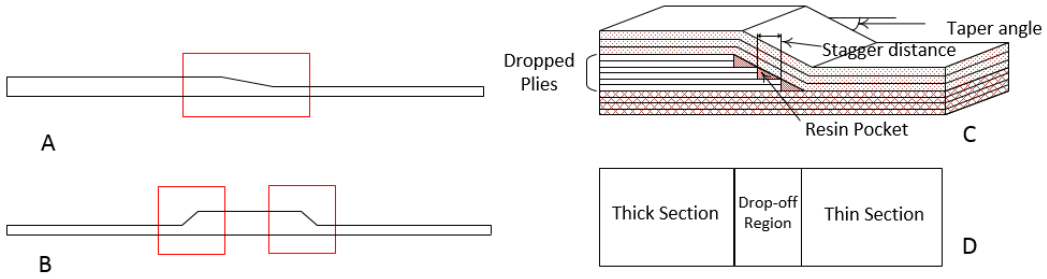

Figure 2.6: A-B) Cross-sections of two composites with ply drop-offs. C) Drop-off configuration and naming conventions. D) Top view of the drop-off region.

to a tapered region in composite artifacts as illustrated by the two examples in Figure 2.6A and B. An example cross-section for taper regions (the red boxes) is shown in Figure 2.6C [33]. As illustrated, resin pockets are formed next to the dropped plies in the taper regions.

2.1.3 Representations for Composite Artifacts

In theory, composite artifacts can be represented by representing starting items as solids that are assembled together using mating constraints. In practice, however, this method is not preferred because representing hundreds of items as individual solids as well as the mating constraints between the solids is computationally expensive. Therefore, special representation methods are used that take advantage of the thin and layered nature of these artifacts. I briefly discuss these representation methods below and also indicate their advantages and disadvantages.

Wireframe and Surface-based Representations

In composite artifacts, items are always laid on top of each other and are supported by a base/tooling surface. Therefore, a base-surface based representation of composite artifacts is common in practice (Figure 2.7). Briefly, a laminate is represented by a *base surface* and a *ply table*, where the ply table stores the details of the starting items laid on the base surface to form the laminate. In the table, each item is assigned a row and a *ply-level*. Ply level is the position of an item relative to other items on the base surface. In general, multiple hierarchical ply tables are needed to record complex composite artifacts, where the hierarchy is based on the hierarchy of the manufacturing structure discussed earlier.

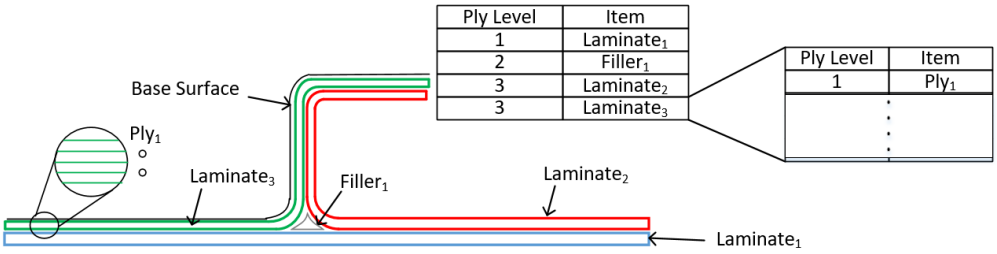

Figure 2.7: A composite part with a filler and three laminates.

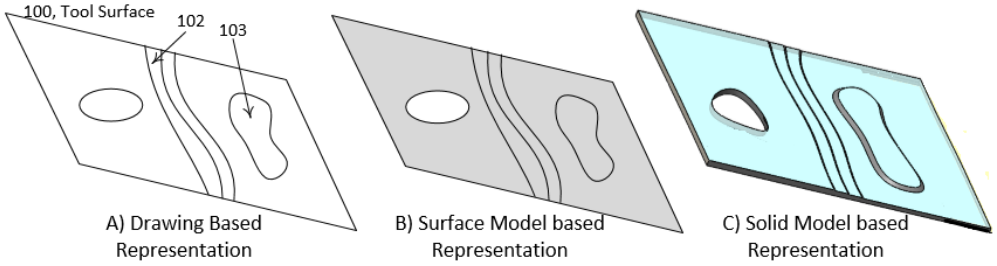

Figure 2.8: A composite artifact represented using different representation methods.

Furthermore, there are various methods to represent the base surface as well. In wireframe representation, the boundaries of the base surface are represented as wireframes [16, 26]. As illustrated in Figure 2.8A, the tooling surface (labeled as 100) and the locations of items (102- Ply, 103- Core) on the tooling surface are recorded using their boundary edges. Items, their materials, and their orientations are listed in ply tables. Cross-section drawings are needed to visualize the thickness information of the items. Wireframe representations are straightforward for simple artifacts, but such representations can easily become ambiguous for even a slightly complex artifact. The inside and outside of items are indistinguishable, and cutouts and holes can be confused with other items in the absence of definitive inside and outside information. Also, new cross-section views are needed every time plies are dropped or added or when the thickness of plies changes.

In surface-based representation, composite artifacts can be represented in two ways [16]: i) by representing tooling surfaces in the computer as surfaces, items using ply-table, and location of the items as edges on the surfaces (as shown in Figure 2.8B), or ii) by representing each item as a surface with material and other information as attributes of the surface. Surface-based representations are better than wireframe for visualization, but they cannot show thickness changes due to ply drop-offs, addition of cores, and so on.

Representation as Solids

Another option is to represent items in composite artifacts as solids whose spatial locations are locked, instead of specifying mating constraints to assemble [16]. The thickness of items is no longer implicit, and material and other information about items are included as attributes of the items. An example of a solid representation of a composite artifact is shown in Figure 2.8C. Some of the disadvantages of using solid representation for complex composite artifacts remains. It is computationally expensive to represent 100s of items, even if mating constraints between the items are not included. Also, every time an item is added or dropped, the shape and location of existing items may have to be updated, which isn't needed for representations where items are represented implicitly. Finally, in all the representation methods above, interfaces between items/laminates are not available, which are regions of interest during structural analysis.

In the next section, I will review the methods used to analyze composite artifacts.

2.2 Analysis of Composite Artifacts

Analysis of a composite artifact is usually carried out using finite element analysis of a simplified analysis model of the artifact, as discussed earlier. I first discuss the behavior models that are used for simplification and then discuss the details of the pre-processing steps needed to carry out FEA of composite artifacts.

2.2.1 Behavior of Functional Elements

In this section, I discuss the mechanical behavior models of common functional elements present in composite artifacts.

Laminated Panels

Composite panels are thin-walled artifacts and show behavior similar to plate and shell artifacts. In-plane and transverse behaviors of laminated panels are modeled independently, and the behavior models differ in the way transverse, or through-the-thickness, behavior is modeled [14, 34–36]. Transverse direction is particularly important in laminated composites, since they are substantially weaker in that direction. The different models for such behavior are as follows.

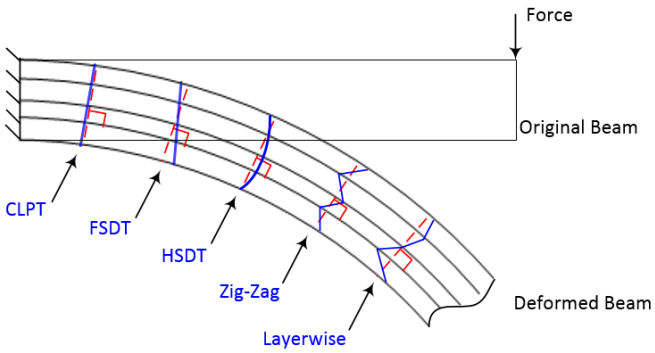

Figure 2.9: Through-thickness deformation for different ESL theories.

A. Global Behavior Models (Equivalent Single Layer Theories) In Equivalent Single Layer (ESL) theories, approximation functions are used to approximate displacement in a panel's transverse direction. This allows the laminated panel to be replaced by an *equivalent single layer* [35]. The number of degrees of freedom to capture deformation in the panel is independent of the number of plies in the panel. So, ESL theories are suitable to model behavior of practical composite panels which usually have hundreds of layers. A few of the popular ESL theories are discussed below and shown in Figure 2.9.

A.1 CLPT, or Classical Lamination Plate Theory, assumes that the panel shows only in-plane stretching and pure bending. In-plane strains, therefore, can vary linearly along the thickness while transverse shear is absent. Application of CLPT results in the popularly known ABD stiffness matrices for the panel, where A is the extensional stiffness matrix, B is the bending stiffness matrix, and D is coupling between extension and bending (details in Chapter 5). CLPT is limited in applicability since it completely ignores transverse shear.

A.2 FSDT, or First-order Shear Deformation Theory, is based on the Reissner-Mindlin hypothesis and allows for constant transverse shear strains in panels, in addition to the linear variation of in-plane strains in the transverse direction [35] (Figure 2.9). A correction factor is needed to compensate for any deviation of the predicted transverse shear strains from the actual shear strains.

FSDT provides better results in comparison to CLPT. However, obtaining a correction factor is not straightforward, and there are different schemes to compute it. Also, the correction factor

is different for different laminates, as it depends on the laminate's ply sequence, material, and thickness [35].

A.3 HOT, or Higher Order Theories, are refinements of FSDT and assume non-linear distributions for transverse shear stress in the panel. Parabolic and cubic approximation (Figure 2.9) of transverse shear displacements are examples of HOTs [14, 35]. Higher order theories give superior results for laminated panels in comparison to CLPT and FSDT.

Higher order theories, as well as CLPT and FSDT, use C^1 continuous functions for approximating displacements in the panel's transverse direction. This results in continuous transverse strains and, therefore, discontinuous stresses at the interfaces of plies made of different materials. However, due to compatibility and equilibrium conditions, transverse stresses must be C^0 continuous at the interface.

A.4 Zig-Zag theories are in a class of ESL theories that captures C^0 continuity of transverse shear stresses in laminated panels. In Zig-Zag theories, the behavior models of laminated panels are enhanced by adding a *warping function* [34]. These functions are capable of representing the deformed profile with a different slope in each layer(Figure 2.9). These warping functions are either provided or constructed using inter-layer shear continuity and zero shear traction boundary conditions.

ESL theories are adequate to model global behavior of laminated panels, but are insufficient if local behavior is also required [12]. Next, I briefly discuss behavior models to capture the local behavior of laminated panels.

B. Local Behavior Models for Panels Local behavior models model behavior of the individual layers in a laminated panel. Some of the local behavior models are as following.

B.1 Layerwise, or discrete-layer, theories are two-dimensional theories, but they model the behavior of each layer in the laminated panel independently [14, 34]. The number of degrees of freedom for deformation, therefore, depends on the number of layers in the panel. There are again different layerwise theories depending on the approximation function chosen to approximate the through-thickness behavior of each layer. Layerwise theories are accurate, but expensive, for practical composite artifacts.

B.2 The full three-dimensional behavior model (3D linear elasticity theory) can be used to model each layer in laminated panels, but the cost of 3D models is extremely high and, therefore, they are considered impractical for composite artifacts.

However, local behavior can be recovered from global behavior using the 3D elasticity theory. Three-dimensional equilibrium equations and constitutive relations can be used to compute approximate local transverse stresses from the stresses and strains obtained using global behavior models [14, 34, 35].

Sandwich Panel

Modeling behavior of sandwich cores using the 3D behavior model is not practical due to the complex internal structure of cores. Therefore, a sandwich core is usually homogenized as an effective material (Figure 2.2C), whose properties are obtained either experimentally, analytically, or numerically [37]. The properties of the effective material have to be accurate, since the response of sandwich panels is very sensitive to transverse shear stiffness of the core [38]. Once the core is replaced by an effective material, the behavior of the sandwich panel is modeled using one of the behavior models for laminated panels.

Modeling core as an effective material, however, is invalid when interaction between the internal structure of the core and the facings introduces new physical phenomena. For such composite artifacts, facings and cores are homogenized together as a continuum. For example, corrugated sandwich panels derive much of their stiffness from the interaction of the corrugated core and the face sheets [39], so the behavior of the core and the sheets cannot be modeled independently.

For modeling behavior of tapered sandwich panels(Figure 2.10A), the natural inclination is to homogenize the core and vary the effective properties as the core's thickness changes [40, 41]. While this approach is valid for tapered beams and plates, it is invalid for tapered sandwich panels. Tapered sandwich panels have two new coupling behaviors— (i) coupling between transverse shear and bending and (ii) coupling between transverse shear and extension —in addition to the commonly occurring couplings in multi-layered artifacts [37]. The reason for transverse shear and stretching coupling is explained with the help of an example tapered sandwich panel under in-plane loading N_x (Figures 2.10B and C). Since cores are softer in the in-plane direction, most of the load is carried by

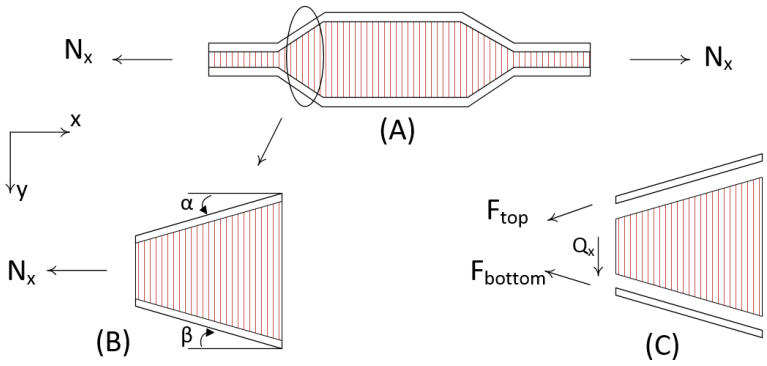

Figure 2.10: A) Tapering of core in sandwich panels B) Zoom-in of the left taper. C) Facings and the core with corresponding loadings due to N_x .

the facings (F_{top} and F_{bottom}). If the top and bottom taper angles (α and β) are unequal, F_{top} and F_{bottom} will also be unequal, with a net component Q_x in the y direction. Q_x leads to transverse shear in the core, leading to coupling between in-plane load and transverse shear. Due to the new coupling effects, additional coupling terms appear in the ABD matrix [40].

Stiffened Panels

The behavior models for stiffened panels can be categorized as 'smeared models' or 'discrete models', which are discussed below and illustrated in Figure 2.11. The panels and stiffeners are assumed to be bonded perfectly and, therefore, adhesive bonding between panel and stiffeners, if present, can be ignored.

1. In smeared behavior models, a panel and its stiffeners are idealized as a new panel by superimposing, or 'smearing', the effect of stiffeners on the behavior of the panel (Figure 2.11B). There are various smearing methods [31, 42, 43], which based on equating final deformation energy, forces-moments, etc. of the original artifact and its smeared model. For a stiffened panel with a regular grid of stiffeners, smearing can be done for a unit repeating cell in the stiffened panel, and the results can be applied to the entire artifact. This is considerably economical in comparison to smearing each stiffener in the grid one by one [31, 44].

   Using smeared behavior models for analysis of stiffened panels is efficient, but are only justified when stiffeners are closely and uniformly spaced and boundary conditions are simple [31,

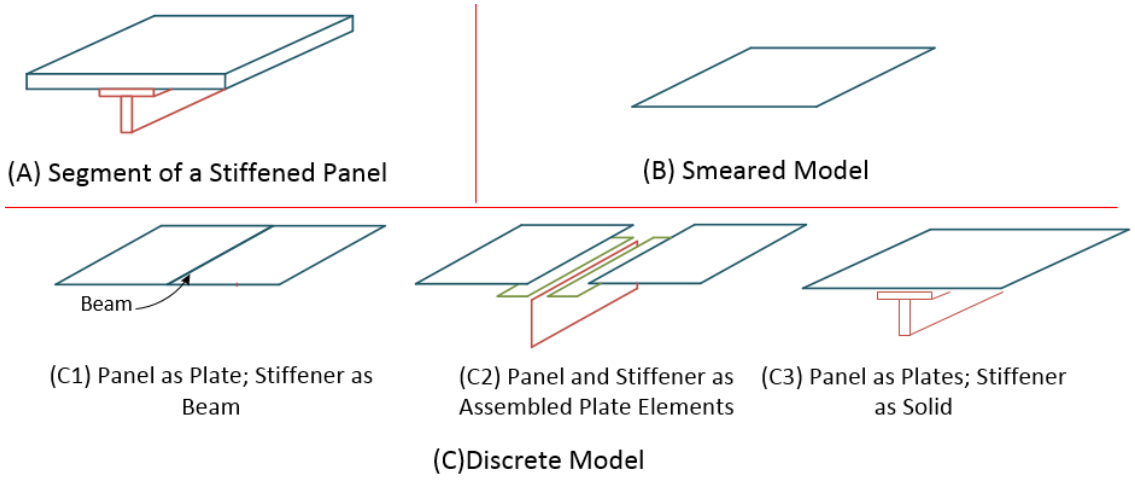

Figure 2.11: A) A stiffened panel. B) Smearing techniques. C) Discrete approaches.

44]. Also, smeared models capture only global behavior and completely miss local behaviors including bending in regions between two stiffeners.

2. In discrete behavior models [1], behaviors of the stiffeners and the panel are modeled separately and are coupled through interface boundary conditions [43]. Discrete models capture behavior in localized regions, in addition to the global behavior. While, behavior of panel is modeled using Equivalent Single Layer Theories, there are different ways to model the behavior of the stiffener (Figure 2.11C).

   C1) Beams Stiffeners can be modeled as 1D beams with extension, bending, and torsional stiffnesses [47]. This model requires symmetry of the stiffener about the panel's mid-surface [44] (Figure 2.12A). When stiffeners are modeled as beams, they essentially lie on the panel's mid surface. As a result, coupling effects due to geometric eccentricity in a stiffened panel which is asymmetric about its mid-plane (Figure 2.12B) is lost. In addition, 1D model for composite beams become extremely complicated if coupling between extension, bending in two directions perpendicular to the axis, and St. Venant's and Vlasov's torsions are included [48–50]. Cross-sectional warping (Vlasov's torsion theory) during torsion is significant for thin-walled composite beams.

   C2) Panels Stiffeners can also be modeled as panels [44, 47] and Equivalent Single Layer

[1] Some authors [44–46] use two different categories (i) discrete models- stiffener modeled as beams (ii) branched plate and shell models- stiffener modeled as plates/shells.

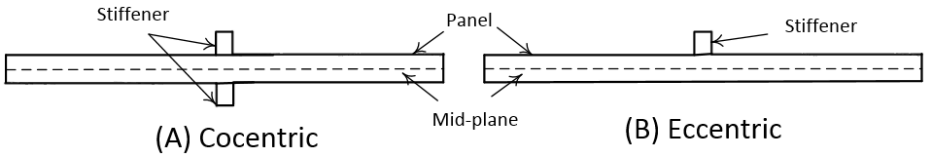

Figure 2.12: Two configurations of stiffeners.

Theories can be used to model the stiffeners' behavior. Coupling effects are always captured, irrespective of the configuration of the stiffeners (Figure 2.12).

C3) Solids Li et al. [51] used the three-dimensional behavior model for stiffeners.

When using discrete models for analysis of stiffened panels, care must be taken to ensure displacement compatibility and traction equilibrium at the stiffener-panel interfaces. This requires the use of compatible mesh or constraint methods during finite element analysis of the stiffened panel.

Neither smeared nor beam model is ideal for arbitrary arrangement of stiffeners. The panel model, on the other hand, requires careful abstraction of the stiffener as an assembly of plates and shells.

Bonded Joints

Bonded joints using adhesives are used to transfer loads between components. Load transfer leads to normal and/or shear stress in the adhesives. Adhesives are usually thin layers and show complex 3D stress-strain fields and stress concentration near the edges. Simplifying assumptions, therefore, are made in the behavior models for the bonded joints [17, 52]. The assumptions are generally regarding the following–

1. the presence of transverse shear and normal (also called peel) stresses in the adhesive.
2. approximation functions to approximate strains or stresses in the adhesive thickness direction.
3. satisfying the zero-stress condition near the adhesive's free edges.
4. the material model, i.e. whether the adhesive material is modeled simply as elastic or inelastic body.
5. whether or not spew fillets near the adhesive edge are being accounted for or not.

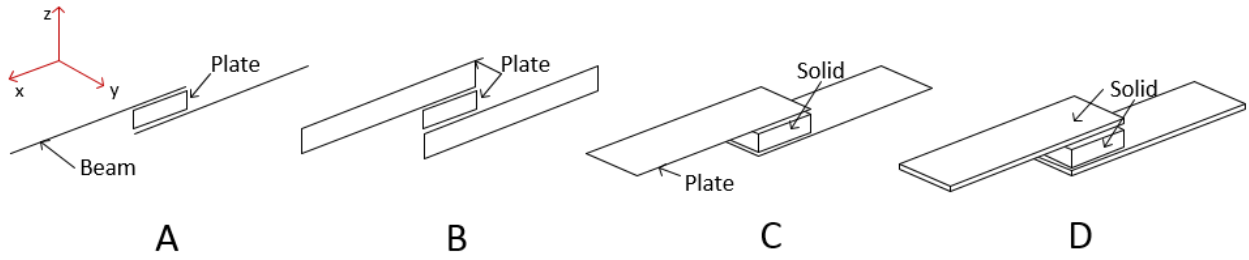

Figure 2.13: Different ways to model lap joints for Finite Element Analysis.

Lap joints are the most studied joints in literature. Examples of different behavior models for the lap joints (Labeled **A** to **D**) are shown in Figure 2.13.

A Behavior of adherents (joined components) is modeled using 1D beams, while the adhesive's behavior is modeled using the 2D behavior model. However, this 2D behavior model is not the same as the panel behavior as discussed above. Assuming adherents and adhesive are flat, the approximation function approximates displacement in one of the in-plane directions (y) and not the thickness direction(z).

B Behavior of adherents and adhesive is modeled as 2D behavior, but as before, approximation function is used for one of the in-plane directions.

C Adherents' behavior is modeled as panels and of the adhesive's using full 3D behavior model.

D Behavior of adherents, as well as adhesives, is modeled using 3D behavior models.

The behavior models in Figures 2.13A and B model only a cross-section of the adhesive and are not valid when lap joint is not flat. Moreover, lap joints show 3D deformation such as bending due to eccentric loading, anticlastic bending, 3D stresses, and stress concentration [17, 18], which cannot be captured by modeling joints using 1D or 2D behavior. Modeling the behavior of adhesives as solids (Figures 2.13C and D) is accurate but expensive.

Capturing high stresses due to stress concentrations in lap joints requires large number of degrees of freedom in the stress concentration regions. Moreover, Bogdanovich et al. [18] point out that extra effort to capture high stresses may not be worthwhile after all. The idealized behavior model ignores the effect of spew fillet at the adhesive edges, residual thermal stresses, and inelastic behavior

of adhesives, which are present in lap joints in practice. These effects play an important role by substantially reducing the actual stresses near the edges. Also, linear elasticity results in singular stresses (infinite stresses) in stress concentration regions, which is not physically possible. Therefore, it is sufficient to capture regions of stress concentrations and use other methods for failure analysis. I have shown in [53] that regions of high stresses are accurately captured by homogenizing the 3D behavior of adherents and joints through the use of layered finite element (Appendix A.1) during analysis, which requires considerably fewer number of degrees of freedom in comparison to using 3D behavior for adherents and adhesives separately.

Ply drop-off Regions

In ply drop-off regions(Figure 2.6C), tapering and the presence of soft resin pockets cause local bending [54, 55]. Also, material discontinuity due to resin pockets causes high stresses and strains and interlaminar stresses. Therefore, full 3D or quasi-3D behavior models are ideal for ply drop-off regions [54–57]. However, full 3D model is expensive as it requires modeling of every layer in the drop-off region. “Homogenizing" the 3D behavior of plies and resin pockets during analysis (done by using layered finite elements) captures the local bending and high stresses [55] without excessive computation cost. Moreover, Varughese et al. [57] have shown that local behavior can be ignored altogether if only global displacements are desired.

Cutout and Boundary Regions in Composite Panels

Regions around holes and free-edges in composite panels are regions where interlaminar[2] stresses and stress concentrations may exist. Interlaminar stresses arise when the in-plane stresses vary along the in-plane directions [58]. Internal cutouts cause a gradient in in-plane stresses by changing the load path around the cutouts, while free edges cause even sharper gradient by forcing in-plane stresses to zero at the boundary. The size of the region where interlaminar stresses are significant vary for the two cases. Interlinear stress due to the free edge occurs within the ‘panel-thickness’ distance from the free edge (from Saint Venant’s Principle [58]), while interlaminar stress around a cutout extends to a distance that is proportional to the length scale of the cutout. Therefore, interlaminar stresses due to cutouts exist in a wider region in comparison to the region of free-edge

[2] At the interface between the layers.

interlaminar stresses.

Global behavior models can predict the in-plane stresses accurately, but they completely miss interlaminar stresses. Full three-dimensional behavior models for each layer in the panel have to be used in order to obtain interlaminar stresses and high stresses due to stress concentration. There are, however, posteriori methods to estimate interlaminar stresses from in-plane stresses obtained using global behavior models [58]. They provide sufficiently accurate stresses and strains, except they fail to accurately capture high stresses in stress concentration zones. Moreover, extra effort to compute such high stresses may not be worthwhile, as discussed earlier.

2.2.2 Finite Element Analysis of Composite Artifacts

Structural analysis of general composite artifacts is carried out using finite element method. Using different behavior models in different regions of the composite artifact results in sufficiently accurate, yet efficient analysis of composite artifacts. Noor et al. [12] have identified following pre-processing steps before finite element analysis of composite artifacts can be carried out:

1. Rational selection of a set of mathematical models and proper identification of the regions in the artifact covered by these models Using the terminologies, this step translates to selecting the simplification behavior models and identifying regions where they are applicable in the composite artifact. In practice, this step is usually carried out by the analyst based on his/her 'intuitive judgment' [12]. A more systematic way, as suggested by Noor et al [12], is to use hierarchical adaptivity. The idea is to start analysis with a coarser behavior model for the entire artifact and adaptively refine the models using sensitivity analysis. Adaptive refinement of behavior models is attractive but requires a complex computational system. Moreover, multiple refinements have to be carried out iteratively, and there are also chances of numerical instabilities. On the other hand, the behaviors of different functional features (structural elements, joints, and transitions) are well studied and known beforehand. So, instead of hierarchical adaptivity, the knowledge of the functional features in an artifact, when FBS structure is provided, can be used to find the appropriate behavior models. Moreover, all of these methods require knowledge and representation for behavior regions, which is one of the contributions of the thesis.

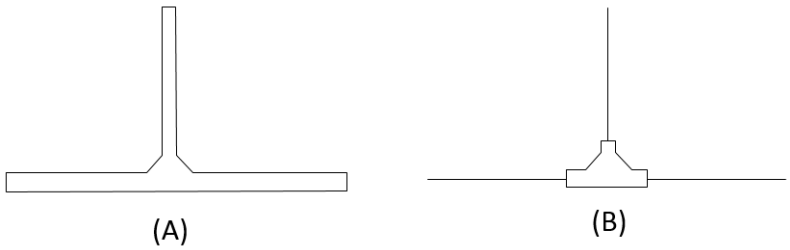

Figure 2.14: A) Artifact B) Mixed dimensional analysis model[4]

2. Proper treatment of interfaces between the regions with different behaviors, as well as of the coupling between different behavior models. Behavior models for two adjacent regions in an artifact are usually not compatible at the interface. Methods such as multi-point constraining methods or a new behavior model for the interface region that is compatible with the models of the adjacent regions must be used.

3. Selection of effective discretization techniques for use with each of the simplification models Regions with different behaviors in the analysis model are discretized independently using appropriate finite elements, which depend on the region's dimension and behavior. A brief description of different types of finite elements used for layered composites can be found in Appendix A. In practice, the application of behavior models usually leads to a mixed-dimensional analysis model [19], which is then discretized for FEA. To obtain the mixed-dimensional model, regions in the original artifact with 2D behavior are dimensionally reduced to a surface, and those with 1D behavior to an axis. An example of a mixed-dimensional analysis model is shown in Figure 2.14. Sometimes, a region is further subdivided into sub-regions, so that each sub-region can be discretized with different mesh densities. The high mesh density provides extra degrees of freedom to capture high fluctuations in stress-strain fields, if any.

In summary, multiple 'pre-processing' tasks have to be carried out before finite element analysis of a composite artifact can be done. There are tools to carry out the pre-processing tasks [19], but many of them are based on heuristics [59] and are error-prone. This makes pre-processing highly manual and time consuming. In fact, it has been estimated that pre-processing tasks can take up to 45% of an analyst's total time [60]. This will be even higher for composite artifacts because of their additional manufacturing complexity.

Attempts have been made, at least for conventional artifacts, to have a more systematic method to generate an analysis model from the original model by establishing a 'link' between the two models. Linking the analysis model to the original model inadvertently requires some kind of intermediate model or structuring method. Nolan, Armstrong el al. [19] link them by capturing 'simulation intent', or the high-level modeling and idealization decisions, through the use of Cellular Modeling, Equivalencing, and Virtual Topology concepts. Additional methods to breakdown and systematize the pre-processing steps are also suggested in [61–63]. However, they, unlike Armstrong's method, are either not generic, do not accommodate all the pre-processing steps, or do not establish a clear bi-directional link between the two models [19]. Moreover, the process of obtaining the analysis model from the original model in all of the above methods is not automatic. In Armstrong's method, the link between the two models is based on the simulation decisions made by the analyst.

Moreover, since several of the pre-processing challenges are faced due of the requirement of the dimension reduction, some 'implicit' reduction methods also have been proposed by researchers that do not require modification of geometry and material properties. These reduction methods incorporates the same dimension reduction assumptions, but in indirect and creative ways.

1. *Solid-shell elements* are 3D elements that use Assumed Natural Strain method and Enhanced Strain method to deform like plates and shells[10, 64–66]. Their three-dimensional nature is well suited for interfacing with other solid elements in assemblies. These elements, however, requires plate/shell direction and, therefore, need the mid/reference surface information. Moreover, the higher the number of assumed and enhanced parameters, the better is the element's performance but at the expense of generality [65, 67].

2. Jorabchi et. al. have proposed an implicit reduction method that is achieved through an algebraic process[68, 69]. The process involves two key steps- i) modify stiffness matrix of the chosen 3D element to only include relevant kinematics (for example, bending strains/stresses for a beam) and ii) project the modified stiffness matrix onto a lower dimensional manifold to result into a lower dimensional stiffness matrix. The lower dimensional stiffness matrix is used during FEA and the results are projected back to the original 3D element to obtain the nodal displacements. This method is computationally efficient, equivalent to the geometric reduction, and implementable in off-the-shelf finite element packages. In addition, several of

the pre-processing steps are eliminated as 3D mesh is used everywhere. Explicit coupling, however, is required when artifacts contain both slender (region with 1D or 2D behavior) and solid regions. The lower dimensional stiffnesses for slender regions obtained after projection (step ii) and the 3D stiffnesses for the solid regions are coupled through Lagrange multipliers in the global stiffness matrix. Finally, the virtual material method can be seen as an extension of the algebraic reduction method, from reduction of geometry to reduction of material. I use the lower dimensional theories to algebraically obtain a simplified virtual material for the purpose of analysis.

For laminates, 3D elements based on the above methods can be used as conforming layered elements (Figure A.1b in Appendix A.1). Since these methods mainly consider homogeneous materials, they do not address the material complexity faced in laminates. Also, although mixed-dimensional interfacing issues are eliminated, coupling is still needed as adjacent elements can still have mismatched 'effective' degrees of freedom when they belong to different functional regions. In the next sections, I review different models for intent in structural design.

2.3 Intent in Design

2.3.1 FBS Framework for Design

I briefly discuss the informal concepts of Function, Behavior, and structure with the help of a simple chair example (Figure 2.15). Function and behavior, specifically, are subjective notions and can be expressed in various ways. I touch upon their fundamental attributes, and the detailed discussion can be found in the literature [70–72].

Structure The structure of an artifact usually refers to its decomposition into a collection of interacting physical elements, typically represented by a graph. In Figure 2.15, the structure of the chair consists of six elements, represented as nodes $S_1 - S_6$ that interact through interfaces represented as edges $r_1 - r_5$. Elements in the structure are perceived through their *states* when they are operational [23], and the states themselves are expressed using *state variables*. If we are concerned with the structural (e.g., elastic) properties of the chair, the state variables are quantities measuring deformation and internal forces in the chair's elements. The same artifact may be viewed

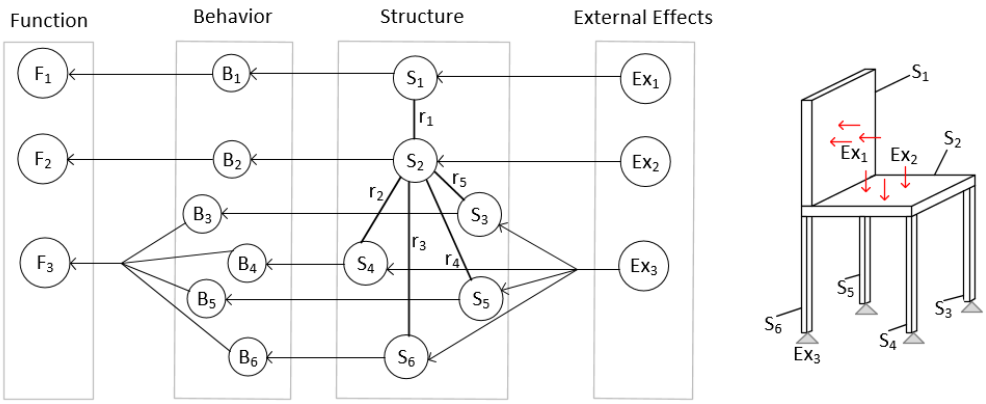

Figure 2.15: Function, behavior, and structure variables and causal relationship between them for a chair design.

in terms of different structures. For example, a calculator is a combination of logical units in one view and a combination of electronic components, such as resistors and capacitors, in another. Many computational design and manufacturing activities are centered around transformations and mappings between different structures and views [70, 73, 74].

Behavior Behavior, informally, is *what* a structure does, usually represented by its response to external stimuli [23]. The legs of the chair are the column elements that are characterized by uniform compression under compressive loads, while the seat and the back are plate elements that bend under flexural loads. These behaviors are denoted using labels $B_1 - B_6$ in Figure 2.15. Behavior is formalized in multiple ways in the literature, but most definitions agree that behavior is expressed through the states of a structure [71, 75]. For example, in one of the definitions, behavior is a device's causal models that are captured through relationships between *dependent* and *independent* state variables. The relationships are either the result of internal constraints due to the interactions between elements in the structure or the result of physical principles and laws such as Ohm's law, Hooke's law, etc. Designers usually postulate the structure's *intended* behavior, which may or may not correspond to its *actual* behavior. One of the goals of the designing process is to devise a structure whose actual behavior meets expectations, which is ensured through analysis of the structure [22].

Function Function captures the teleological knowledge behind an artifact, which captures the artifact's goals, purposes, requirements, etc. For example, the chair's function may be (1) to support a person's back and weight (F_1 and F_2, respectively) and (2) to support the seat at an elevated height (F_3). Due to its subjective nature, many definitions of function have been proposed in literature [70, 71, 76]. One of the reasons for differences is the so-called *device-centric* and *environment-centric* view of the function. In the former view, for example, the function of a buzzer is to make a sound when a switch is pressed, while the function in the latter view is to inform the residents of a house of a visitor outside [70]. The two views have their respective importance in design and diagnosis [70, 76]. While designing, the environment-view function is transformed to device-centric function and then the device-centric function is decomposed hierarchically into sub-functions until sub-functions can be associated to some physical phenomena and/or components.

Together, the concepts of function, behavior and structure are commonly referred to as the *FBS framework*, which is used to formulate the workflow in support of design, analysis, and manufacturing activities [22]. For example, a typical workflow may consist of the following steps: (1) a function is achieved by mapping it to a set of expected behaviors (requirements); (2) a synthesized artifact should possess a structure which should have an expected behavior (synthesis); (3) analysis/simulation are deployed to predict the actual behavior of the structure; and (4) validation that the actual behavior matches the expected behavior and ultimately achieves the desired function.

2.3.2 Other Models of Intent

While the above and other FBS frameworks are popular in design, they are not directly related to or supported by solid and geometric modeling systems that ultimately must represent all designed and simulated artifacts. Instead, computer-aided design and engineering activities are often cast in terms of user "intent," an ill-defined concept that is implied by heuristic geometric constructions that reflect common application-specific practices. For example, parameteric feature-based modeling is widely accepted as a particularly effective method of capturing design and/or manufacturing intent in a variety of applications [73]. Methods to capture intended physical behavior and/or function of artifacts through geometric constructions and transformations have also been proposed [11, 77–80], focusing mainly on creation, parametrization, idealization, simplification, and preprocessing of solid

models for simulation and analysis. Most of these constructions appear to be based on empirical knowledge and heuristics [12, 59, 60]. As such, these purely geometric techniques cannot be easily extended to support FBS tasks in the design and manufacturing of complex material structures, e.g. those arising in 3D printing or composite manufacturing.

One of the main motivations for developing a formal extension of solid modeling that includes the physics of behavior and function is to support the formal notion and modeling of intent, as well as other tasks within the FBS framework. It is reasonable that the starting point for such extension should be the classical notion of a well-posed boundary value problem [81]. More general notions of physical solids as fiber bundles were proposed in the context of computational analysis in [82] and heterogeneous material modeling in [83]; a combinatorial physical model in terms of (co)chain complexes was advocated in [84] and [85]. None of these proposals dealt with formal notions of behavior and its use within FBS framework. The proposed approach and concepts are general, but for concreteness, I will focus on behaviors and functions governed by elastostatics, arguably the most common model of physical analysis.

Chapter 3

FBS For Engineering Artifacts

I present the formal definitions of Function-Behavior-Structure terminologies in this chapter. The definitions are based on the extension of solid modeling to include physics, which is discussed in the first section. I present two applications of the definitions of function, behavior, and structure— a precise formulation of design and analysis problems in Section 3.2 and a concrete FBS framework for structural engineering in Section 3.3. I focus on linear elasticity physics in the definitions below, but they can be easily extended to include other types of physics.

3.1 Physical Solid Modeling

Informally, a physical solid is the classical solid model with a physical state, which in turn supports the systematic definition of a physical solid's structure, behavior, and function. In this section, I make these notions precise, focusing specifically on elastic solids.

3.1.1 Elastic Solid and Its Structure

Solid, R

Several mathematical models for solids have been proposed in the literature[83, 86] to model the geometry and topology of physical objects. I adopt the classical notion of an n-dimensional 'manifold solid'[87–89]. To be precise, a **solid** R is a compact n-dimensional manifold with a boundary, where the boundary is a compact, oriented, $(n-1)$-dimensional manifold, and $n = 1, 2$ or 3. A **decomposition** of n-solid R is a collection $\mathcal{R} = \{ r_1, r_2, ..., r_k \}$ of n-solids such that

1. $R = \bigcup_i r_i$, and
2. for $(i \neq j)$, $r_i \cap r_j = \emptyset$ or F_{ij}, where F_{ij} is a $(n-1)$-dimensional manifold with boundary, called an **interface** between the solids r_i and r_j.

Individual solids r_1 and r_2 can be composed into $R = r_1 \cup r_2$ whenever they share a valid interface $r_1 \cap r_2 = F_{12}$.

State of a solid, T

In physical systems, solids are perceived through their states. Temperature field, displacement field, and stress field defined over the domain of the solid are examples of physical states. Formally, **state** T of a solid R for some physics is an ordered set of admissible fields defined over the solid[90, 91]. Admissibility conditions for the fields are conditions such as continuity or differentiability and depend on the laws of the particular physics. Some popular physics are thermodynamics, elasticity, and electrostatics.

In general elasticity, the state of a 3D solid consists of displacement, strain, and stress fields defined over the solid and is referred to as the **elastic state**[90]. Based on the theory of elasticity and some additional assumptions, the state can be generalized to lower dimensional solids as well[92–94]. The generalized elastic state T of an n-dimensional solid is given as

$$T = [u, \mathcal{E}, \Sigma], \tag{3.1}$$

where (1) u is the *displacement vector* field, (2) Σ is the *resultant stress vector* field consisting of forces and moments which are statically equivalent to some stress distribution, (3) $\mathcal{E}$ is the *resultant strain vector* field and has quantities which measure changes in lengths, angles, curvatures, etc. at a point. Also, the vectors Σ and $\mathcal{E}$ are linearly related by a constitutive relationship—

$$\Sigma(p) = C(p) \cdot \mathcal{E}(p), \;\; p \in R \tag{3.2}$$

where C is the elasticity, or the material stiffness, field.

In general elasticity, the resultant stress, strain, and constitutive relationship correspond to the classical concepts of stress, strain, and material stiffness tensor[90]. In one-dimensional pure

bending theory, the resultant stress, strain, and constitutive relationship are bending moments, radius of curvature of the neutral axis, and bending stiffness, respectively. They are related by

$$[\text{Moment}] = C \cdot [\frac{1}{\text{Radius of Curvature}}] \tag{3.3}$$
$$C = (\text{Young's Modulus}) \cdot (\text{Moment of Inertia})$$

Physical Solid, S, and its Structure

A physical solid S is an n-solid R with a state T for some physics. However, the state is determined by a solution to some well-posed boundary (and possibly, initial) value problem that is defined by the constraints and boundary conditions L and internal material's constitutive relation C for the relevant physics. Thus, we can choose to define the physical solid directly in terms of its geometry, constitutive material properties, and constraints/boundary conditions. In the case of linear elasticity, we can define an **elastic solid** to be a triple

$$S = [R, C, L], \tag{3.4}$$

where

1. R is the solid domain of the boundary value problem (BVP).
2. C is the constitutive relation and implies that Σ and $\mathcal{E}$ are defined (from Equation 3.2).
3. *Loading* L specifying constraints on state variables Σ and/or u of the boundary points (Dirichlet and Neumann) and of the interior points (body forces).

Similarly to the decomposition of solids, a physical solid can always be decomposed into smaller boundary value problems, as illustrated in Figure 3.1. I define a physical **decomposition** of an n-dimensional elastic solid $S = [R, C, L]$ as $\mathcal{S} = \{ s_1, s_2, ..., s_k \}$ where $s_i = [r_i, c_i, l_i]$ is an elastic sub-solid such that:

1. $\mathcal{R} = \{ r_1, r_2, ..., r_k \}$ is a decomposition of R.
2. $c_i = C\big|_{r_i}$ is the restriction of C to r_i.

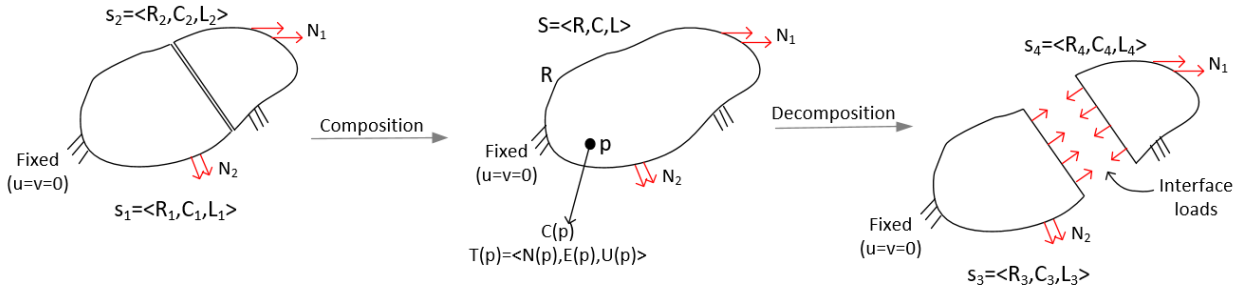

Figure 3.1: Illustration of a physical solid and composition and decomposition operations.

3. l_i is the set of loading applied to r_i plus the interface loads for all r_i's interfaces with other regions.

Based on the equilibrium and compatibility conditions in linear elasticity, **interface loads** are the conditions that, at each point in the interface, the two solids meet at the interface have equal but opposite tractions and identical displacements.

It should be noted that a physical decomposition of an elastic solid preserves the original state of the elastic solid. If T is the state of a elastic solid S, the state t_i of s_i, an element in the decomposition $\mathcal{S} = \{ s_1, s_2, ..., s_k \}$, is simply the restriction of T to r_i, i.e., $t_i = T\big|_{r_i}$. In other words, a physical decomposition of elastic solids represents its **physical structure.**

We can also define a **composition** $\odot$ of two elastic solids $s_1 =< r_1, c_1, l_1 >$ and $s_2 =< r_2, c_2, l_2 >$ into a larger elastic solid as

$$S = s_1 \odot s_2 \quad = \quad < r_1 \cup r_2,\ C,\ l_1 + l_2 > \tag{3.5}$$

where C is such that $C\big|_{r_i} = c_i$, $l_1 + l_2$ is the superimposition of loads, and solids r_1 and r_2 share an interface. In contrast to decomposition, composition of elastic solids clearly does not preserve their state, as an interface is created that leads to new interface loads. The composition and decomposition operations are compared in Figure 3.1. In general, the elastic state of $s = s_1 \odot s_2$ will have to be reevaluated.

3.1.2 Behavior of a Physical Solid

Behavior as a mapping

The simplest model of th behavior of a physical solid is its physical state. This model, however, is not very useful in design, as the physical state is usually not known *a priori* and also cannot be used to describe intended behavior and function of an artifact. In contrast, *bending, compression*, and *twisting* behaviors are frequently used terminologies in structural engineering. The terms referring to simplified states are used to specify the variation of the displacement field in some 'cross-section' located along a lower dimensional solid. Note that these terms implicitly describe the properties of simplified elastic state fields including the assumed loadings (constraints and boundary conditions.) Hence, I propose to define **behavior** of a physical solid s as a map $b : s \mapsto s^d$, where s^d is a (simpler) physical solid with a physical state that reasonably approximates the state of s in some metric. Map b induces following mappings for elastic solid:

$$f^R(R) = R^d,\ f^C(C) = C^d,\ f^L(L) = L^d, \tag{3.6}$$

where R^d, C^d, and L^d are the simplified solid, constitutive relation, and load, respectively.

Using this definition, the solid in Figure 3.2a behaves as a beam, if the 3D region R is mapped into a 1D axis R^d, the constitutive relationship C is mapped into a bending stiffness C^d, and the distributed force on the end-face is mapped into a bending moment F^d. This statement, however, does not imply that the mapping is somehow "correct;" the model of the behavior is only as good as the mapping b. When the model s cannot be simplified, map b is an identity map (denoted as b^I) such that $b^I(s) = s$, signifying that the simplest behavior of s is its general 3D elastic state.

The notion of behavior extends naturally to the decomposition $\mathcal{S} = \{ s_1, s_2, .., s_n \}$ of S. In this case, behavior of the structure $\mathcal{S}$ becomes a collection of behaviors

$$B(\mathcal{S}) = \{ b_1(s_1), b_2(s_2), ..., b_n(s_n) \} \tag{3.7}$$

$$= \{ s_1^d, s_2^d, ..., s_n^d \} \tag{3.8}$$

In other words, B is a piecewise map $\{ b_i \}$ which associates a set of simplified physical solids $\{ s_i^d \}$ with different parts of S. An example of such more complex behavior map is illustrated in Figure

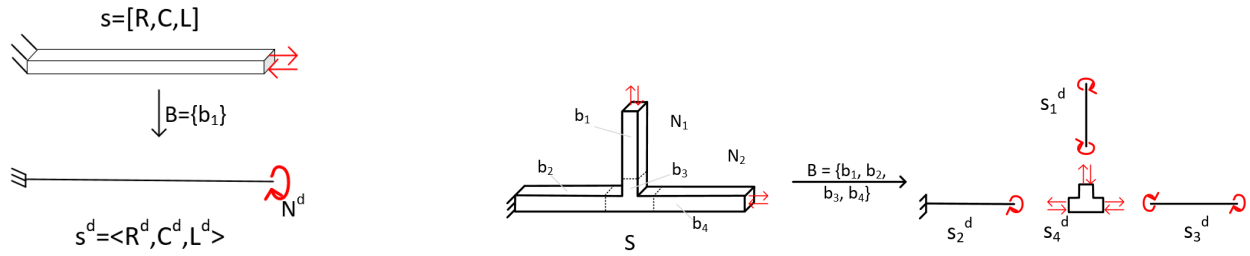

(a) A simple beam behavior map b.

(b) A more complex behavior map B.

Figure 3.2: Examples of behaviors: (a) of a single solid; (b) of a structure

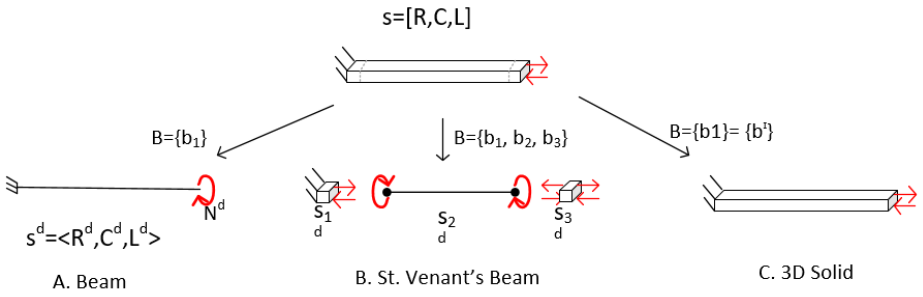

Figure 3.3: Illustration that behavior is not unique.

3.2b: the three arms have beam behavior with a 3D behavior map for the junction portion of the structure.

Behavior is not unique for a physical solid. For example, Figure 3.3 shows three possible behaviors of solid S. S can be treated as a simple beam, a beam with end-regions (St. Venant's Principle), or as the identical 3D solid. The level of fidelity is different for the three behaviors with the first being the least accurate and the last the most accurate.

Types of a Behavior

The above definition of behavior requires a fully evaluated instance of the simplified physical solid. In practice, to say that solid s behaves as **B** implies that *there exists* a simplified physical solid of type **B**. The simple beam behavior illustrated above is a type of behavior, and there are other common behavior types in structural engineering such as thick beam, shafts, plates, and shells. We will say that a behavior $b(s)$ is of a certain type when the domain R^d, loading L^d, and constitutive relation C^d of the simplified physical solid $\{ s_i^d \}$ satisfies a set of properties common to that type.

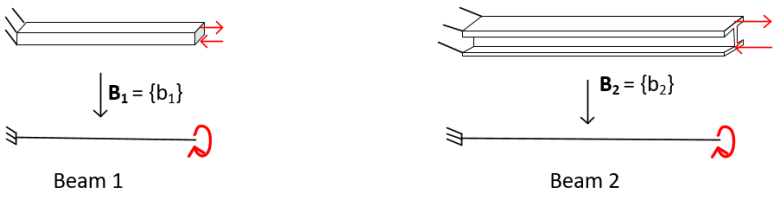

Figure 3.4: Example of two behaviors which are of the Type beam behavior.

For example, we can say that a behavior $b(s)$ is of type *beam* if following conditions are satisfied:

1. $s^d = [r, c, l]$ is a 1D physical solid.
2. r is a line segment.
3. c is a bending stiffness.
4. l can only consists of a) fixed displacement, b) moments out of the normal plane at the end-points, and (c) uniformly distributed force transverse to the line segment.

Any behavior $b(s)$ satisfying these constraints is then an instance of the beam behavior. Two instances of the beam behavior are illustrated in Figure 3.4. Other types of elastic behaviors can be defined similarly. Behavior types also could have a hierarchy where a behavior type has sub-types. For example, 1D behavior is a more general behavior type than the beam, column, and shaft behaviors, which are the sub-types of the 1D behavior.

3.1.3 Function of a Physical Solid

Informal definition of function for elastic solids, such as to “support/brace", “strengthen/stiffen", and “transfer load" have different meanings in different contexts. I posit that such informal concepts may be replaced with formal constraints on physical behaviors. For example, when a designer decides to “resist some load only through compression", he/she may want to use a physical solid with the *column* behavior. To be more precise, I propose that a physical **function F** of a artifact S should be identified with a *set of design requirements* that are expressed as constraints on the behavior $B(S)$ of S. Since $B(S)$ evaluates to a simplified solid s^d, the constraints may be stated in terms of the geometry, material, or physical state of s^d, including constraints on the maximum allowed deflection, required extension stiffness, maximum allowed stress, etc. For example, for the leg of the

chair, which is designed to have the column (compression) behavior, the function could include the requirement that the maximum allowable compression is $1 inch$; when this constraint is violated, the chair will not satisfy its design requirements and will lose its ability to provide the intended function. When the decomposition of S is a collection $\{ s_i \}$ with behaviors $\{ B_i \}$, the design requirements may be stated in terms on the conditions on each s_i in the decomposition. Thus, the function of the chair reduces to specific constraints on the chair's seat, back, and four legs, as shown in Figure 3.9.

Design requirements are effective means for specifying intended functions of physical solids. For example, an office chair and a theater chair may possess very similar models of structure and behavior, but can be distinguished through their design requirements: the office chair may be required to constrain maximum deflection at the mid-point of the chair's back to ensure sufficient stiffness for the back support, while the theater chair may be constrained by maximum deflection at the top of the chair's back to maintain a certain leg-space between seating rows while providing the back support.

In the next sections, I discuss two applications of the above definitions in the context of design and analysis of engineering artifacts.

3.2 Application 1: Formal Expressions For Design and Analysis Problems

The proposed definitions of physical structure, behavior, and function allow precise formulation of fundamental problems in design (synthesis) and analysis of physical artifacts. I briefly discuss some of these problems below. The top seven problems are related to behavior and the last problem is related to function.

1. Behavior instance test Does a physical solid or structure $\mathcal{S}$ exhibit the specified behavior instance $B(\mathcal{S}) = \{ s_i^d \}$? If the map B is given, the problem becomes a relatively straightforward fidelity test that involves comparing the states of $\mathcal{S}$ with the corresponding states of simplified solids $\{ s_i^d \}$ to see if they are within an acceptable margin of error. For example, for the beam behavior illustrated in Figure 3.5, the map B is the dimensional reduction that assigns the state at a point

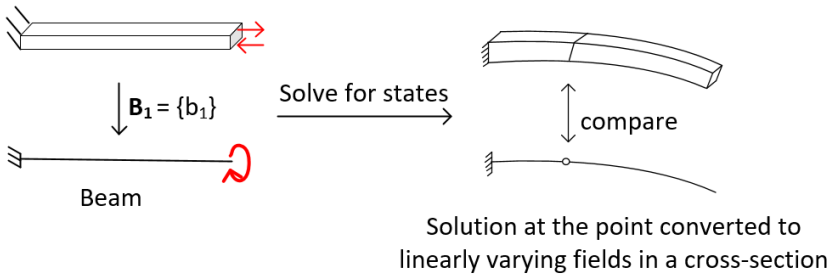

Figure 3.5: Evaluating if a physical solid behaves like a given beam.

on the center axis to the state of a cross-section of the 3D physical solid. If the behavior map B is not given explicitly, the problem becomes more challenging, requiring generating (non-unique) candidate maps and testing each of them for fidelity.

2. Behavior type test Does a physical solid S possess a given behavior type $\mathbf{B}$? And if so, can the behavior be determined? In fact, constructing an instance of an acceptable behavior map $B(S)$ immediately solves this problem. For example, the widely practiced dimensional reduction techniques provide many examples of such constructions [11, 95]. More generally, the task of deciding if there exists a behavior of type $\mathbf{B}$ is non-trivial. For example, to test if S has behavior of type beam, we will have to find at least one beam whose state approximates the state of S. There can also be indirect ways to ascertain if a physical solid $S = [R, C, L]$ has a behavior type $\mathbf{B}$. For example, in Figure 3.6, we know that the physical solid A has beam behavior since we know that there exist some mapping $B(S)$ of type beam if the geometry of R is obtain by sweeping a cross-section along an axis, has field C that is constant along the axis, and L has forces on the end-faces whose resultants are only moments. Deciding whether the solid B in Figure 3.6 behaves as a beam requires a very different argument. And such tests break down completely in presence of additional local features (holes, ribs, fillets, etc.) and may require a complete physical analysis to validate any hypothetical type of behavior.

3. Behavior of decomposition We earlier saw that the operation of decomposition does not change the physical state of a solid. However, the behavior of a solid is very much affected by its structure, and different decompositions $\mathcal{S} = \{ s_1, s_2, ...s_n \}$ of physical solid S will usually result in very different behavior models. This observation underlies apparent challenge in manufactur-

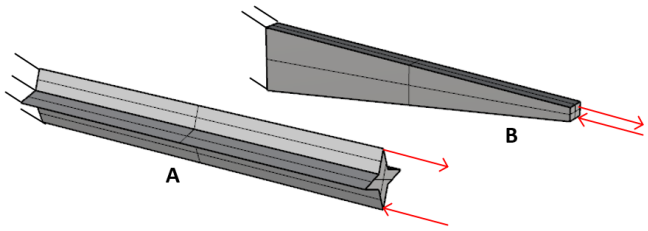

Figure 3.6: Two physical solids tested if they have beam behavior.

ing: intended/actual behaviors of the manufacturing structure are usually quite different from intended/actual behaviors of the functional structure of an artifact. Generally speaking, determination of behavior for a particular decomposition is an ill-posed problem without additional constraints on the behaviors or behavior types.

4. Behavior of composition On the other hand, given two physical solid S_1 and S_2 with behaviors B_1 and B_2 respectively, a common design problem is to determine the behavior and behavior type of their composition $S_1 \odot S_2$, assuming the original solids can be composed. This situation arises, for example, whenever structural elements with known behaviors are joined together in order to achieve a particular intended structural function. We shall see in Section 4.3 that behaviors of a composition play a key role in the design and analysis of composite artifacts.

5. Optimal structures and behaviors For a given physical solid S, we may want to find a decomposition $\mathcal{S} = \{ s_1, s_2, ..., s_n \}$ and behavior $B_i(s_i)$ such that S exhibit the most intuitive or simplest behaviors, appropriately defined. These and other criteria may be formulated in terms of minimizing the total number of components in the structure, or simplicity/dimension of individual components, or restricting to components of particular types. The fidelity of behavior must also be taken into account.

6. Behavior comparison Two behavior types can be compared for simplicity based on the relative computational effort required to solve simplified boundary value problems. It is widely accepted (though does not need to be true) that $(n-1)$-dimensional behaviors[1] are simpler than n-dimensional behaviors. So, a 1D rod behavior is usually simpler that a 2D membrane behavior.

[1] Dimension of behavior $B(S) = \{ s^d \}$ is the highest geometric dimension of the simplified physical solid s^d

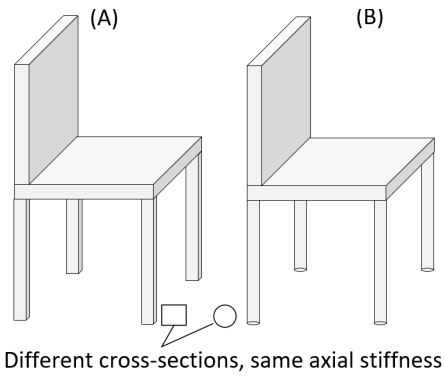

Figure 3.7: The chair artifacts are physically different but behaviorally equivalent.

Behavior types are of the same dimension can be further compared in terms of total degrees of freedom in the physical solid's model and so on. Thus, one may judge a 1D rod behavior to be simpler than a 1D thick beam behavior, as the former has one degree of freedom (axial strain) while the latter has two (curvature and shear strain).

7. Behavior equivalence When can we say that two physical solids exhibit equivalent behaviors? By definition, physical solids S and S' are *behaviorally equivalent* if there exists B and B' such that $B'(S') = B(S)$, or, in other words, S and S' can be mapped to the same simplified physical solid. For example, the two chairs in Figure 3.7 are behaviorally equivalent even though they are geometrically different: the legs have different cross-sections, but they can be mapped to the identical simplified solid. Equivalence can be also defined with respect to behavior types and/or fidelity. We shall see in Section 4.2 that equivalent behaviors hold a key to dramatic improvements in efficiency of analysis and simulation of composite artifacts.

8. Function Equivalence Similarly to behavior equivalence, we can also define the notion of function equivalence. Two artifacts are functionally equivalent if they are behaviorally equivalent and have identical design requirements on their respective simplified models. So, even if two chairs are behaviorally and/or structurally equivalent, they may not be functionally equivalent. For example, two chairs which are structurally and behaviorally equivalent can be functionally different in the following scenario, which was also discussed earlier.

1. In a home/office setting, the design requirement may constrain maximum deflection at the

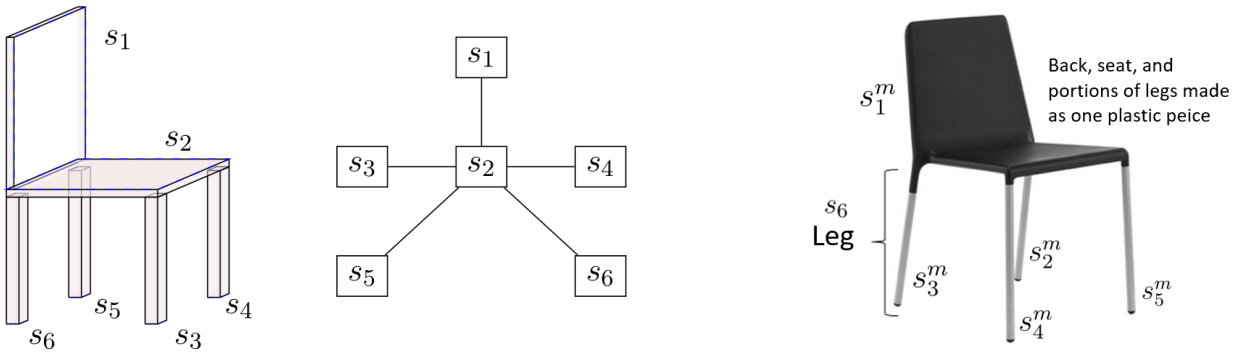

(a) Functional Structure of the chair example as per the definition.

(b) Manufacturing structure of the chair.

Figure 3.8: Structures of an example chair.

mid-point of the chair's back, which is to ensure sufficient stiffness for back support.

2. In a theater setting, the design requirement may constrain maximum deflection at the top of the chair's back to maintain a certain leg-space between seating rows while providing back support.

3.3 Application 2: Formal FBS Framework

Formalized notions of structure, behavior, and function allow systematic application of FBS framework in design and manufacturing applications, where workflows are abstracted as FBS paths[24].

I defined the structure of a physical artifact S as a particular decomposition $\mathcal{S} = \{ s_i \}$ of S. A structure is typically represented by a graph [24], whose nodes represent the components in the decomposition and edges represent the relationship between them. When S is a physical solid, the nodes represent the sub-solids in $\mathcal{S}$ and the edges represent the interfaces between the sub-solids. Graph representation of the chair structure is illustrated in Figure 3.8a. The graph can be seen as the *dual* of the decomposition $\mathcal{S} = \{ s_i \}$, where the nodes are the dual of sub-solids s_i's and the edges are the dual of the interfaces between the sub-solids.

However, note that a structure of a physical artifact is not unique, but it is usually implied by an application view of the artifact: different views imply different structures [74]. My focus is the design view and the manufacturing view, where the former leads to the *functional structure* and the latter leads to the *manufacturing structure* of a physical artifact, as discussed in detail below.

Functional Structure Functional structure $\mathcal{S}^F = \{ s_i^f \}$ is the structure of a physical artifact from the design perspective. Components s_i^f in the structure are physical elements that were chosen by the designer for their known behavior B_i. We will call the pair $[s_i^f, B_i]$ as a *functional element*. For the chair example in Figure 3.8a, the legs, seat, and back are functional elements. Note that the functional structure of an artifact S does not depend on how S is manufactured.

Manufacturing Structure Manufacturing structure $\mathcal{S}^M = \{ s_i^m \}$ is the structure of an engineering solid from the manufacturing perspective. In traditional manufacturing, components s_i^m are individually manufactured parts that are assembled together to get a physical artifact. Multiple functional elements are sometimes manufactured as one part to reduce the assembling cost. For example, the chair in Figure 3.8b has only five components in its manufacturing structure. The component s_1^m consist of the seat, back, and portions of the legs.

In general, the components s_i^m depend on the type of manufacturing method. In manufacturing using 3D printing, $\mathcal{S}^M$ will consist of roads and layers and, in composite manufacturing, $\mathcal{S}^M$ will consist of plies that are laid on each other to form laminates. Physical solid s_i^m can be assumed to have the default 3D behavior type B^I (or other simplified behaviors). For our case, the pair $[s_i^m, B^I]$ will be referred to as a *manufacturing element*.

Intended/Expected Behavior In FBS framework, systems have two types of behaviors (1) intended and (2) actual. This distinction is needed because behavior as expected by the designer are not preserved after composition due to the emergent behaviors. Behaviors of functional elements such as beam, plate, and shell behaviors is what the designer expects to be present in the solid. If an artifact was designed to include functional elements $[s_i^f, B_i]$, the *expected behavior* B^e of an engineering solid can be defined to be

$$B^e(S) = \bigcup_i B_i. \tag{3.9}$$

Actual Behavior Behavior types in actual behavior B^a of S are often unknown. By default, B^a can be assumed to be a 3D behavior, that is, $B^a(S) = \{ b^I(S) \}$. However, this approach is intrinsically inefficient because it does not take advantage of the artifact's structure and simpler behaviors exhibited by the individual elements of that structure. For example, some of the sub-

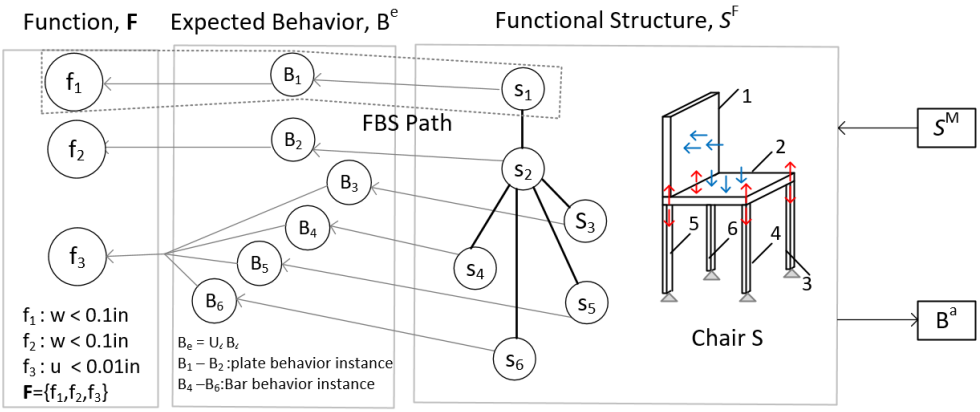

Figure 3.9: Function, behavior, and structures for the chair

solids in S could exhibit lower-dimensional simpler behaviors that could lead to faster structural analysis of S.

As we saw in the last section, finding the simplified behaviors for a general structure is non-trivial (Problem 5), and predicting the actual behavior B^a when S is a composition of simpler elements requires identification of all the emerging behaviors (Problem 4). The latter may be possible for some restricted well-understood composition operations, but not in general.

Function of an Engineering Solid As defined earlier, function **F** of an engineering solid that consists of functional elements $E_i = [s_i^f, B_i]$ is the set of design requirements f_i for E_i, that is,

$$\mathbf{F} = \{ f_i \} \tag{3.10}$$

FBS Paths for Representing Design Knowledge FBS paths [24] are used to define and record the flow of information by establishing causal relationships between function, behavior, and structure for modeling activities. My definitions allow to transform such FBS paths into formally defined and computable objects. For example, FBS relationships for the chair are shown in Figure 3.9. For the functional structure S^F of the chair, there are several possibilities for its manufacturing structure (e.g., Figure 3.8b). A correspondence between the two structures is established to record how each functional element was physically realized. Also, the expected behavior of the chair is given by the designer, but the actual behavior B^a of the artifact has to be determined, or can be assumed to be the general 3D behavior.

I apply this formal FBS framework to composite artifacts in the next chapter.

Chapter 4

Design and Analysis of Laminate Composites Using FBS

In this chapter, I use the formal FBS framework from the last chapter to address several difficulties faced in the design and analysis of composite artifacts, with some potential design applications. The first section discusses the management of manufacturing and functional structures of composite artifacts. The second section discusses the application of the behavior equivalence concept for a new type of analysis method, called the Virtual Material method. An artifact may have a new functional structure due to emergent behaviors after the functional elements are composed, which I discuss in the third section. In the fourth section, I demonstrate how the complete design knowledge, including function and manufacturing structure correspondence and emergent behaviors, can be documented for composite artifacts using FBS diagrams. The fifth section shows that a new type of simplified analysis model can be used for efficient FEA of composite artifacts using the virtual material method and FBS knowledge. Finally, in the sixth section, I show how the FBS framework can be used to generate new designs for artifacts to be manufactured using composite manufacturing as a possible design application.

4.1 Manufacturing versus Functional Structure

Functional structure of a laminate composite is straightforward: $S^F = \{ s_i^f \}$ where s_i^f are the solids representing all the functional elements in the laminate composite. Organization of manufacturing

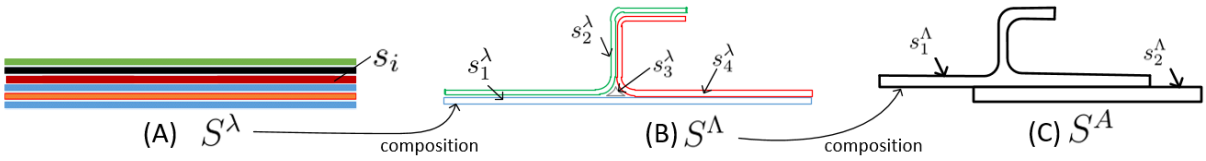

Figure 4.1: (A) A laminate S^λ (B) A Laminated component S^Λ (C) A Composite Assembly S^A

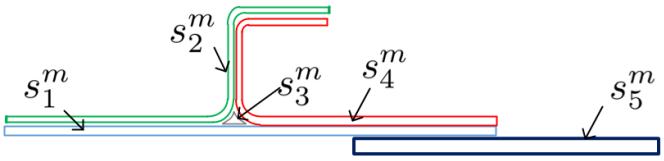

Figure 4.2: Manufacturing structure of a composite artifact.

elements in composite artifacts, however, is hierarchical in nature, as discussed earlier using the UML diagram in Figure 2.1. There are three sub-structures in the hierarchy, which are defined below using the proposed definition for physical solids and structures.

Hierarchical Manufacturing Structure The components in the structural hierarchy can be defined using the proposed definitions of solid and structure as follows.

- The starting items (plies, cores, and embedding) are 3D solids s_i's with uniform material constitutive relationships. Any internal material structure in the starting item is assumed to be homogenized.
- Laminate structure is a structure denoted with the subscript λ, that is, $\mathcal{S}^\lambda = \{ s_i \}$, where s_i's are the starting items in the laminate. Figure 4.1A illustrates a simple laminate structure. We will refer to the composition of all the components in a laminate structure $\mathcal{S}^\lambda$ as a laminate solid and denote it as s^λ's.
- A laminated component also has a structure $\mathcal{S}^\Lambda = \{ s_i^\lambda \}$, where s_i^λ's are the laminate solids. A structure of a laminated component is illustrated in Figure 4.1B. The laminated component is denoted as s^Λ's.
- Finally, a composite assembly is a structure $\mathcal{S}^A = \{ s_i^\Lambda \}$, where s_i^Λ's are the laminated components. Figure 4.1C illustrates a composite assembly. The composition of all the components in $\mathcal{S}^A$ results in a composite artifact.

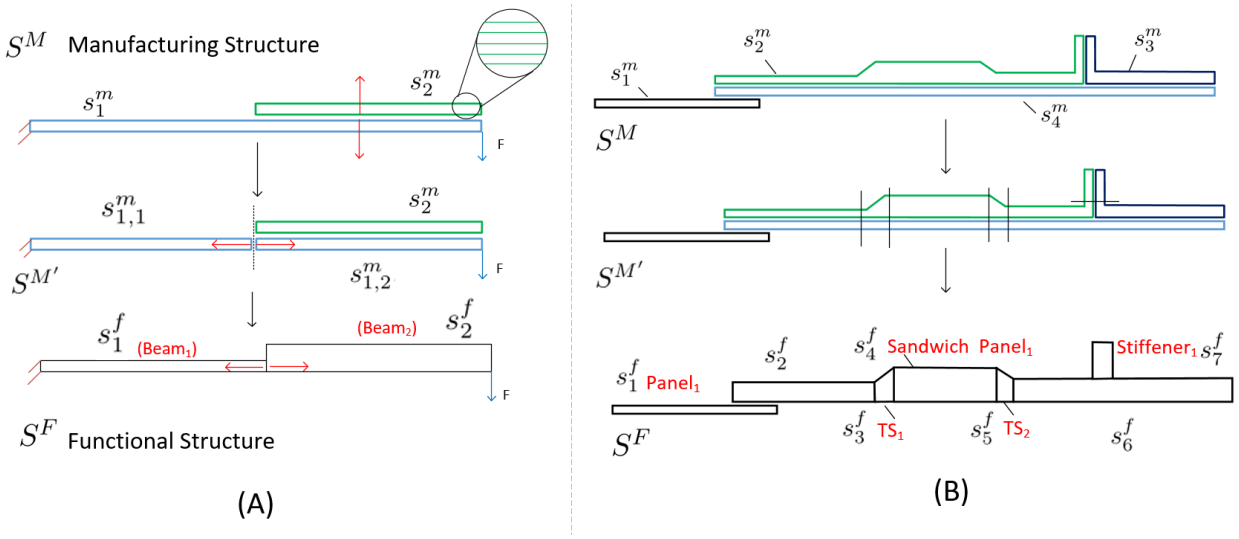

Figure 4.3: Mapping between manufacturing structure and functional structure.

Laminate-based definition for Computer Representation A hierarchical definition of the manufacturing structure is mainly needed for the manufacturing process and planning. However, all the material, geometry, and loading information for a composite artifact can be documented on a computer by representing any one of the levels in the hierarchy. I, therefore, propose a laminate-centric definition for manufacturing structure, wherein the manufacturing structure is simply a collection of all the laminate solids s_i^λ (denoted as s_i^m for consistency) in the composite artifact. That is,

$$S^M = \{\, s_i^m \,\}, \tag{4.1}$$

where $i = 1, 2, .., n$, and n is the total number of laminates in the artifact. Note that S^Λ above only consists of laminate solids which are present in a laminated component, while S^M is the collection of all the laminate solids in the artifact. Based on the current definition, the manufacturing structure S^M of the composite artifact in Figure 4.1 is illustrated in Figure 4.2. The proposed definition is logical because CAD models represent composite artifacts by representing the constituent laminates as tooling surfaces and a ply-table, as discussed in Section 2.1.3. Moreover, this definition is also convenient for establishing a correspondence between S^M and S^F of a composite artifact, as a laminate solid can be implicitly decomposed by decomposing its tooling surface, the details of which I discuss next.

Correspondence between Functional and Manufacturing Structure In unitized composite artifacts, as discussed in the Introduction (Figure 1.3), plies are shared between multiple structural elements. From the definitions of S^F and S^M ($S^F = \{ s_i^f \}$ and $S^M = \{ s_i^m \}$), this translates into some of the laminate solids s_i^m's being shared between multiple structural elements s_i^f's. A correspondence can be established by decomposing every shared laminate solid s_i^m into sub-solids such that each sub-solid's domain is contained entirely in the domain of only one functional element. For example, in Figure 4.3A, laminate solid s_1^m is shared between two structural elements s_1^o and s_2^o. So, s_1^m is decomposed into $s_{1,1}^m$ and $s_{1,2}^m$. Now, $s_{1,1}^m$ corresponds to s_1^f, and $s_{1,2}^m$ and s_2^m corresponds to s_2^f. The decomposition of the shared laminate solids essentially results in a new, refined structure $S^{M'}$. Figure 4.3B shows how the S^F and S^M correspondence is established for the unitized laminate artifact in Figure 1.3 which consisted of a stiffener, a sandwich panel, three thin panels, and two smooth transitions. By introducing transition solids (TS_1 and TS_2) as structural elements, the smooth transitions can be accounted by designers as transition-solids.

4.2 Efficient Analysis Through Behavior Equivalence

In theory, application of 3D finite element analysis to multi-ply artifacts is straightforward: we can simply mesh each ply, making sure that the finite element mesh is fine enough to resolve (usually a few elements across) each ply's thickness. Given that ply's thickness is often a fraction of a millimeter and the composite artifact could span meters, the approach is clearly impractical. A common method for predicting the performance of such artifacts is to (manually) represent them by simpler artifacts, usually 2D artifacts such as plates or shells, which approximate the intended behavior of the 3D layered artifact using classical lamination theories[96]. In other words, this is a clear example where a simple intended elastic behavior is implemented in terms of a complex layered artifact.

Instead of analyzing this complex manufactured structure, we can find another manufacturing structure for the same composite solid with equivalent elastic behavior. It turns out that a considerable simple manufacturing structure can be obtained that could be used as a replacement of the original structure during analysis. We will refer to the method of finding the new simpler manufacturing structure as the virtual material method, which is discussed in full detail in the next

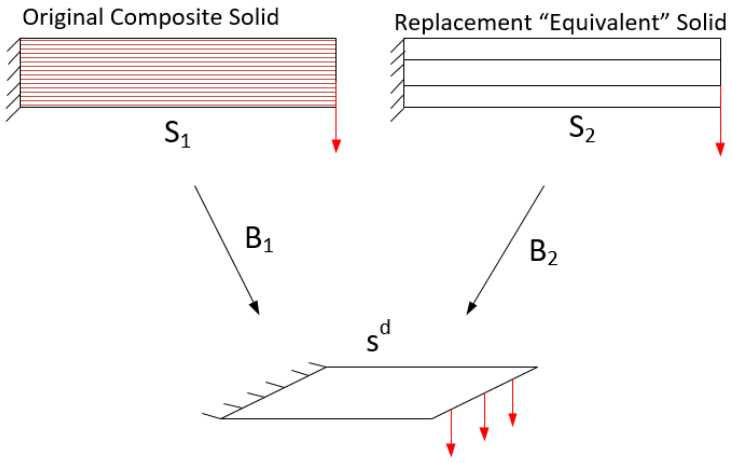

Figure 4.4: Replacement solid that is behaviorally equivalent to the original composite solid.

Chapter. Conceptually, as illustrated in Figure 4.4, the original composite laminate S_1 (made of 100s of plies) with, say, thin plate behavior $B_1(S_1) = \{ s^d \}$ can be replaced by another 3D laminate S_2 made of a small number of plies (3 plies in this case), but has the behavior $B_2(S_2) = \{ s^d \}$. The geometry and boundary conditions of the replacement physical solid are identical to the original solid. The procedure of obtaining the replacement solid involves solving a inverse problem which is based on the behavior model (lamination theory). The finite elements analysis on this solid gives identical results (by construction) at a fraction of computational cost.

4.3 Functional Structure under Composition

To reduce the cost of assembly, as discussed earlier, realistic composite artifacts are increasingly being manufactured as unitized artifacts [2, 5], wherein multiple functional elements are realized as one monolithic part. In order to be able to use the virtual material method for such an artifact, one needs to establish and maintain the explicit relationship between (portions of) the layered artifact and its intended mechanical behavior. This is challenging because joining of individual components with known behaviors not only changes the behavior of these components, but in fact changes the behavior *types* in the final structure. Typically, this happens for several reasons: (1) composition of two composite solids $S_1 \odot S_2$ creates new interfaces invalidating the behavior types of S_1 and S_2; (2) new emergent behaviors may appear in the decomposition of the structure; and (3) 3D behavior

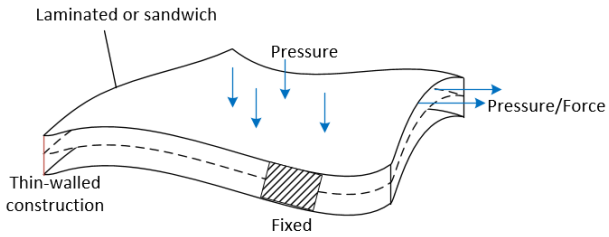

(a) Geometry and loading of Laminated Panel or Sandwich Panel.

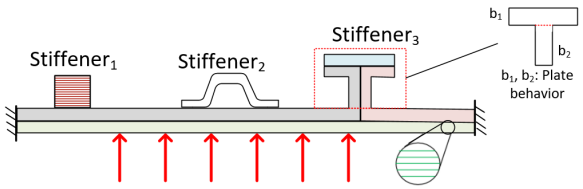

(b) Example of solid (Stiffener_1) and open cross-sections (Stiffener_2 and Stiffener_3) of stiffeners.

Figure 4.5: Panel and Stiffener solids

in the *transition regions*[1]. An example of a unitized composite artifact with two panels (functional elements) connected through a smooth transition is shown in Figure 4.6A. The emergent behavior is three-dimensional and is found in a region around the interface as shown in Figure 4.6B (details in Appendix B.3).

In general, automatic determination of the behavior after composition is an open and challenging problem. However, the behavior types are known *a priori* for many common functional elements and emergent behaviors can be predicted based on the type of joining operations. Below, I discuss the 1) common functional elements and their behavior types and 2) common joints and the associated emergent behavior for composite artifacts. This approach can be easily extended to other types of functional elements and joints to deterministically predict the emergent behaviors.

Common Functional Elements in Composite Solids Composite solids are thin-walled artifacts which mainly consist of one-dimensional and two-dimensional functional elements. The common functional elements and their behavior types are as follows.

1. Laminated panels and sandwich panels are the primary functional elements in composite solids, as discussed earlier. They have thin-walled construction with arbitrary loading on the end-faces and pressure loads in the interior faces (illustrated in Figure 4.5a). They have a general 2D behavior of either thin or thick plates and shells. General 2D behavior includes extension, bending, and extension-bending coupling, and it is discussed in more detail in the Sections 5.2.1 and 5.2.2. Additional details, including sub-classes of 2D elements, are discussed in Appendix B.2

[1] Transition regions are typically established using St. Venant's principle[17, 18] near the interfaces in the composite solid and requires either specialized behavior or a full 3D analysis.

2. Stiffener elements are used to stiffen laminated panels. Geometry of stiffener is obtained by sweeping a cross-section along an axis. A stiffener has interface loads due to its connection to a panel and may have loading on its end cross-sections that is consistent to the loading on the adjacent panel. Behavior of a stiffener depends on the *stiffener type*, where the types are based on the cross-section geometry(illustrated in Figure 4.5b): (1) solid cross-section stiffeners have 1D thin or thick beam behavior with extension-bending-twisting coupling and (2) thin-walled cross-section stiffeners have 1D behavior or a set of 2D plate and 3D behaviors (Stiffener_3 in Figure 4.5b). More details, including the sub-classes of 1D elements, are presented in Appendix B.1.

3. Finally, there are transition solids, which are regions of ply drop-off, core taper, and junctions (Figure 4.6). These solids have 3D behavior and cannot be dimensionally reduced.

The behaviors of 1D and 2D elements can be lost due to emergent behaviors after the elements are composed to form an engineering solid. However, we can predict the new behavior types in the engineering solid if the functional elements are joined using the standard joining methods. The common standard joining methods and the associated emergent behaviors are as follows.

Common Joining Methods and Associated Emergent Behaviors Two popular methods to join functional elements in composite solids are using [7, 97](1) bonded joints and (2) transition regions, which we will refer to as *transition-joints*. In bonded joints, the functional elements are manufactured separately and then bonded together using adhesives, while, in transition-joints, they are manufactured as one monolithic part and one functional element transitions into the another. I model the transition using *transition solid*(Figure 1.3). Examples of bonded joints are illustrated in Figure 4.8a, and the same 'joint configurations' can be achieved using transition solids as shown in Figure 4.9.

Designers usually join the 1D and 2D functional elements in composite solids in a way that the original behaviors (behavior type in our case) are somewhat preserved. Emergent behaviors, if any, are localized in regions around the joint interface. Using my formalizations, this can be expressed as following. Given solids S_1 and S_2 whose behavior are B_1 and B_2, the original behaviors B_1 and B_2 are destroyed after composition $S_3 = S_1 \odot S_2$. Their behavior types $\mathbf{B}_1$ and $\mathbf{B}_2$, however, are

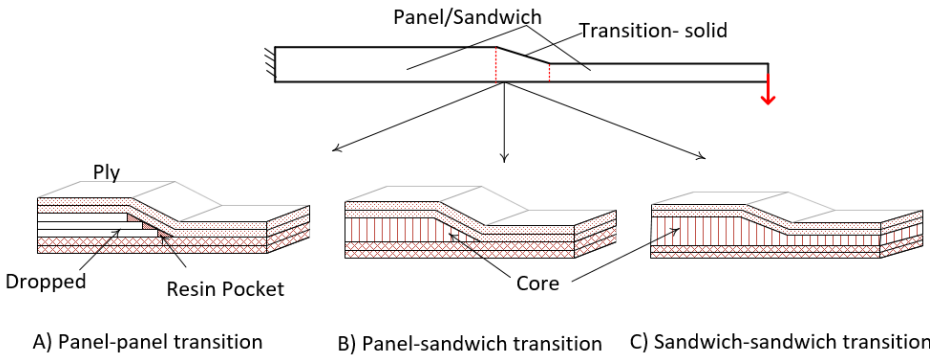

Figure 4.6: Joints using transition-solids.

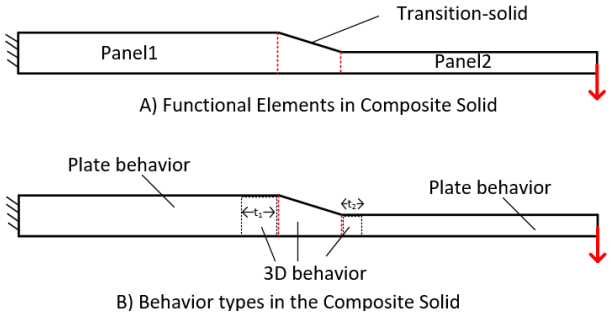

Figure 4.7: Emergent behavior in transition joints.

still preserved for some sub-solids in S_3 depending on the type of joint. I discuss this in detail for the common joint types below.

Transition joint between panels and sandwich It is easy in composite solids to use thick plate elements for regions with higher load by adding extra plies or a sandwich core. The joining between thick and thin plate elements is achieved through a transition solid whose domain is the region of a ply drop-off in case of the laminated panel and a tapered core in the sandwich panel, as illustrated in Figure 4.6.

In such joints, the emergent behavior is present in a small region around the joint interface (Figure 4.7), which is in the form of local bending and 3D stresses (Section 2.2.1). Such regions have 3D behavior and, according to the St. Venant's principle, they are the size of the *characteristic thickness* h^v, which is of the order of the thickness of the panel. The region can be evaluated using the Minkowski sum operation (Appendix B.3) of a ball of size h^v and the joint interface. The behavior type is preserved at the rest of the points in each region.

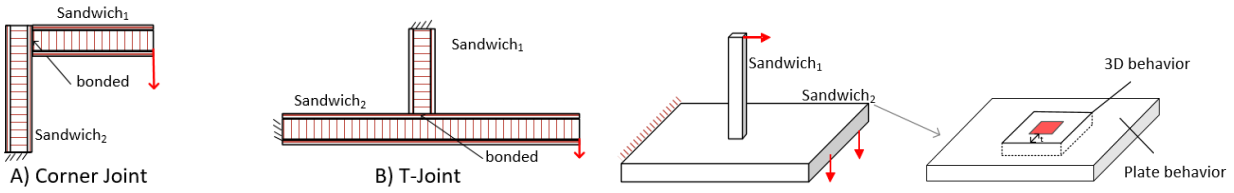

(a) Corner and T-joints in sandwich Panels. **(b)** Region of 3D behavior in T-joint.

Figure 4.8: Bonded joint and emergent behavior in T-joint.

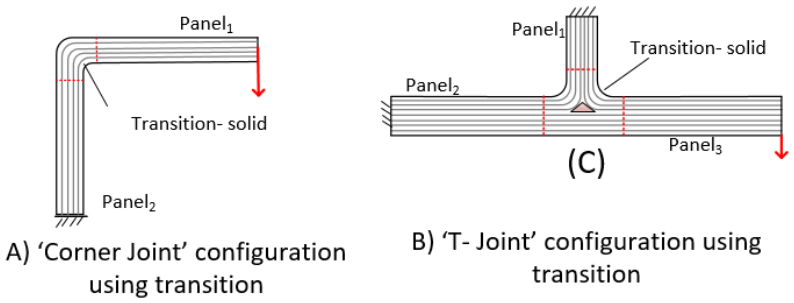

Figure 4.9: 'Corner and T-joint' configuration using transition joints.

Corner and T-joints These joint-configurations are used to join panels and beams that are at some 'angle' to each other. Bonded corner and T-joint in sandwich panels is shown in Figure 4.8a. A transition solid can be used as an angle or T "bracket" for joining laminated panels, as illustrated in Figure 4.9. Again, the emergent 3D behavior is localized in a region near the interface and its exact region can be obtained as described above and shown in Figure 4.7. The original behavior type is present at the rest of the points in each region. Figure 4.8b illustrates solid with the emergent joint behavior in a sandwich panel that is joined to another sandwich panel in T-joint.

Joint between a panel and a stiffener Joint between a stiffener and a panel can be either a bonded or a transition joint. Behaviors of the stiffener and the panel are preserved[44, 47]. Note that stiffener is a sub-type of 1D solid because, in stiffeners, the loadings has more restrictions.

Based on the emergent behaviors for the above joint types, we can find the final behavior types in the chair example that I discussed in the previous chapter (Figure 3.9). The legs and the back elements are joined to the seat through corner joints and, therefore, will have emergent 3D behavior

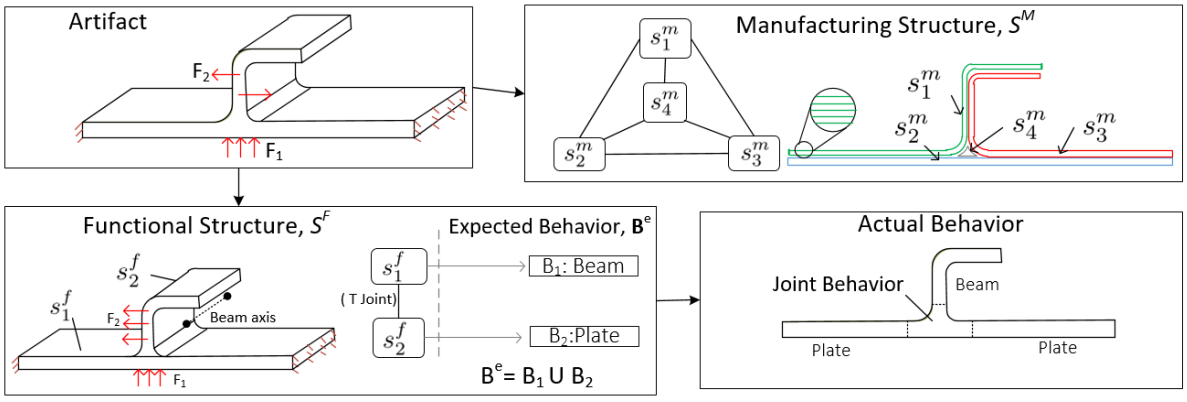

Figure 4.10: Behavior and structures in a stiffened plate.

in the vicinity of the interfaces. Rest of the regions will preserve their behavior types. The behavior types in the chair after composition are shown in Figure 4.13A.

4.4 Design Knowledge Through FBS Diagrams

We earlier saw the formal FBS knowledge diagram for a simple chair example in Figure 3.9. The diagram did not include 1) correspondence between the chair's manufacturing and functional structures and 2) the behavior types in the artifact's actual behavior. In this section, I include these details in the diagram and demonstrate for two example composite artifacts.

Example I— Beam and Panel Assembly

The beam-panel assembly and the loading are shown in Figure 4.10. The artifact is manufactured using four laminates denoted as s_i^m (i=1 to 4). Functionally, the artifact consist of only two functional elements, s_1^f (a panel), and s_2^f (a beam), which are composed using a T-Joint. Laminates s_i^m (i=2 and 3) are shared between the two functional elements and are decomposed into smaller laminates such that each new laminate lies within either the beam or the plate. The expected behaviors are supplied as labels (beam and plate in this case) and the details of the behaviors (the simplified models) can also be included as described in Appendix B. A designer also specifies the design requirements such as maximum deflection or desired resultant stiffness as the function. Based on the proposed approach to predict emergent behaviors, the actual behavior will consist of an emergent behavior at the interface of the beam and the plate because of the T-joint between

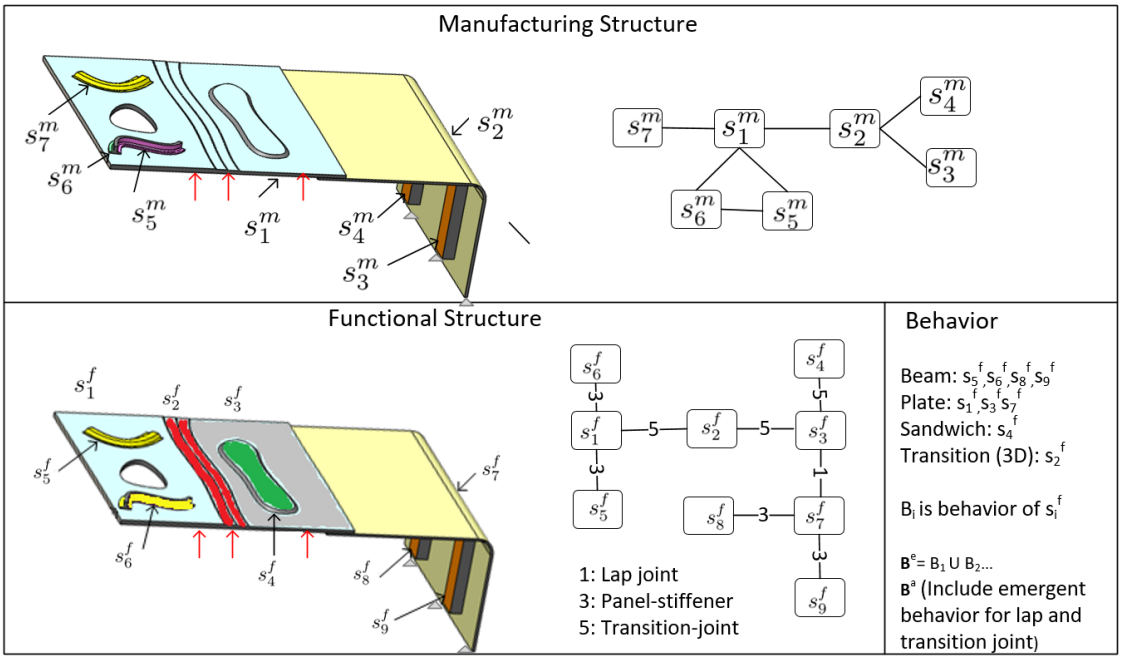

Figure 4.11: Manufacturing and functional Structure of the toy composite artifact.

them. The joint-region is obtained using the method in Appendix B.3. Once the behavior types are known for the functional structure after composition, the artifact can be analyzed using one of the simplified analysis models, which will be discussed in detail in the next section (Section 4.5).

Example II— A Complex Unitized Structure

The composite artifact shown in Figure 4.11 is a complex unitized artifact consisting of composite features such as ply drop-offs, sandwich structure, and sandwich core. The complexity was discussed in detail in the Introduction Section (Figure 1.1). The artifact was manufactured as a combination of seven laminates s_i^m (i=1 to 7) as shown in the figure. Functionally, however, the artifact consist of nine functional elements s_i^f (i=1 to 9) where s_1^f, s_3^f, and s_7^f are panels; s_5^f, s_6^f, s_8^f and s_9^f are stiffeners; s_4^f is the sandwich panel; and s_2^f is the transition element.

So the laminate solid s_1^m contains the four functional elements s_i^f (i=1 to 4), while the laminates s_5^m and s_6^m together form the functional element s_6^f. There is a 1:1 correspondence between the rest of the sub-solids: $s_7^m = s_5^f$, $s_2^m = s_7^f$, $s_4^m = s_8^f$, and $s_3^m = s_9^f$. The expected behaviors are again supplied as labels, and the details of the behaviors (the simplified models) can also be included as described in Appendix B. To obtain the actual behavior, all the emergent joint-solids are computed, which are

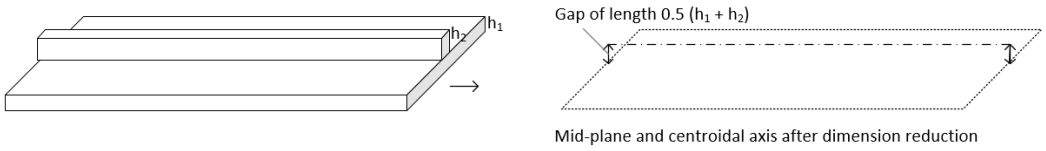

Figure 4.12: Loss of contact between the panel and stiffener elements after dimension reduction.

due to the lap-joints and the transition-joints in this example. The emergent joint-behaviors again can be obtained using the method in Appendix B.3. Finally, once the behavior types are known for the functional structure after composition, the artifact can be analyzed using one of the simplified analysis models, as discussed next.

4.5 Behavior-based Analysis of Composite Solids

Explicit representation of the correspondence between the functional and manufacturing structure of composites supports fully automated analysis of complex manufactured structures, and the accuracy and efficiency of the analysis are determined by the complexity of the functional structure. After predicting the regions of the emergent behaviors from the functional structure, efficient analysis of composite artifacts can be carried out using either (1) a mixed dimensional analysis model or (2) the virtual material method. Mixed dimensional analysis will require preprocessing for the function elements with 1D behavior to 1D physical solids and those with the 2D behavior to 2D physical solids. Additional processing may be required as dimension reduction usually breaks contacts. For example, in the panel stiffener assembly in Figure 4.12, if the stiffener is reduced to a 1D solid whose geometry is the centroidal axis and the panel is reduced to a 2D solid whose geometry is the mid-plane, there is no contact between the axis and the plane (see gap length in Figure 4.12). The 1D geometry will either have to be translated to lie on the plane or some other way to constrain the degrees of freedom of the two lower dimensional elements will have to be used. Analysis using the virtual material based analysis model does not induce any changes to the geometry, so the above issues are absent. The analysis models for the chair artifact with behavior types in Figure 4.13A obtained using Method 1 (dimension reduction) is shown in Figure 4.13B and using Method 2 (virtual material method) is shown in Figure 4.13C.

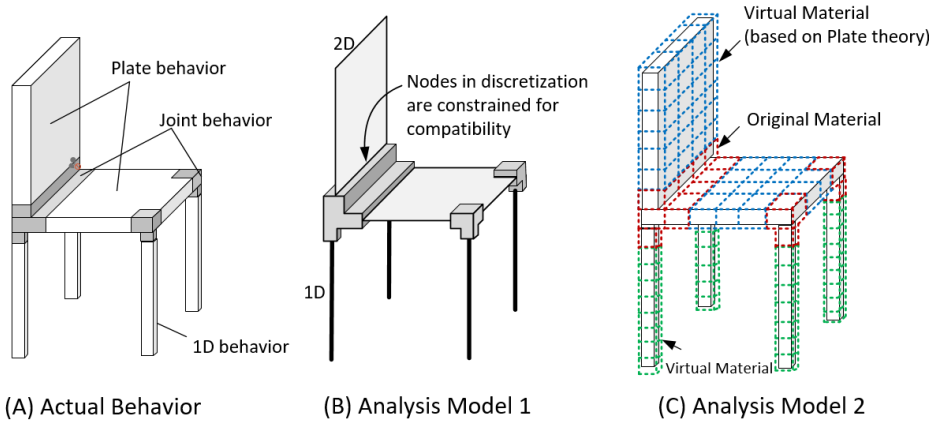

Figure 4.13: Analysis models for chair based on its predicted behavior

4.6 Design for Composite Manufacturing through Functional Equivalence

As the manufacturing technology progresses, an existing functionality can be realized using new manufacturing methods. The manufacturing method could be cheaper or may have some other advantages. For example, the functionality of the traditional plate-stiffener assembly can be realized as a 'unitized structure' using composite materials (Figure 4.14B). Such an artifact doesn't require assembling and are also stronger because of the reduced stress concentration at the joint. An another example from [5] in Figure 4.14C demonstrates that the intersection of fuel floor, skin, and bulkhead, traditionally separate parts in an airplane, can now be manufactured using composites as a unitized artifact. This synthesis method uses the notion of behavior equivalence, as shown in Figure 3.7. For an existing Function F and expected behavior B^e, the designer can synthesize a new artifact with manufacturing and functional structure S^F and S^M, respectively.

In this chapter, we saw how formal FBS framework can allow us to systematically analyze composite artifacts. I also discussed some application of the FBS framework in design of composite artifacts. The FBS framework has potential in design of not only composite artifacts, but also other artifacts that have complex manufacturing structures, including 3D printed structures. Such discussion, however, is out of the scope of the current thesis.

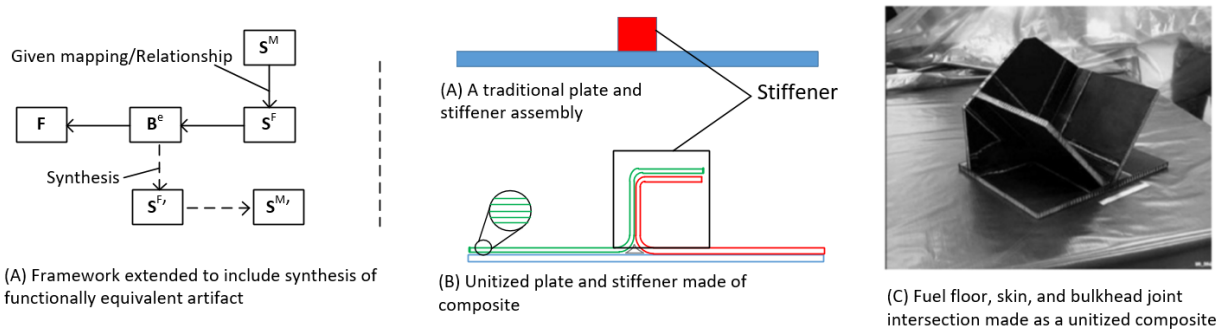

(A) Framework extended to include synthesis of functionally equivalent artifact

(B) Unitized plate and stiffener made of composite

(C) Fuel floor, skin, and bulkhead joint intersection made as a unitized composite

Figure 4.14: Synthesizing new artifacts that are functionally equivalent to an existing artifact.

Chapter 5

Virtual Material Method

In this chapter, I derive virtual materials for different behavior types using the notion of behavioral equivalence, as introduced in the previous chapter. But, first I summarize the elastic material model for orthotropic plies that will be used for obtaining the virtual materials.

5.1 Constitutive Relations for Orthotropic Plies

The general constitutive relation for an arbitrary homogeneous anisotropic material is given as

$$\sigma_i = C_{ij} \cdot \epsilon_j \qquad i, j = 1, 2, .., 6, \tag{5.1}$$

where

1. σ_i is the stress vector and ϵ_j is the strain vector. Both have the dimension 6×1.
2. $\mathbf{C} = \{C_{ij}\}$ is the 6×6 material stiffness matrix.
3. $i, j = 1, 2,$ and 3 are $x, y,$ and z coordinate axes, while $i, j = 4, 5,$ and 6 are $yz, zx,$ and xy planes respectively.

The fiber-reinforced plies and sandwich core are modeled as orthotropic materials, for which, $\mathbf{C}$ requires 9 independent elastic constants: Young's Modulus E_1, E_2, and E_3; Poisson's Ratio ν_1, ν_2, and ν_3; and Shear Modulus G_{12}, G_{23}, and G_{13}. Unlike for isotropic materials, $\mathbf{C}$ is direction dependent for orthotropic materials and needs to be transformed if the coordinate system of the

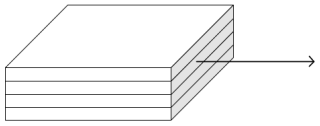

$\mathbf{C} = \{C_{ij}\}$	$\mathbf{Q} = \{Q_{ij}\}$	$\mathbf{C} = \{Q_{ij}\}$
General 3D constitutive matrix (Equation 5.1).	Plane stress constitutive matrix (Equation 5.2).	3D constitutive matrix with plane stress assumption (Equation 5.4).

Figure 5.1: Different material models for orthotropic plies.

material does not align with the xyz coordinate system. Full matrix form of Equation 5.1 and the procedure for transformation of $\mathbf{C}$ from its principal to an arbitrary coordinate system is given in Appendix C.1.1.

In laminated composite artifacts, orthotropic plies are extremely thin in one of the directions, called the thickness or out-of-plane direction, in comparison to the other two directions, called the in-plane directions. So, the stresses in the thickness direction can be assumed to be negligible (plane-stress assumption), in which case, the material stiffness $\mathbf{C}$ reduces to a 3×3 matrix $\mathbf{Q}$, given as [4]:

$$\sigma_i = Q_{ij} \cdot \epsilon_j \qquad i, j = 1, 2, 3, \tag{5.2}$$

where $i, j = 1$ and 2 stand for x and y axes respectively, while 3 stand for the xy plane. Full matrix form of the equation is in C.1.2.

In thick-walled laminated artifacts, however, out-of-plane shear strains ϵ_{yz} and ϵ_{xz} can be significant; therefore, out-of-plane shear stiffness, in addition to the in-plane stiffnesses, are needed to characterize the material. In an arbitrary coordinate system, shear stresses σ_{yz} and σ_{xz} are related to shear strains ϵ_{yz} and ϵ_{xz} as [13]:

$$\begin{bmatrix} \sigma_4 \\ \sigma_5 \end{bmatrix} = \begin{bmatrix} Q_{44} & Q_{45} \\ Q_{45} & Q_{55} \end{bmatrix} \cdot \begin{bmatrix} \epsilon_4 \\ \epsilon_5 \end{bmatrix}, \tag{5.3}$$

where indices 4 and 5 stand for planes yz and xz respectively.

Let us now assume that, in a laminate, z direction is the thickness direction for both the laminate and its plies, which is also the third principal direction of the orthotropic ply materials. Recall that the plate theories assumes that the thickness of a plate in stretching and bending remains constant, or in other words, Poisson's ratios ν_{xz} and ν_{yz} are zero [10]. These assumptions reduce the general

stress-strain relation in Equation 5.1 to

$$\begin{bmatrix} \sigma_1 \\ \sigma_2 \\ \sigma_3 \\ \sigma_4 \\ \sigma_5 \\ \sigma_6 \end{bmatrix} = \begin{bmatrix} Q_{11} & Q_{12} & Q_{13} & 0 & 0 & 0 \\ Q_{12} & Q_{22} & Q_{13} & 0 & 0 & 0 \\ Q_{13} & Q_{23} & Q_{33} & 0 & 0 & 0 \\ 0 & 0 & 0 & Q_{44} & Q_{45} & 0 \\ 0 & 0 & 0 & Q_{45} & Q_{55} & 0 \\ 0 & 0 & 0 & 0 & 0 & E_3 \end{bmatrix} \cdot \begin{bmatrix} \epsilon_1 \\ \epsilon_2 \\ \epsilon_3 \\ \epsilon_4 \\ \epsilon_5 \\ \epsilon_6 \end{bmatrix}, \tag{5.4}$$

where

$[\sigma_1, \sigma_2, \sigma_3, \sigma_4, \sigma_5, \sigma_6] = [\sigma_x, \sigma_y, \tau_{xy}, \tau_{yz}, \tau_{xz}, \sigma_z]$ and $[\epsilon_1, \epsilon_2, \epsilon_3, \epsilon_4, \epsilon_5, \epsilon_6] = [\epsilon_x, \epsilon_y, \gamma_{xy}, \gamma_{yz}, \gamma_{xz}, \epsilon_z]$. Q_{ij} for indices $i, j = 1, 2, 3$ are the in-plane normal and shear stiffness terms for the ply from plane-stress assumption, while Q_{ij} for indices $i, j = 4, 5$ are the out-of-plane shear stiffness terms. Q_{66} is the out-of-plane normal stiffness, which is the *Young's Modulus* E_3 in the z-direction. Q_{66} is ignored in 2D analysis, but we need it for the 3D formulation.

5.2 Virtual Material for Panels

5.2.1 Thin and Moderately Thick Panels

1. First-order Lamination Theory

The First-order Shear Deformation Theory (FSDT) is obtained by adding transverse shear terms to the Classical Lamination Plate Theory. CLPT, as mentioned earlier, assumes that laminated panels undergo stretching and pure bending, for which strain ϵ_i field is given as a linear combination of mid-plane strain ϵ_i^o and curvature κ_i [4]:

$$\epsilon_i = \epsilon_i^o + z \cdot \kappa_i \qquad \text{i = 1,2, and 3,} \tag{5.5}$$

where z is the distance of the point from the mid-plane.

The stress resultants for CLPT are the mid-plane forces N_i and moments M_i given as

$$N_i = \int_{-\frac{t}{2}}^{\frac{t}{2}} \sigma_i \, dz \quad \text{and} \quad M_i = \int_{-\frac{t}{2}}^{\frac{t}{2}} \sigma_i \, z dz, \tag{5.6}$$

where t is the total thickness of the panel.

Combining this equation with plane-stress constitutive relationship from Equation 5.2 and strain field from Equation 5.5 leads to the so-called *ABD matrix model*, the global constitutive relation for CLPT, for laminates:

$$\begin{bmatrix} \mathbf{N} \\ \mathbf{M} \end{bmatrix} = \begin{bmatrix} \mathbf{A} & \mathbf{B} \\ \mathbf{B} & \mathbf{D} \end{bmatrix} \cdot \begin{bmatrix} \epsilon^o \\ \kappa \end{bmatrix}. \tag{5.7}$$

The individual coefficients of $\mathbf{A}$, $\mathbf{B}$ and $\mathbf{D}$ matrices for indices $i = 1, 2,$ and 3 are given as:

$$A_{ij} = \int_{-\frac{t}{2}}^{\frac{t}{2}} Q_{ij} \, dz, \qquad B_{ij} = \int_{-\frac{t}{2}}^{\frac{t}{2}} Q_{ij} \, z dz, \qquad D_{ij} = \int_{-\frac{t}{2}}^{\frac{t}{2}} Q_{ij} \, z^2 dz. \tag{5.8}$$

where Q_{ij} is the material stiffness of the laminate. The details of the derivation can be found in Appendix C.2. Intuitively, $\mathbf{A}$ and $\mathbf{D}$ are *extensional* and *bending* components of the stiffness respectively, while $\mathbf{B}$ couples stiffness between bending and stretching that occurs in a laminate if its material properties are asymmetrical about its mid-plane. If $\mathbf{B}$ is a non-zero matrix, a normal pull in x or y direction can lead to bending and vice versa.

FSDT is obtained by introducing out-of-plane shear strains and stresses to CLPT. The stress resultants for out-of-plane shear stresses are the mid-plane shear forces Γ_4 and Γ_5 and has the same form as the mid-plane forces N_i in Equations 5.6. The global constitutive equation for FSDT has the following additional terms in comparison to that for CLPT (Equation 5.7).

$$\begin{bmatrix} \Gamma_4 \\ \Gamma_5 \end{bmatrix} = K \cdot \begin{bmatrix} A_{44} & A_{45} \\ A_{45} & A_{55} \end{bmatrix} \cdot \begin{bmatrix} \epsilon_4 \\ \epsilon_5 \end{bmatrix}. \tag{5.9}$$

Here, strains ϵ_4 and ϵ_5 are assumed constant in the z direction, and any deviation from the actual field is corrected using a *correction factor* K [13]. The *extensional* shear stiffness coefficients A_{44}, A_{45}, and A_{55} are defined as A_{ij} in Equation 5.8.

2. Virtual Material Derivation

Based on the concept of behavior equivalence introduced in Section 4.2, a new layup is behaviorally equivalent to the original layup based on the First-order Shear Deformation Theory when it satisfies the following equivalence relationship:

$$\begin{aligned} \boldsymbol{A}^o = & \int_{-\frac{t}{2}}^{\frac{t}{2}} Q^o(z) \quad dz \quad = \int_{-\frac{t}{2}}^{\frac{t}{2}} Q^*(z) \quad dz, \\ \boldsymbol{B}^o = & \int_{-\frac{t}{2}}^{\frac{t}{2}} Q^o(z) \ z dz \quad = \int_{-\frac{t}{2}}^{\frac{t}{2}} Q^*(z) z \ dz, \\ \boldsymbol{D}^o = & \int_{-\frac{t}{2}}^{\frac{t}{2}} Q^o(z) z^2 dz \quad = \int_{-\frac{t}{2}}^{\frac{t}{2}} Q^*(z) z^2 dz, \end{aligned} \tag{5.10}$$

where the original layup Q^o defines the matrices A^o, B^o and D^o, and Q^* is the virtual layup.

Since the above integral equations are a system of three equations for each entry of ABD matrices, they can be completely determined by a layup Q^* in which the material variation is fully specified by 3 or more independent coefficients. There are infinitely many such layups, and any two of them are interchangeable based on the behavior model FSDT. In other words, during structural analysis of a composite artifact using a behavior model, any arbitrarily complex layup with numerous items can be replaced by a much simpler layup, yet yielding identical results. Furthermore, since the new layup is virtual, it is not subjected to manufacturing constraints and doesn't necessarily have to be ply-based.

For demonstration, I choose two such layups: a 3-ply layup and a quadratically graded material as the virtual materials for the behavior model FSDT. In the next two paragraphs, the in-plane material properties of the two virtual layups are derived, followed by the derivation of out-of-plane material properties that are common for both the layups.

In-plane stiffness coefficients for the 3-Ply layup model: In the equivalence class of layups for a given ABD matrix, a 3-ply material model is the simplest ply-based layup. Figure 5.2A shows a 3-ply layup with Q_{ij}^{ek} as the material of the k^{th} ply, and for simplicity, each ply is assumed to be of identical thickness. With these assumptions, Equation 5.10 can be solved for material properties

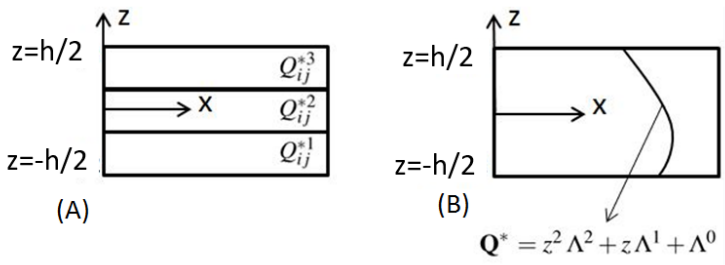

Figure 5.2: A) A 3-ply ABD-equivalent virtual layup. B) A quadratically graded ABD-equivalent virtual layup.

Q_{ij}^{ek}, and in terms of ABD matrices of the original laminate, are given as:

$$Q_{ij}^{e1} = \frac{36D_{ij}^o - 18tB_{ij}^o - t^2A_{ij}^o}{8t^3}, \quad Q_{ij}^{e2} = \frac{13t^2A_{ij}^o - 36D_{ij}^o}{4t^3}, \quad Q_{ij}^{e3} = \frac{36D_{ij}^o + 18tB_{ij}^o - t^2A_{ij}^o}{8t^3}, \tag{5.11}$$

where t is the laminate's total thickness and indices $i, j = 1, 2,$ and 3. Clearly, there always exists a unique 3-ply laminate that is ABD-equivalent to the original laminate. Note that only the top and bottom plies depend on the **B** matrix and capture any material asymmetry about the mid-plane. If the original laminate is symmetrical, the **B** matrix is zero, and the two plies Q_{ij}^{e1} and Q_{ij}^{e3} are identical.

In-plane stiffness coefficients for the quadratically graded layup model: Instead of a ply-based layup, we can also replace the original layup by a layup with a continuously varying, or graded, material. Since there are 3 equations to be satisfied, a quadratic variation with 3 independent coefficients θ_{ij}^k with $k = 1, 2, 3$ is sufficient. A layup with quadratically varying material, or quadratically graded layup, is shown in Figure 5.2B, and the material for the layup is given as:

$$Q_{ij}^* = z^2\,\theta_{ij}^2 + z\,\theta_{ij}^1 + \theta_{ij}^0. \tag{5.12}$$

θ_{ij}^k can be found from the equivalence relations in Equation 5.10, and are given as

$$\theta_{ij}^0 = \frac{15(12D_{ij}^o - tA_{ij}^o)}{t^5}, \qquad \theta_{ij}^1 = \frac{12B_{ij}^o}{t^3}, \qquad \theta_{ij}^2 = \frac{3(3tA_{ij}^o - 20D_{ij}^o)}{4t^3}. \tag{5.13}$$

Interestingly, coefficients θ_{ij}^k take different roles in the material model: together, the quadratic

coefficient θ^2_{ij} and the constant coefficient θ^0_{ij} capture the bending and in-plane stiffness, while the linear coefficient θ^1_{ij} captures the coupling stiffness of the given laminate. Again, there is a unique quadratically varying graded material for the given ABD matrices.

Out-of-plane stiffness coefficients: In addition to the in-plane, we also require out-of-plane material properties to completely characterize the ABD-equivalent models. These out-of-plane, or transverse, material properties can be derived using approaches similar to above, and are common for both the ply-based and graded virtual materials.

From Equations 5.8 and 5.9, the transverse shear properties of a laminated panel are given by the extensional stiffness matrix A_{ij} for $i, j = 4$ and 5. Since we are only interested in the equivalent material behavior, transverse shear stiffness Q^{ek}_{ij} can be assumed constant along the laminate's thickness. When substituted in Equation 5.10, Q^*_{ij} are obtained as the average values of A^o_{ij} over the laminate's thickness t:

$$Q^*_{ij} = \frac{A^o_{ij}}{t} \quad for\ i,j = 4, 5. \tag{5.14}$$

Transverse normal stiffness of laminates, which is not required for 2D FEA, is needed for 3D FEA using virtual materials. From Equation 5.4, transverse normal stiffness for plate elements reduces to Young's Modulus E_3. It is well known that for thin layered artifacts, the resultant out-of-plane Young's Modulus E^o_3 can be approximated as the harmonic average of the *Young's Modulus* E^{ok}_3 of the individual plies of the original laminate [4, 98]. Again, since I am only interested in the equivalent material behavior of the ABD-equivalent virtual materials, their *Young's Modulus* E^*_3 can be assumed constant throughout the laminate thickness. This assumption makes E^*_3 identical to E^o_3:

$$\frac{1}{E^e_3} = \frac{1}{E^o_3} = \sum_{k=1}^{k=n} \frac{h^k}{E^{ok}_3}, \tag{5.15}$$

where h^k is the thickness of the k^{th} ply and n is the total number of plies in the original laminate.

To summarize, we can efficiently construct various virtual materials that are ABD-equivalent to the original layup. Any one of these virtual materials can be used during analysis; however, some materials could be easier to implement than others in a particular system. For example, the 3-ply layup is straightforward to implement in systems which already support ply-based definition

of composite artifacts. On the other hand, the graded material model can be used to analyze laminated panels in systems that are meant for graded materials, but do not support laminates.

5.2.2 Thick Panels

The first-order deformation theory models thin and moderately thick panels accurately, but falls sort for thick panels like sandwich panels, as discussed in Section 2.2.1. In order to model thick panels, higher-order lamination theories must be used. In this section, I propose virtual material for higher-order theories to accurately analyze thick panels using the proposed virtual material based 3D FEA. There are several higher order theories as discussed in Chapter 2. I use higher-order theories based on Touratier's and Schmidt's kinematic assumption to derive the virtual material for thick panels. Touratier proposed a unified presentation for a class of lamination theories, which includes theories based on his assumption of sinusoidal variation and Schmidt's assumption of cubic variation for the out-of-plane displacement.

1. Touratier Unified Presentation for Lamination Theories

According to Touratier el al [99], the displacement fields in x, y and z directions, that is, u_1, u_1 and u_3, for different shear-deformation theories can be given using a general expression, that is,

$$\begin{aligned} u_i(x_1, x_2, x_3) &= u_i^o - z w_{,i} + f(z)\gamma_i^o(x, y) \\ &\qquad (i = 1, 2) \\ u_3(x_1, x_2, z) &= w(x_1, x_2) \end{aligned} \tag{5.16}$$

where $x_1 = x, x_2 = y$, and $x_3 = z$ axes, $w_{,i} = \frac{\partial w}{\partial x_i}$, f(z) is the *shear function*, and $\gamma_i^0 (i = 1, 2)$ are the transverse shear strains at the mid-plane of the panel. γ_i^0 can be further expanded as:

$$\gamma_i^0(x, y) = \omega_i(x, y) + w_{,i}(x, y) \tag{5.17}$$

where ω_i are the rotations of the mid-plane normal about the x_i axes. I have included the in-plane extension u_i^o of the mid-plane in the Touratier's expressions for shear-bending kinematics, as we will also be considering the coupling of in-plane extension with bending and transverse shear

deformation. Finally, different expressions for $f(z)$ result in different lamination theories as following [99].

- $f(z) = z(1 - \frac{4z^2}{3h^2})$, or Schmidt kinematic assumptions also used by Reddy for linear laminates.
- $f(z) = \frac{h}{\pi} sin \frac{\pi z}{h}$, or Touratier kinematic assumption.

In fact, $f(z) = z$ results in the first-order deformation theory, which we saw in the earlier section.

Now, for the Touratier's unified kinematic assumption in Equation 5.16, the equilibrium equations are given as [99]:

$$
\begin{aligned}
[N_i, M_i, \tilde{M}_i] &= \int_{-h/2}^{+h/2} [1, z, f(z)]\sigma_i dz \qquad (i = 1, 2, 3) \\
\tilde{\Gamma}_k &= \int_{-h/2}^{+h/2} \frac{df(z)}{dz}\sigma_k dz \qquad (k = 4, 5)
\end{aligned} \tag{5.18}
$$

where N_i are the resultant in-plane forces, M_i are classical moments, $\tilde{M}_i$ are refined moments, and $\tilde{\Gamma}_k$ are resultant transverse shear forces.

Substituting expression for σ_i from Equation 5.4, the above equilibrium equations result in the following constitutive relationship [99]:

$$
\begin{bmatrix} \mathbf{N} \\ \mathbf{M} \\ \tilde{\mathbf{M}} \end{bmatrix} = \begin{bmatrix} \mathbf{A} & \mathbf{B} & \tilde{\mathbf{A}} \\ \mathbf{B} & \mathbf{D} & \tilde{\mathbf{B}} \\ \tilde{\mathbf{A}} & \tilde{\mathbf{B}} & \tilde{\mathbf{D}} \end{bmatrix} \cdot \begin{bmatrix} \boldsymbol{\epsilon^o} \\ \boldsymbol{\kappa} \\ \tilde{\boldsymbol{\kappa}} \end{bmatrix}
$$
$$
\text{and} \qquad \tilde{\mathbf{\Gamma}} = \mathbf{A^s} \cdot \boldsymbol{\gamma^o} \tag{5.19}
$$

where, using the displacement expression in Equation 5.16, the resultant strain terms are given as

$\boldsymbol{\epsilon^o} = [u^o_{1,1}, u^o_{2,2}, u^o_{1,2} + u^o_{2,1}]^T$ are the in-plane strains,

$\boldsymbol{\kappa} = -[w_{,11}, w_{,22}, 2w_{,12}]^T$ are curvatures of the mid-plane,

$\tilde{\boldsymbol{\kappa}} = [\gamma^o_{1,1}, \gamma^o_{2,2}, \gamma^o_{1,2} + \gamma^o_{2,1}]^T$ are change in transverse shear strains γ^o_α, and

$\boldsymbol{\gamma^o} = [\gamma^o_1, \gamma^o_2]$, as given in Equation 5.17, are transverse shear strains,

while the resultant stiffness matrices are given as

$$[A_{ij}, B_{ij}, D_{ij}, \tilde{A}_{ij}, \tilde{B}_{ij}, \tilde{D}_{ij}] = \int_{-h/2}^{+h/2} Q_{ij}(z)[1, z, z^2, f(z), zf(z), (f(z))^2]dz \qquad (5.20)$$

$$(i, j = 1, 2, 3),$$

$$\text{and,} \quad \tilde{A}^s_{kl} = \int_{-h/2}^{+h/2} \left(\frac{df(z)}{dz}\right)^2 Q_{kl}(z)dz \qquad (k, l = 4, 5). \qquad (5.21)$$

Depending on the type of theory, appropriate expression of $f(z)$ can be substituted in the above equation to obtain the exact resultant stiffness matrices for a given layup Q_{ij}. Next, we will obtain virtual material for refined theories using the above expression of resultant stiffness matrices.

2. Virtual Material Derivation

In the above resultant stiffness matrix for Touratier's unified formulation, any arbitrary layup Q_{ij} is reduced to six in-plane ((Equation 5.20)) and one out-of-plane stiffness matrices (Equation 5.21). Using the notion of behavior equivalence from Section 4.2, we can obtain a virtual material model for a given layup and lamination theory as following. Let the original material model be Q^o_{ij} for which the six resultant in-plane stiffness matrices are $A^o_{ij}, B^o_{ij}, D^o_{ij}, \tilde{A}^o_{ij}, \tilde{B}^o_{ij}$, and $\tilde{D}^o_{ij}$, respectively, and the out-of-plane stiffness matrix is $\tilde{A}^{s^o}_{kl}$. The virtual material Q^*_{ij} is equivalent to the original material Q^o_{ij} when both of them result in identical resultant stiffness matrices, that is

$$[A^o_{ij}, B^o_{ij}, D^o_{ij}, \tilde{A}^o_{ij}, \tilde{B}^o_{ij}, \tilde{D}^o_{ij}] = \int_{-h/2}^{+h/2} Q^*_{ij}(z)[1, z, z^2, f(z), zf(z), (f(z))^2]dz \qquad (5.22)$$

$$(i, j = 1, 2, 3),$$

$$\text{and} \quad \tilde{A}^{s^o}_{kl} = \int_{-h/2}^{+h/2} \left(\frac{df(z)}{dz}\right)^2 Q^*_{kl}dz \qquad (k, l = 4, 5). \qquad (5.23)$$

In the next two subsections, I discuss how to obtain the in-plane and out-of-plane stiffness coefficients for the virtual material Q^*_{ij}.

In-plane Stiffness Coefficients: Unified Graded Layup Model The in-plane coefficients $Q^*_{ij}(z)(i, j = 1, 2, 3)$ of the virtual material must satisfy the six equations in Equation 5.22. There is a class of materials, in principle, that satisfies these equations, among which the simplest ones will

be a function of at least six unknown coefficients. The inverse problem of finding simplest $Q^*_{ij}(z)$'s for higher-order theories, however, is not as intuitive as it was for FSDT. For example, based on the intuition behind the 3-ply and 2^{nd}-order graded virtual material for FSDT, a 6-ply or a 5^{th}-order graded material seem a suitable choice for virtual material $Q^*_{ij}(z)$. It can be, however, easily shown that both the models do not satisfy the six equations simultaneously for all laminate configurations. Consider a symmetric layup $Q^o_{ij}(z)$, for which we essentially have 3 unknown coefficients to satisfy 4 stiffness equations ($B^o_{ij} = \tilde{A}^o_{ij} = 0$ is automatically satisfied). Depending on the configuration of the original laminate, one can carefully derive a virtual material from the class of materials that satisfy the six stiffness equations in Equation 5.22.

I propose a simple graded virtual material which is valid for any ply configuration and is given as

$$Q^*_{ij}(z) = \theta^5_{ij}\{f(z)\}^2 + \theta^4_{ij}\{zf(z)\} + \theta^3_{ij}\{f(z)\} + \theta^2_{ij}\{z^2\} + \theta^1_{ij}\{z\} + \theta^0_{ij} \tag{5.24}$$

where $\theta^0_{ij}, \theta^1_{ij}, ..., \theta^5_{ij}$ are the unknown coefficients to be found for a given set of resultant matrices. Virtual material of this form satisfies the six stiffness equations for any of the expressions for $f(z)$ in the Touratier's unified kinematic model. This makes the virtual material independent of the type (sinusoidal or polynomial) of the shear function $f(z)$ for a particular lamination theory.

I, now, show that $Q^*_{ij}(z)$ satisfies the six stiffness equations for arbitrary laminate configuration when $f(z)$ is Schmidt's or Touratier's kinematic assumption. First, substitute the expression for Q^*_{ij} (Equation 5.24) into the equivalence expression (Equation 5.22) to obtain a system of six linear equations. Let the matrix form of the linear system be

$$\boldsymbol{\alpha} \cdot \boldsymbol{\theta}_{ij} = \boldsymbol{B}_{ij} \tag{5.25}$$

where $\boldsymbol{\alpha}$ is a 6×6 matrix, $\boldsymbol{\theta}_{ij} = [\theta^0_{ij}, \theta^1_{ij}, \theta^2_{ij}, \theta^3_{ij}, \theta^4_{ij}, \theta^5_{ij}]^T$, and $\boldsymbol{B}_{ij} = [A^o_{ij}, B^o_{ij}, D^o_{ij}, \tilde{A}^o_{ij}, \tilde{B}^o_{ij}, \tilde{D}^o_{ij}]^T$.

Using the fact that (1) the shear functions $f(z)$ are odd functions[1] (2) product of an even and an odd function is an odd function, and (3) integration of an odd function from some limit $(-t)$ to (t) is zero, $\boldsymbol{\alpha}$ in the above linear system simplifies to the following matrix.

[1] Except when $f(z) = 0$, for which the following statements are automatically true.

$$\begin{bmatrix} \alpha_0 & 0 & \alpha_1 & 0 & \alpha_2 & \alpha_3 \\ & \alpha_1 & 0 & \alpha_2 & 0 & 0 \\ & & \alpha_4 & 0 & \alpha_5 & \alpha_6 \\ & & & \alpha_3 & 0 & 0 \\ & sym. & & & \alpha_6 & \alpha_7 \\ & & & & & \alpha_8 \end{bmatrix}$$

where, $[\alpha_0, \alpha_1, \alpha_2, \alpha_3] = \int_{-t}^{t}[1, z^2, zf, f^2]dz;$

$[\alpha_4, \alpha_5, \alpha_6] = \int_{-t}^{t}[z^4, z^3 f, z^2 f^2]dz$

$[\alpha_7, \alpha_8] = \int_{-t}^{t}[zf^3, f^4]dz.$

(assuming $t = \frac{h}{2}$)

So, $\boldsymbol{\alpha}$ matrix is a function of the shear function $f(z)$ and automatically adapts based on the lamination theory being considered. Moreover, after substituting the expression for $f(z)$ for Schmidt's and Touratier's kinematic assumptions, it can be shown that the determinant of $\boldsymbol{\alpha}$ is non-zero: approximately $3.376 \times 10^{-18} h^{22}$ when $f(z) = z(1 - \frac{4z^2}{3h^2})$ and $5.423 \times 10^{-18} h^{22}$ when $f(z) = \frac{h}{\pi} sin\frac{\pi z}{h}$, respectively. A solution to the above linear system, therefore, exists for any arbitrary laminate Q_{ij}^{o} and thickness h, and the values of the unknown coefficients $\boldsymbol{\theta}_{ij}$ in the virtual material Q_{ij}^{*} are given as

$$\boldsymbol{\theta}_{ij} = \boldsymbol{\alpha}^{-1} \cdot \boldsymbol{B}_{ij}. \tag{5.26}$$

By substituting $\boldsymbol{\theta}_{ij}$ from above to Equation 5.24, we obtain the in-plane coefficients of the virtual material Q_{ij}^{*}. Next, I discuss how to obtain the out-of-plane stiffness coefficients of the virtual material.

Out-of-plane Stiffness coefficients The out-of-plane shear stiffness coefficients $Q_{ij}^{*}(i, j = 4, 5)$ of the virtual materials have to satisfy only one equation, that is, Equation 5.23. So, for the simplest virtual material, transverse shear stiffness $Q_{ij}^{*}(i, j = 4, 5)$ can be chosen to be

$$Q_{ij}^{*} = \frac{\tilde{A}_{ij}^{s^o}}{\alpha}, \text{ where } \quad \alpha = \int_{-h/2}^{+h/2} \left(\frac{df(z)}{dz}\right)^2 dz \text{ and } (i, j = 4, 5) \tag{5.27}$$

This is true for any of the expressions for $f(z)$ presented above. However, Reddy et al [100] in their work formulated transverse shear stiffness as a combination of three stiffness terms (Λ^k, k=1,2,3), each associated to different orders of z, as shown below.

$$\text{for } f(z) = z(1 - \tfrac{4z^2}{3h^2}),$$
$$\tilde{A}^{s^o}_{ij} = \int_{-h/2}^{+h/2} (1 - \tfrac{8z^2}{h^2} + \tfrac{16z^4}{h^4}) Q^o_{ij} dz = \Lambda^0_{ij} + \Lambda^1_{ij} + \Lambda^2_{ij},$$
$$\text{where} \quad [\Lambda^0_{ij}, \Lambda^1_{ij}, \Lambda^2_{ij}] = \int_{-h/2}^{+h/2} [1, (-\tfrac{8z^2}{h^2}), (\tfrac{16z^4}{h^4})] Q^o_{ij} dz$$

Since I will be using results from Reddy [100] for comparison, I ensure that the virtual material Q^*_{ij} has not only the total shear stiffness $\tilde{A}^{s^o}_{kl}$, but also components Λ's, identical to the original material Q^o_{ij}. This can be achieved using the following form for the transverse shear coefficients of the virtual material Q^*_{ij}:

$$Q^*_{ij} = \phi^2_{ij}(zf(z)) + \phi^1_{ij}(z^2) + \phi^0_{ij} \qquad (i, j = 4, 5) \tag{5.28}$$

where $\phi^0_{ij}, \phi^1_{ij}, \phi^2_{ij}$ are the unknown coefficients. Following steps similar to steps in the previous sub-section, the unknown coefficients can be obtained as a solution to the following linear system.

$$\begin{bmatrix} \beta_0 & \beta_1 & \beta_2 \\ & \beta_3 & \beta_4 \\ sym. & & \beta_5 \end{bmatrix} \cdot \begin{bmatrix} \phi^0_{ij} \\ \phi^1_{ij} \\ \phi^2_{ij} \end{bmatrix} = \begin{bmatrix} \Lambda^0_{ij} \\ \Lambda^1_{ij} \\ \Lambda^2_{ij} \end{bmatrix} \text{ or, } \qquad \boldsymbol{\beta} \cdot \boldsymbol{\phi}_{ij} = \boldsymbol{\Lambda}_{ij}, \tag{5.29}$$
$$\text{where, assuming } t = \tfrac{h}{2}, \quad [\beta_0, \beta_1, \beta_2, \beta_3, \beta_4, \beta_5] = \int_{-t}^{t} [1, z^2, zf, z^4, z^3 f, z^2 f^2] dz;$$

The determinant of the $\boldsymbol{\beta}$ matrix is non-zero ($2.24 \times 10^7 h^{11}$) and, therefore, a solution to the above linear system exists for arbitrary laminate configuration and thickness. The unknown coefficients $\boldsymbol{\phi}_{ij}$ are given as

$$\boldsymbol{\phi}_{ij} = \boldsymbol{\beta}^{-1} \cdot \boldsymbol{\Lambda}_{ij}, \tag{5.30}$$

and, by substituting ϕ_{ij} in Equation 5.28, we obtain the transverse shear stiffness of the virtual material Q^*_{ij}.

Finally, as pointed out earlier, transverse normal stiffness Q^*_{66} is needed for virtual material models that can be obtained using Equation 5.15, since the assumptions made earlier are applicable now as well. In summary, the proposed virtual material Q^*_{ij} for higher-order lamination theories is a graded material whose in-plane stiffness coefficients are given by Equation 5.24, transverse shear stiffness coefficients by Equation 5.27 or 5.28, and transverse normal coefficients by 5.15. Other ply-based or graded virtual materials are also possible, but the proposed graded virtual material is special, as the variables (terms that are function of z) in the above expressions for the virtual material (Equation 5.24, 5.27, and 5.28) correspond to the coefficients of original laminate Q^o_{ij} in the expressions for resultant stiffness matrices.

5.2.3 Implementation and Numerical results

Virtual materials are implemented by (1) replacing the original laminate by a virtual material obtained using the suitable lamination theory and (2) using new virtual material for stiffness matrix formulation during 3D FEA. For demonstration, I implement virtual materials in a meshfree system called Scan and Solve(SnS) [101], the details of which are presented in the next chapter. Some important points relevant to the discussion in this chapter are:

1. I use second order multi-variate B-spline basis function , and, due to the fact that B-spline basis is hierarchical in nature, potential problems of locking and ill-conditioning of stiffness matrix when using 3D elements for thin-walled structures are eliminated [102, 103].

2. Volume integration during stiffness matrix computation is approximated by integration over surfaces. Each laminate is replaced by a set of integration surfaces parallel to the base surface of a laminate (Figure 6.5), where locations and thicknesses (weights) of the integration surfaces are obtained using Lobatto quadrature rules [104].

3. The material stiffness coefficients for each integration surface is assigned based on the distance of the surface from the mid-plane of the laminate, that is, the z value in Equations 5.24, 5.27, and 5.28.

Graded virtual materials are also more efficient compared to ply-based virtual materials. In fact, using graded material can be almost twice as efficient as using ply-based virtual material: for a symmetric laminate, virtual material for Schmidt/Reddy theory is a sixth-order graded material using the proposed scheme and will be at least a 7-ply laminate if using a ply-based virtual material. So, the total number of integration surfaces required based on Lobatto quadrature rule[2] will be 21 for the 7-ply virtual material (3 surfaces for each ply) and 13 for the graded virtual material.

Next, I compare results of linear static analysis of laminate panels using my proposed method to results from the literature, as well as commercial software ANSYS [105] and SolidWorks [106] for few cases. I use the virtual material models based on (1) first-order deformation theory (2) Schmidt's higher-order theory and (3) Touratier's higher-order theory. For brevity, we will refer to the virtual material obtained form them as FSDT-virtual, HEX-virtual, and SINE-virtual materials, respectively. For comparison, I consider five different benchmark problems. The problems with their objectives are listed as following.

- Demonstrate that both ply-based and graded material can be used as a virtual material through *Problem* 1— a clamped rectangular plate under out-of-plane distributed loading.
- Demonstrate that virtual material method can model stretching-bending coupling in plates through *Problem* 2— a clamped rectangular plate with in-plane loading. Also, I discuss the degree of increase in efficiency for 3D FEA when using virtual materials.
- Compare accuracy of all three types of virtual materials for plates of different aspect ratio through *Problem* 3— a simply supported, symmetric rectangular plate under a doubly sinusoidal transverse load.
- Show that virtual material can be used for panels made of large number of plies through *Problem* 4— a simply supported, multi-layered laminated square plate under a doubly sinusoidal transverse load.
- Show that virtual material method gives accurate results for laminated curved panels, or shells, through *Problem* 5— a singly-curved cylindrical shell under its own weight and *Problem* 6 — a simply supported, doubly-curved spherical shell under a uniformly distributed transverse load.

[2] N integration points accurately integrate polynomials of order up to $2N-1$.

Benchmark problems 3–6 have been used in the literature [13, 107–110] to establish accuracy of different lamination theories. For all the problems, plies in each laminate are assumed to be of the identical thickness and made of the same material. I only consider one material for orthotropic plies whose engineering constants are as following.

$$\begin{aligned} &E_1 = 25 \times 10^6 \text{ psi}, E_2 = E_3 = 25 \times 10^6 \text{ psi}, \\ &\nu_{12} = 0.25, \nu_{23} = \nu_{13} = 0.0, \\ &G_{12} = G_{13} = 0.5 \times 10^6 \text{ psi}, G_{23} = 0.2 \times 10^6 \text{ psi}, \end{aligned} \tag{5.31}$$

where E, ν, G are the Young's modulus, Poisson's ratio and Shear modulus respectively, and indices 1, 2 and 3 indicate the three principal material directions. This material is identical to the material used in literature except that I set ν_{23} and ν_{13} to zero, as explained in Equation 5.4. The elements used in different FEA systems are as following.

- ANSYS: I use Shell181 elements for 2D analysis, which are four node elements with six degrees of freedom at each node— 3 translation and 3 rotation degrees of freedom.
- SolidWorks: I use two-dimensional parabolic triangular shell elements.
- SnS: Scan and Solve uses second-order tri-variate B-spline functions on a uniform Cartesian non-conforming grid for analysis. The Lobatto quadrature rule implies that 5 integration surfaces for the FSDT equivalent model, and 6 integration surfaces for the HEX and SINE equivalent models are sufficient for full integration.

Problem 1: Clamped Rectangular Plate with Out-of-plane Loading

Our first benchmark problem is a plate clamped on all four sides and a normal pressure on the top surface (Figure 5.4A). A plate under these boundary conditions shows pure bending, with maximum displacement at the center of the plate. The plate consists of 10 plies in cross-ply and angle-ply configurations. Table 5.1 compares the maximum displacements using ANSYS, SolidWorks (SW), and proposed method (SnS) for different laminates. Tests were done for three different aspect ratios: thin (a/h = 1000), moderately thick (a/h = 100), and thick (a/h = 10).

For both cross-ply and angle-ply laminates with moderate thickness, SnS accurately predicts the

Table 5.1: Maximum displacement value in inches for plate problem in Figure 5.4A for different cases.

Laminate	Thickness	a/h	ANSYS	SW	SnS– 3-Ply		SnS– Graded	
(Number of elements)			10k	1k	1k	3k	1k	3k
$[0/90]_5$	1	10	$4.748e^{-3}$	$4.058e^{-3}$	$3.855e^{-3}$	$3.762e^{-3}$	$4.567e^{-3}$	$3.755e^{-3}$
	0.1	100	$1.543e^{+0}$	$1.550e^{+0}$	$1.532e^{+0}$	$1.543e^{+0}$	$1.532e^{+0}$	$1.543e^{+0}$
	0.01	1000	$1.510e^{+3}$	$1.552e^{+3}$	$1.145e^{+3}$	$1.661e^{+3}$	$1.145e^{+3}$	$1.662e^{+3}$
$[-45/45]_5$	1	10	$5.094e^{-3}$	$4.360e^{-3}$	$4.057e^{-3}$	$4.152e^{-3}$	$4.880e^{-3}$	$4.050e^{-3}$
	0.1	100	$1.629e^{+0}$	$1.620e^{+0}$	$1.597e^{+0}$	$1.611e^{+0}$	$1.598e^{+0}$	$1.611e^{+0}$
	0.01	1000	$1.581e^{+3}$	$1.578e^{+3}$	$1.163e^{+3}$	$1.684e^{+3}$	$1.163e^{+3}$	$1.685e^{+3}$

Table 5.2: Von Mises stress at the mid-point (x=0, y=0) of the top face of the plate in Figure 5.4A

Laminate	Thickness	a/h	ANSYS	SW	SnS– 3-Ply		SnS– Graded	
(Number of elements)			10k	1k	1k	3k	1k	3k
$[0/90]_5$	1	10	$2.42e^{3}$	$2.43e^{3}$	$2.50e^{3}$	$2.40e^{3}$	$3.20e^{3}$	$2.35e^{3}$
	0.1	100	$2.54e^{5}$	$2.55e^{5}$	$2.04e^{5}$	$2.06e^{5}$	$2.05e^{5}$	$2.06e^{5}$
	0.01	1000	$2.50e^{7}$	$2.60e^{7}$	$1.60e^{7}$	$1.94e^{7}$	$1.60e^{7}$	$1.93e^{7}$
$[-45/45]_5$	1	10	$2.70e^{3}$	$2.66e^{3}$	$2.67e^{3}$	$2.60e^{3}$	$3.20e^{3}$	$2.60e^{3}$
	0.1	100	$2.25e^{5}$	$2.26e^{5}$	$1.80e^{5}$	$1.82e^{5}$	$1.80e^{5}$	$1.82e^{5}$
	0.01	1000	$2.25e^{7}$	$2.22e^{7}$	$1.52e^{7}$	$1.70e^{7}$	$1.52e^{7}$	$1.69e^{7}$

maximum displacement values, and the results from all the systems are in close agreement. There are more noticeable differences in the displacements computed by the three systems for thin and thick laminates, e.g., SnS and SW tend to differ by 5%. Importantly, SnS is not under-predicting displacements for thin plates, suggesting that locking is is not an issue.

I also compare, in Table 5.2, the Von Mises stresses at the mid-point $(x = 0, y = 0)$ of the top face for different plates. For both cross-ply and angle-ply laminates, stresses from different methods are in agreement for the thick plate with aspect ratio 10, but there is some deviation for other aspect ratios, which increases with plate aspect ratio. A comparison of the entire stress field for the moderate thickness plate (aspect ratio 100) is shown in Figure 5.3 for cross-ply and angle ply laminates. The stress patterns match for the two laminates, and the highest stress due to stress concentration are also within 15% of each other. Solid elements generally better capture the stresses

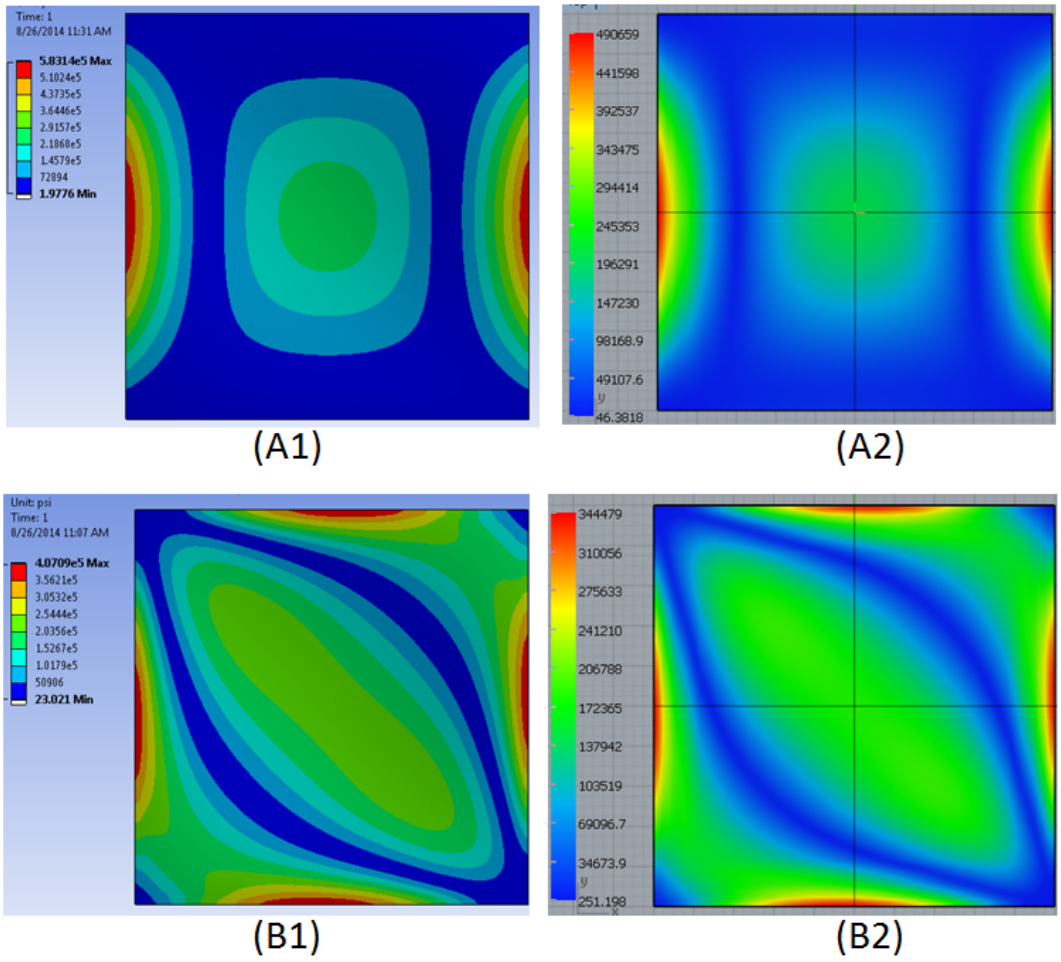

Figure 5.3: Comparison of Von Mises stress for top face of the plate in Figure 5.4 with aspect ratio 100 for A1) $[0, 90]_5$ analyzed in ANSYS (Max stress- $5.83e^5$) 2.$[0, 90]_5$ analyzed using the proposed method (Max stress- $4.91e^5$). B) $[-45, 45]_5$ analyzed in ANSYS (Max stress- $4.08e^5$) 2. $[-45, 45]_5$ analyzed using the proposed method (Max stress- $3.44e^5$.)

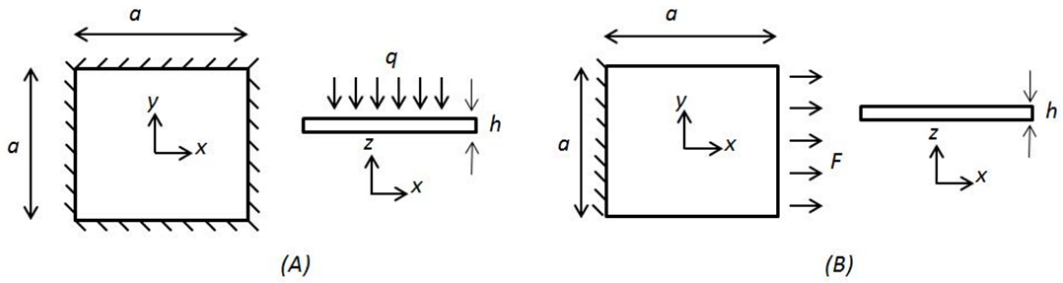

Figure 5.4: A) Plate with geometry parameters $a = 10in$ and $h = 1, 0.1, 0.01in$, clamped from all four sides with a surface pressure, $q = 100psi$. B) Plate with $a = 10in$ and $h = 0.1in$, fixed on one end with a force, $F = 1.0e^4 lbf$ on the opposite end.

near edges as they explicitly model the finite thickness of plates.

Problem 2: Clamped Rectangular Plate with In-plane Loading

Next, I test the same rectangular plate, but with different boundary conditions: plate is under in-plane load of $1.0e^4$ lbf on one end and clamped at the opposite end (Figure 5.4B). The plate is made of 50 random plies whose angles are given as:

$$\begin{aligned} &-45, 45, 0, -45, 90, 45, -50, -75, 60, -45, 90, -45, -45, 45, -45, -75, -5, \\ &80, 30, -45, -45, 60, 90, -75, -45, 25, -45, -45, 45, -75, 60, 60, -45, 90, \\ &-45, -45, -75, -50, 45, -45, 60, -45, 50, -75, -45, -75, 10, -45, 60, \text{ and } 90. \end{aligned} \tag{5.32}$$

This particular problem was chosen to validate the claim that virtual material method successfully captures coupling behavior in asymmetrical laminates. Due to stretching-bending coupling in asymmetrical laminates, the in-plane load F results into bending and produces out-of-plane deformation. The proposed method did capture this coupling phenomena accurately as shown in Figure 5.5, which compares the z displacement fields from SnS and and ANSYS. The maximum z displacement are in agreement with $0.3730in$ in ANSYS and $0.3734in$ in SnS.

I also carried out a time analysis in order to estimate the net efficiency achieved using proposed method when using 3D FEA. Complete analysis of the 50-ply laminate plate using the ABD-equivalent 3-ply model took 14.9 seconds, out of which 12.8 seconds were spent integrating 9 integration surfaces (3 surfaces per ply). Therefore, an average of 1.42 seconds were spent

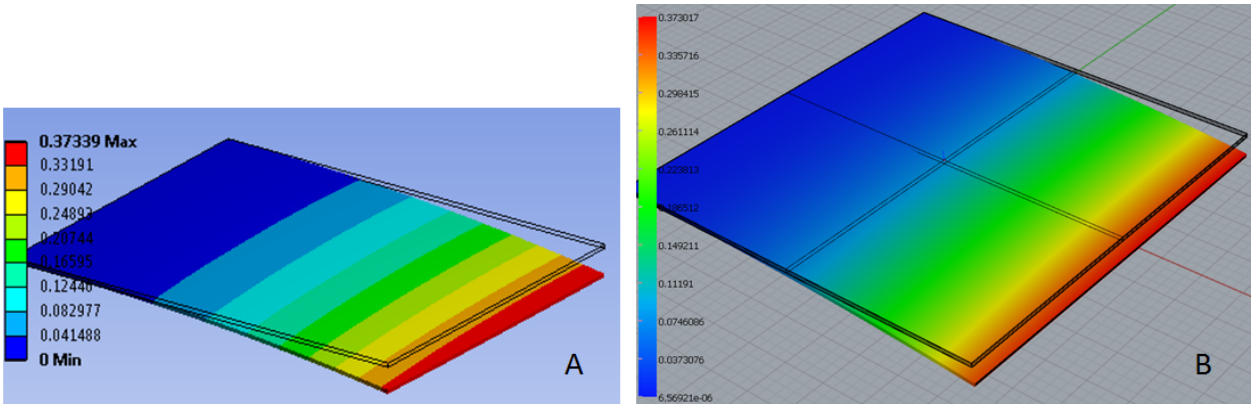

Figure 5.5: The deformed plate and color map of out-of-plane displacement obtained using A) ANSYS B) Scan&Solve with ABD-equivalent 3-ply material model, for a laminate plate made of 50 plies. As expected, the in-plane load leads to out-of-plane bending.

integrating each surface. This implies that integrating over 150 surfaces in the original 50-ply model would require roughly 215 seconds for the same analysis. The gain in efficiency is even higher when using graded material model, as it needs only 4 integration surfaces in comparison to 9 for the 3-ply laminate. The total time taken for analysis was only 6.8 seconds, decreasing the total computation cost of analysis by more than 30 times. Similar speedup should be expected in any 3D FEA of laminated structures relying on layered elements.

Problem 3: Symmetric Rectangular plate

Current benchmark problem is a simply supported [0/90/0] rectangular plate used by Pagano [107]. I choose this problem to test if the proposed method yields accurate bending in plates of different aspect ratios. The plate geometry and boundary conditions are illustrated in Figure 5.6. A doubly sinusoidal transverse load q is applied on the top face of the plate as shown in the figure.

For this benchmark problem, the normalized center plane deflections from different methods and for different aspect ratios are plotted in Figure 5.7a. The aspect ratios for which the computed results are a/h = 4, 10, 20, 50, and 100. The plot confirms that the FSDT-virtual material is accurate for higher aspect ratios but underestimates deflection at lower aspect ratios. SINE-virtual and HEX-virtual materials, however, yield results consistent with the elasticity solution for all the aspect ratios. The maximum deviation when using HEX-virtual and SINE-virtual materials is for

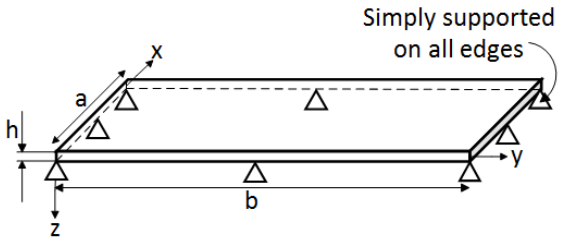

Load on the top face

$$q = q_0 sin(\frac{\pi x}{a}) sin(\frac{\pi y}{b})$$

$$\text{At } x = 0, a: \quad \sigma_1 = u_2 = u_3 = 0$$
$$\text{At } y = 0, b: \quad \sigma_2 = u_1 = u_3 = 0$$

Figure 5.6: Rectangular plate with geometry parameters $b = 3a$ and height h, simply supported on all four edges and subjected to a doubly sinusoidal load on the top surface.

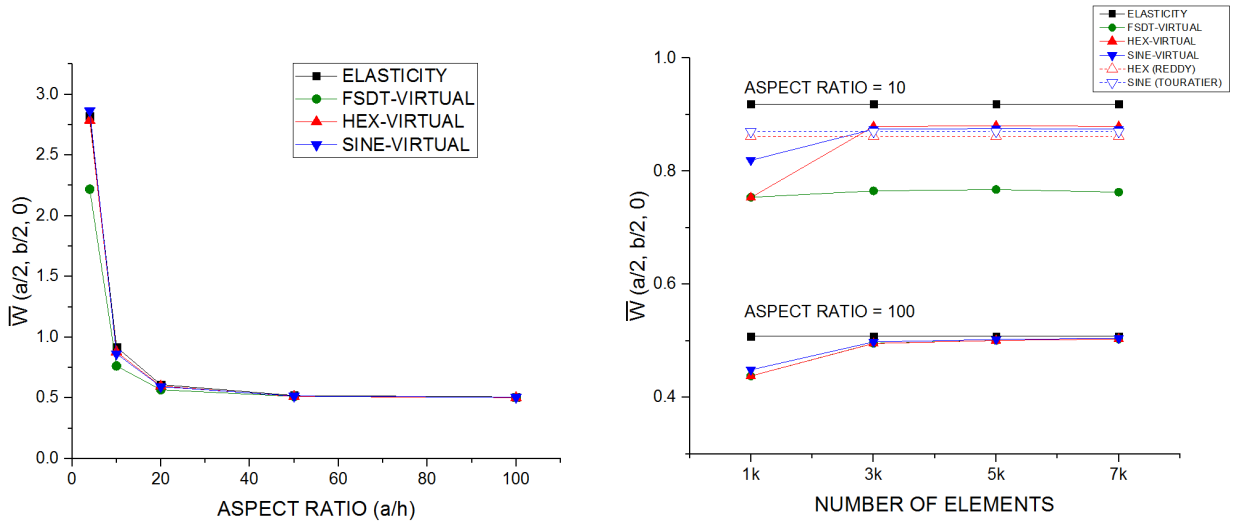

(a) $\overline{W}$ as a function of aspect ratio.

(b) Plot of Normalized central plane deflection, $\overline{W} = W(\frac{a}{2}, \frac{b}{2}, 0)\frac{100E_2h^3}{q_0a^4}$

Figure 5.7: $\overline{W}$ as a function of number of elements for $\frac{a}{h} = 10$ and 100.

the lowest aspect ratio ($a/h = 4$), which is 1.2% and 1.6%, respectively.

Results from my method converge rapidly when the number of finite elements is increased, as shown by the plot in Figure 5.7b. The plot illustrates the variation of normalized central plane deflection for aspect ratios 10 and 100. For comparison, results from 3D elasticity solutions, as well as solutions using higher-order theories by Reddy [100] and Touratier [99] (available for a/h=10), are also included in the plot. For both aspect ratios, all solutions stabilize after 3000 elements. Furthermore, converged solutions from HEX-virtual and SINE-virtual materials are in closer agreement to the elasticity solution than the higher-order solutions by Reddy and Touratier. Error in results is higher for a/h=10 in comparison to a/h=100, but it is within 5% of the displacements

Table 5.3: Comparison of normalized stress values. For each a/h, first row has the reference stress values from [Touratier and Pagano] while the second row has values computed using the SINE-virtual material.

a/h	$\bar{\sigma_1}$	$\bar{\sigma_3}$	$\bar{\sigma_4}$	$\bar{\sigma_5}$
4	$1.10e^{+0}$	$-2.81e^{-2}$	$3.30e^{-2}$	$3.87e^{-1}$
	$9.65e^{-1}$	$-2.75e^{-2}$	$3.25e^{-2}$	$3.53e^{-1}$
20	$6.50e^{-1}$	$-9.30e^{-3}$	$1.20e^{-2}$	$4.34e^{-1}$
	$6.42e^{-1}$	$-9.30e^{-3}$	$1.12e^{-2}$	$5.21e^{-1}$
100	$6.24e^{-1}$	$-8.30e^{-3}$	$1.08e^{-2}$	$4.39e^{-1}$
	$6.23e^{-1}$	$-8.35e^{-3}$	$1.52e^{-2}$	$4.43e^{-1}$

using general elasticity.

I also compare the maximum stress values from Pagano [107] for three different aspect ratios, as shown in Table 5.3. Stress values are normalized as following.

$$\bar{\sigma}_i = \sigma_i h^2/(q_o a^2) \quad (i = 1, 3), \text{ and } \bar{\sigma}_i = \sigma_i h/(q_o a) \quad (i = 4, 5) \tag{5.33}$$

I do not compare the maximum normal stress in the y-direction, that is σ_2, since maximum σ_2 occurs at the interface of 0 and 90 plies [107] and I not modeling interfacial stresses in the current work. I only use SINE-virtual material (values are in the second row for each aspect ratio) for comparison and the stress values are consistent with the stress values from exact elasticity solutions.

Problem 4: Multi-layered square plate

Next, to demonstrate the accuracy of the method for different types of laminates with a large number of plies, I consider a square plate made of the following laminate configurations:

Case 1 4-ply $[(0, 90)_2]$ asymmetric laminate,

Case 2 8-ply $[(0, 90)_4]$ asymmetric laminate,

Case 3 5-ply $[0, 90, \bar{0}]_S$ symmetric laminate,

Case 4 9-ply $[(0, 90)_2, \bar{0}]_S$ symmetric laminate,

Case 5 50-ply asymmetric laminate (Ply orientation in Figure 5.32).

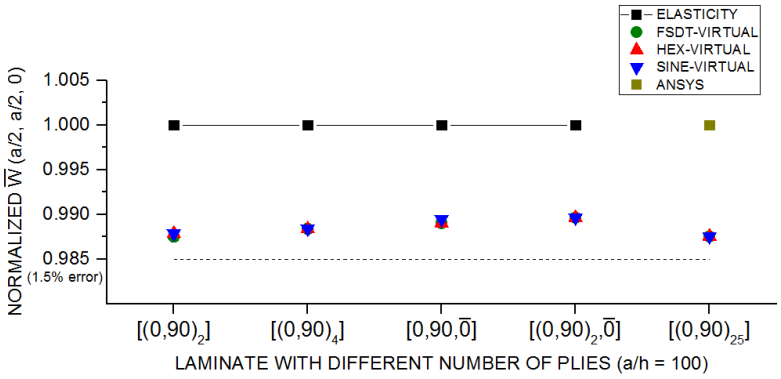

Figure 5.8: Normalized central plane deflection for different laminate configurations when a/h = 100

The plate is simply supported with a doubly sinusoidal load as the previous rectangular plate (Figure 5.6 with $a = b$) with an aspect ratio of 100. I compare the normalized center deflection for the different cases in Figure 5.8. The exact elasticity solutions for Cases 1 and 2 are provided by Zenkour [109], while Pagano [108] provides exact solutions for Cases 3 and 4. There are no exact solutions present in literature for extremely large number of plies, so I use results from ANSYS as the benchmark for comparison in Case 5. The results are normalized by the benchmark solutions. Clearly, both higher-order equivalent material models accurately predict displacements for all cases. For the 9-layer symmetric laminate, deflections using HEX and SINE models differ from the elasticity solution by only 1%. For the 50-ply laminate, results from my method has 1.25% error in comparison to the ANSYS solution.

Problem 5: Singly-curved shell

We now move to laminated shells and show that the proposed method can also be extended to shells of different aspect ratios and curvatures. First, consider a laminated singly-curved cylindrical shell fixed at its curved ends, also known as the Barrel Vault problem. The detailed loading and boundary conditions are shown in Figure 5.9A.

The maximum vertical displacements of the shell computed using different methods are given in Table 5.4. The superscript 'v' denotes virtual material. The comparison is done for various cross-ply and angle-ply laminates and the 50-ply laminate with three different aspect ratios— 20, 50, and 100. Reddy [13] uses Q81 elements, which are eighth order elements (p-level = 8). There is some

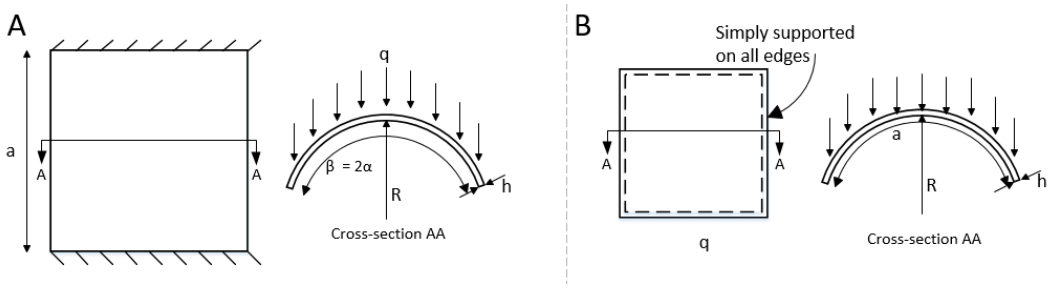

Figure 5.9: (A) Barrel vault with vertical pressure $q = 0.625$psi. The curved ends are fixed and $\beta = 80°$, $R = 300$ in, $a = 600$ in, $h = 3, 6, 15$ in (B) Top and side views of the doubly-curved spherical shell. The inner radius is R, thickness is h, arc length is a, and $q = 1$psi.

Table 5.4: Maximum vertical deflection (inches) of Barrel vault for different cross-ply and angle-ply laminates.

Laminate	R/h	Reddy [13]	ANSYS	SolidWorks	FSDT^{v}	HEX^{v}	SINE^{v}
[0, 90]	100	$2.339e^{+0}$	$2.407e^{+0}$	$2.460e^{+0}$	$2.416e^{+0}$	$2.402e^{+0}$	$2.402e^{+0}$
	50	$5.082e^{-1}$	$5.291e^{-1}$	$5.659e^{-1}$	$5.503e^{-1}$	$5.765e^{-1}$	$5.765e^{-1}$
	20	$7.292e^{-2}$	$7.449e^{-2}$	$7.560e^{-2}$	$7.016e^{-2}$	$7.998e^{-2}$	$8.262e^{-2}$
[-45, 45]	100	$3.597e^{+0}$	$3.871e^{+0}$	$3.866e^{+0}$	$3.699e^{+0}$	$3.636e^{+0}$	$3.637e^{+0}$
	50	$6.760e^{-1}$	$7.652e^{-1}$	$7.170e^{-1}$	$7.780e^{-1}$	$7.083e^{-1}$	$7.080e^{-1}$
	20	$1.205e^{-1}$	$1.397e^{-1}$	$1.130e^{-1}$	$1.386e^{-1}$	$1.094e^{-1}$	$1.095e^{-1}$
$[(0,90)_5]$	100	$1.415e^{+0}$	$1.434e^{+0}$	$1.564e^{+0}$	$1.593e^{+0}$	$1.523e^{+0}$	$1.523e^{+0}$
	50	$2.940e^{-1}$	$2.979e^{-1}$	$3.270e^{-1}$	$3.412e^{-1}$	$3.424e^{-1}$	$3.423e^{-1}$
	20	$5.234e^{-2}$	$5.246e^{-2}$	$5.370e^{-2}$	$5.399e^{-2}$	$5.407e^{-2}$	$5.406e^{-2}$
$[(-45, 45)_5]$	100	$1.818e^{+0}$	$1.836e^{+0}$	$1.955e^{+0}$	$1.912e^{+0}$	$1.867e^{+0}$	$1.867e^{+0}$
	50	$4.096e^{-1}$	$4.082e^{-1}$	$4.089e^{-1}$	$3.940e^{-1}$	$3.951e^{-1}$	$3.951e^{-1}$
	20	$1.004e^{-1}$	$9.727e^{-2}$	$8.959e^{-2}$	$8.088e^{-2}$	$8.122e^{-2}$	$8.120e^{-2}$
50-ply	100		$1.411e^{+0}$	$1.478e^{+0}$	$1.445e^{+0}$	$1.432e^{+0}$	$1.430e^{+0}$

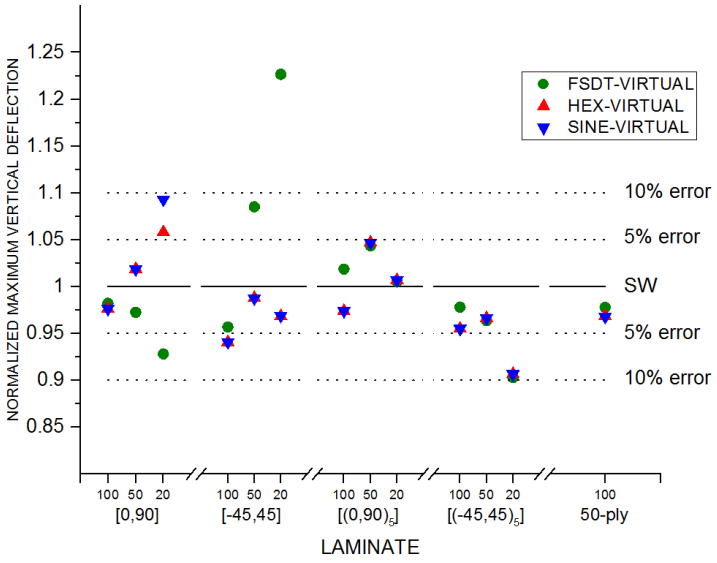

Figure 5.10: Normalized maximum vertical deflection for various cross-ply and angle-ply laminates

variability in reference results from Reddy, ANSYS, and SolidWorks, and my results compare best against the results from SolidWorks. To illustrate this, I plot the displacements from my methods normalized by displacements from SolidWorks(SW) in Figure 5.10. There is a close agreement between results from both higher-order virtual materials with the results from SolidWorks(SW). Errors in deflection are within 5% for all but three cases, and the error is highest for thick laminates (aspect ratio 20). For the random 50-ply laminate, HEX-virtual and SINE-virtual materials show a 3.1% and 3.2% difference from the SolidWorks results, respectively.

Problem 6: Doubly-curved shell

Next, I consider a doubly-curved spherical shell that is simply supported and under a uniform load. The dimensions and boundary conditions of the shell are shown in Figure 5.9B. Let us consider two laminates:

Case 1 asymmetric $[0, 90]$ laminate

Case 2 symmetric $[0, 90, 0]$ laminate,

each with aspect ratios 10 and 100. I will be using results provided by Reddy [110] as the benchmark.

Variation of normalized center deflection with five values of R/h is plotted for Cases 1 and 2 in Figures 5.11a and 5.11b, respectively. Both figures also show variation for the two aspect ratios.

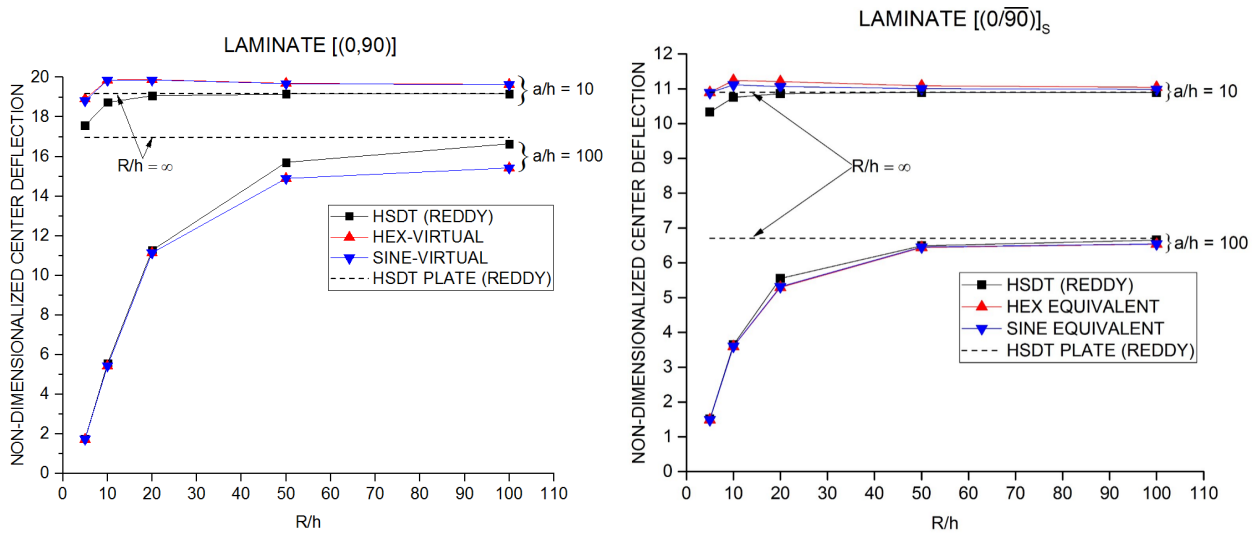

(a) $\overline{W}$ for laminate $0, 90$. **(b)** $\overline{W}$ for laminate $0, 90, 0$.

Figure 5.11: Plot of Non-dimensionalized center deflection, $\overline{W} = -W(\frac{a}{2}, \frac{a}{2}, 0)\frac{1000E_2h^3}{q_0a^4}$ as a function of curvature ratio.

Again, there is a close agreement between the higher-order virtual models and Reddy's HSDT solution [110] for all cases. As expected, results converge to the plate solution with increasing R/h. For the symmetric laminate, errors in deflection between both my models and Reddy's solution are within 5% for all cases.

5.3 Virtual Material for Generalized Beams

Stiffener functional elements are modeled as beams. There are two broad types of beams based on their cross-sections: 1) beams with solid cross-sections and 2) beams with thin-walled cross-sections. The latter is common in composite and is distinguished from the former by their thin walls compared to the overall dimension of the cross-section, as illustrated in Figure 5.12. The kinematics of the two types of beams consist of the generalized beam deformations, which are extensions in normal (X) and shear(XY and YZ) directions, bending in the two transverse (Y and Z) directions, twisting (St. Venant's torsion), and cross-section warping (Vlasov's torsion).

One-dimensional behavior model for composite beams with arbitrary cross-section and loading is extremely complex, as (1) they exhibit several types of deformation, (2) the different deformation

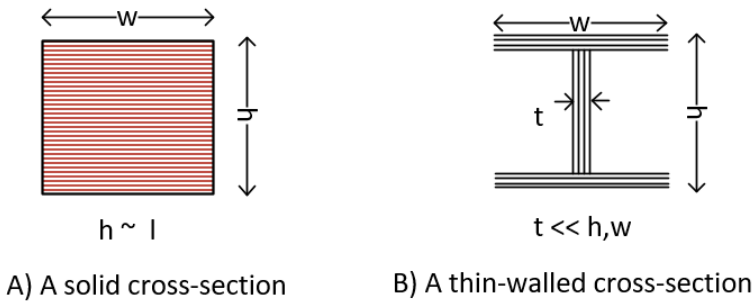

Figure 5.12: Illustration a solid cross-section and a thin-walled cross-section.

types are coupled to each other (normal force can produce twist), and (3) shape of the cross-sectional warping depends on the shape of cross-section (I-section and T-section warps differently). As a result, the number of independent stiffness coefficients for beam models are extremely high. For instance, there are 45 stiffness coefficient for I-beam [48]. This further results into a large number of equations that the virtual material for beam models have to satisfy. Even in practice, designers usually have specialized models for different cross-section types (I, box, etc.) and layup types (symmetric, balanced, etc.).

Modeling beams as collection of plates, on the other hand, is straightforward. Since plate model abstracts the stiffener into a set of surfaces and not an axis, all the '1D deformations' do not have to be modeled explicitly: 1D torsion and warping are automatically captured due to 2D shear strains and curvatures (ϵ_{xy} and κ_{xy}) in plates. Modeling of beams as a collection of plates was discussed in Section 2.2.1 and illustrated in Figure 2.11.

I propose to use the plate behavior models to obtain virtual materials for the composite beams. Therefore, beams with solid cross-sections can simply be modeled as a plate, while thin-walled beams like I-section, T-section, hat-section, etc. are modeled as a collection of plates, one for each web and flange. In the next section, I analyze example beams to show that virtual material for thin plates can be used for the FEA of stiffeners.

5.3.1 Numerical Results

We studied the accuracy of the virtual material for first-order plate behavior using benchmark problems in Section 5.2. In this section, I use virtual material for FSDT plate to analyze two types of beams 1) a solid square cross-section beam and 2) a thin-walled I-beam. My main objective is

Table 5.5: Mid-span displacement for square cross-section beams with layup [0,90,0].

Boundary Condition	Aspect-Ratio	CBT	HOBT	SnS
Clamped-Free	10	$2.20e^{-4}$	$3.46e^{-4}$	$4.00e^{-4}$
	50	$1.37e^{-1}$	$1.41e^{-1}$	$1.42e^{-1}$
Clamped-Clamped	10	$1.29e^{-5}$	$5.32e^{-5}$	$7.48e^{-5}$
	50	$8.06e^{-3}$	$9.19e^{-3}$	$9.65e^{-3}$

to demonstrate that deformations found in beams but not modeled by plates, that is, torsion and warping, can be accurately captured using plate models. Finally, I use Solid186 [105] elements in ANSYS to analyze multi-laminate artifacts. ANSYS also used Conta174, Targe170, and Surf154 to model contacts between laminates, as well as other surface effects.

Problem 1: Square Cross-section Beam

I first analyze a solid square ($1in \times 1in$) cross-section beams under three different loading conditions.

1. Clamped-Clamped (c-c): The beam is clamped at both ends with a distributed pressure of $1\,psi$ on the top surface.

2. Clamped-Free (c-f): The beam is clamped at one end with a distributed load of $1\,psi$ on the top surface.

3. Clamped-Loaded (c-l): The beam is clamped at one end with an axial load (compressive pressure) of $1\,psi$ on the other end.

For c-c and c-f beams, the laminate configuration is [0,90,0]. I compare the mid-span displacement for c-c and c-f beams using FSDT virtual material with results from literature in Table 5.5. Results from literature are for Classical Beam Theory (CBT) and Higher-order Beam Theory (HOBT) [111]. The higher order beam theory was more accurate from lower aspect ratio beams. Results using FSDT virtual material are within 5% for beams with aspect ratio 50. For aspect ratio 10, the virtual material is somewhat over-predicting the result as it did for plates.

To show that we can capture torsion as well as torsion-extension coupling using virtual material for plate theory, I analyze a clamped-loaded beam with aspect ratio of 50. The beam is made of [-45,45] plies which shows torsion under axial load. The deformation is illustrated in Figure 5.13 from

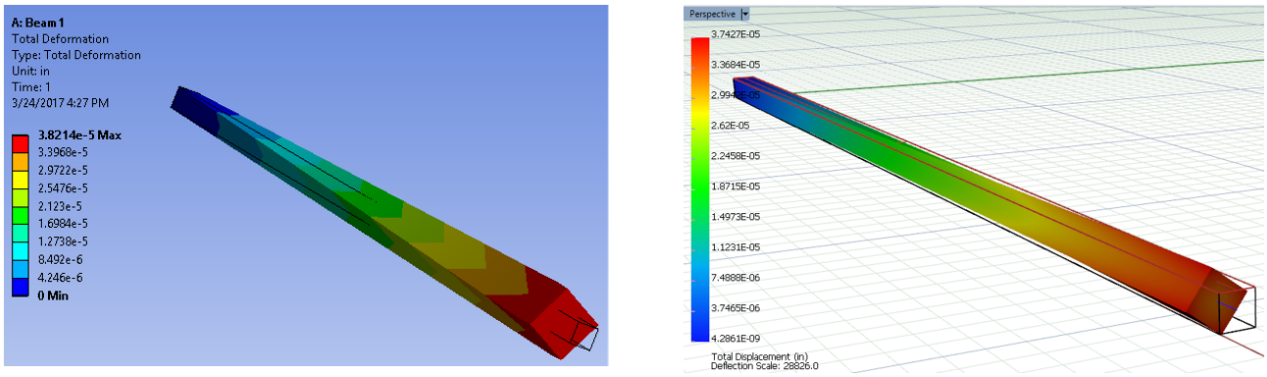

(A) ANSYS (B) SnS

Figure 5.13: Twisting of beam made of $[-45, 45]$ laminate in axial loading due to extension-twisting coupling.

my method and ANSYS. Virtual material for plate theory is able to capture the torsion accurately due to the coupling effect. The maximum value of the deformation using my method is within 5% of the value using ANSYS.

Problem 2: I-beam

The final beam example is a thin-walled beam with I-section and . The cross-section is as shown in Figure 5.12B with $w = h = 1in$, wall-thickness $t = .04in$, and axial length of $l = 36in$. The web and two flanges are made of [0,90] plies. The beam is clamped on one end and axially loaded on the other end with a load of $1lb$. First, such a beam will show extension-bending coupling due to asymmetric ply configuration of the web. In addition, the unclamped end will also show cross-sectional warping due to asymmetric ply configuration in the two flanges and the web. This is confirmed through analysis in ANSYS, as shown in Figure 5.14A. Analysis using the virtual material method successfully captures the warping, as shown in Figure 5.14B. The maximum displacement value has around 7% difference between the two methods.

In the next section, I analyze composite artifacts with functional features other than just a panel or a beam.

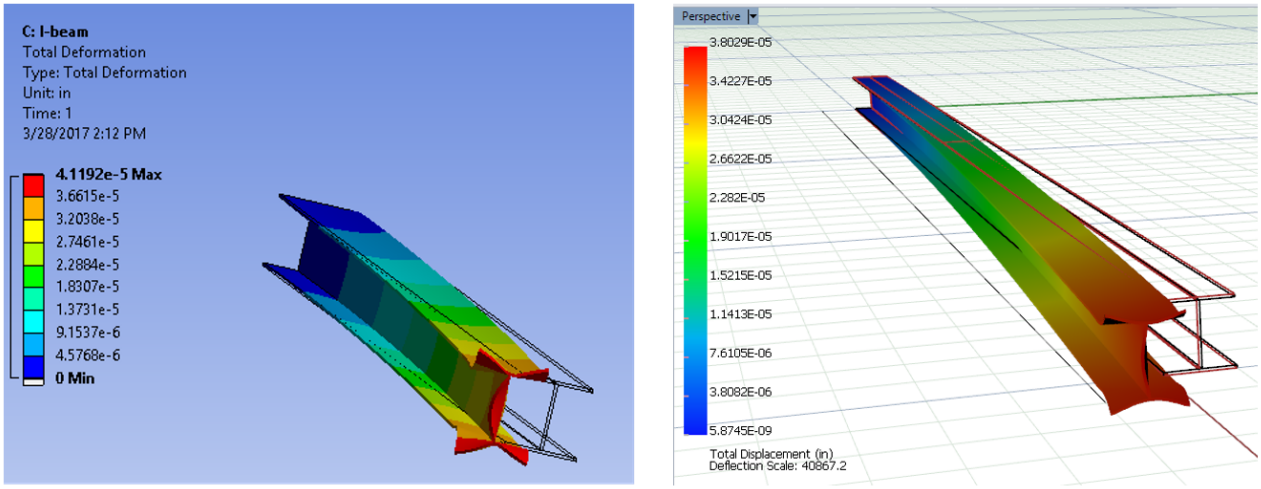

Figure 5.14: Cross-sectional warping in I-beam made of $[0, 90]$ laminate in axial loading.

5.4 Virtual Material Based Analysis of Composite Artifacts with Different Functional Features

Let us now consider simple composite artifacts that also have 3D behavior due to some common functional features. Specifically, I look at four problems

1. Two panels in a lap joint.
2. Composite artifact with a transition region through ply drop-off.
3. Sandwich composite artifact with tapered honeycomb core.
4. Three panels in a T-joint.

The second and fourth problems also involve filler/resin pockets. There are two objectives behind these tests: (1) demonstrate how composite artifacts which does not have 1:1 correspondence between functional and manufacturing structures are analyzed and (2) show that we can capture the complex 3D deformations while using virtual material method. The composite material of the plies are as given in Equation 5.31. The resin pockets and fillers are isotropic materials with following Young's Modulus and Poisson's Ratio.

$$E_1 = 5 \times 10^5 \text{ psi}, \nu = 0.36 \tag{5.34}$$

The sandwich core is a honeycomb core with transversely isotropic material properties.

$$
\begin{aligned}
&E_1 = E_2 = 4 \times 10^4 \text{ psi}, E_3 = 5 \times 10^5 \text{ psi}, \\
&\nu_{12} = 0.25, \nu_{23} = \nu_{13} = 0.0, \\
&G_{12} = 1.6 \times 10^4 \text{ psi}, G_{13} = G_{23} = 6.0 \times 10^4 \text{ psi},
\end{aligned} \tag{5.35}
$$

Directions 1 and 2 are in-plane direction and 3 is the core thickness direction. Finally, for all the simulations, I used 1500 second-order elements in SnS.

5.4.1 Panels in a Lap Joint

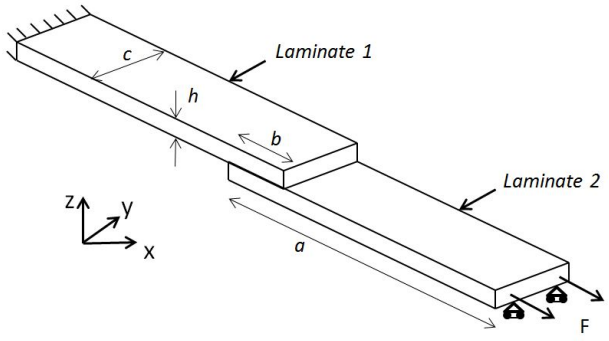

Figure 5.15: A lap joint made of two laminates that are identical in geometry. Dimensions: $a = 10in$, $b = 2in$, $c = 2.5in$ and $h = 0.1in$. The left end is fully fixed, and the right end is allowed to slide in the x direction. A force $F = 10e^4 lb$ is also applied on the right end.

As discussed earlier, direct application of 2D methods do not capture 3D phenomena in lap joints, and special theories are needed if conducting simplified analysis. By contrast, I have shown in my earlier work [53] that 3D FEA using non-conforming mesh can be used to simulate lap joints made of homogeneous materials. I now demonstrate that this approach extends to laminate structures using virtual materials as well.

The geometry and boundary conditions of the lap joint analyzed are shown in Figure 5.15. The two laminates are made of the composite material in Equation 5.31, and I have ignored the adhesive layer for simplicity. I compare the results computed using virtual material method to those computed in ANSYS using a 20-node layered solid element (since 2D shell elements are not

Table 5.6: Maximum displacement value in inches for the lap joint in Figure 5.15. The second row shows the number of elements used.

Laminate	ANSYS	SnS– 3-Ply		SnS– Graded	
	760	1k	3k	1k	3k
$[0, 90]_5$	1.251	1.147	1.212	1.147	1.212
$[-45, 45]_5$	7.975	6.540	7.641	6.540	7.641
50 Plies	3.304	2.937	3.194	2.938	3.195

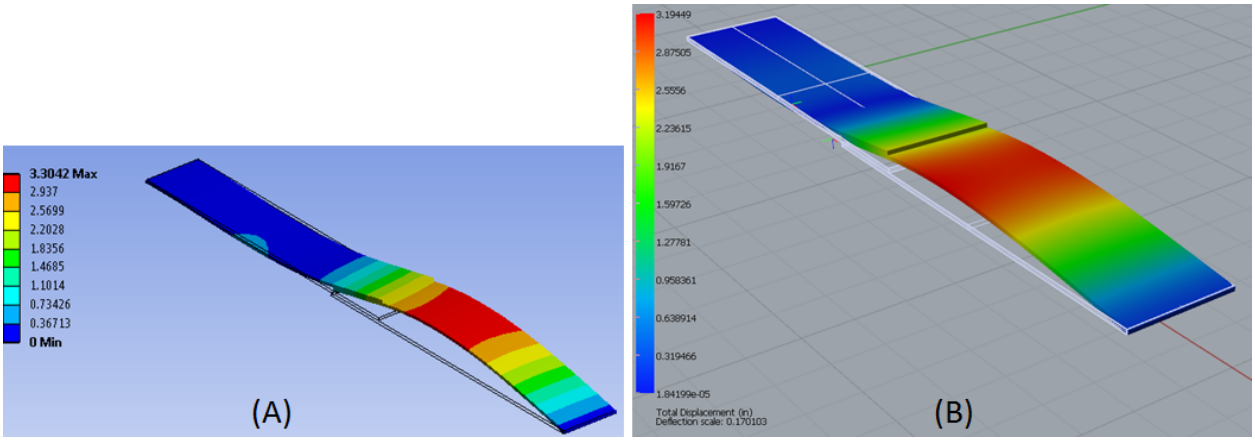

Figure 5.16: Deformed plate and colormap of out-of-plane displacement obtained using A) ANSYS B) Present method, for a laminate plate made of 50 plies. Due to non-zero coupling matrix **B**, in-plane loads leads to out-of-plane bending.

appropriate). Table 4 shows that the maximum displacement values are in close agreement. Figure 5.16 shows displacement colormap as well as the deformed lap joint for the 50-ply laminate.

For the final test, I show that my method also accurately captures coupling phenomena in multi-laminate structure. We will study the same lap joint, but it is now made of laminates with substantial stretching-bending coupling properties. In laminate [0/90], there is a strong coupling between in-plane stretching and out-of-plane cylindrical bending, while in laminate [−45/45], there is a strong coupling between in-plane stretching and out-of-plane twisting. For both the laminates, I compare deformation in the lap joint in two cases: (1) for laminate [0/90], when 0^o plies are bonded together (Figure 5.17A) and when 90^o plies are bonded together (Figure 5.17B); (2) for laminate [−45/45], when 45^o plies are bonded together (Figure 5.18A) and when -45^o plies are bonded together (Figure 5.18B). As predicted, the deformation in the lap joints obtained using my

method and ANSYS agree.

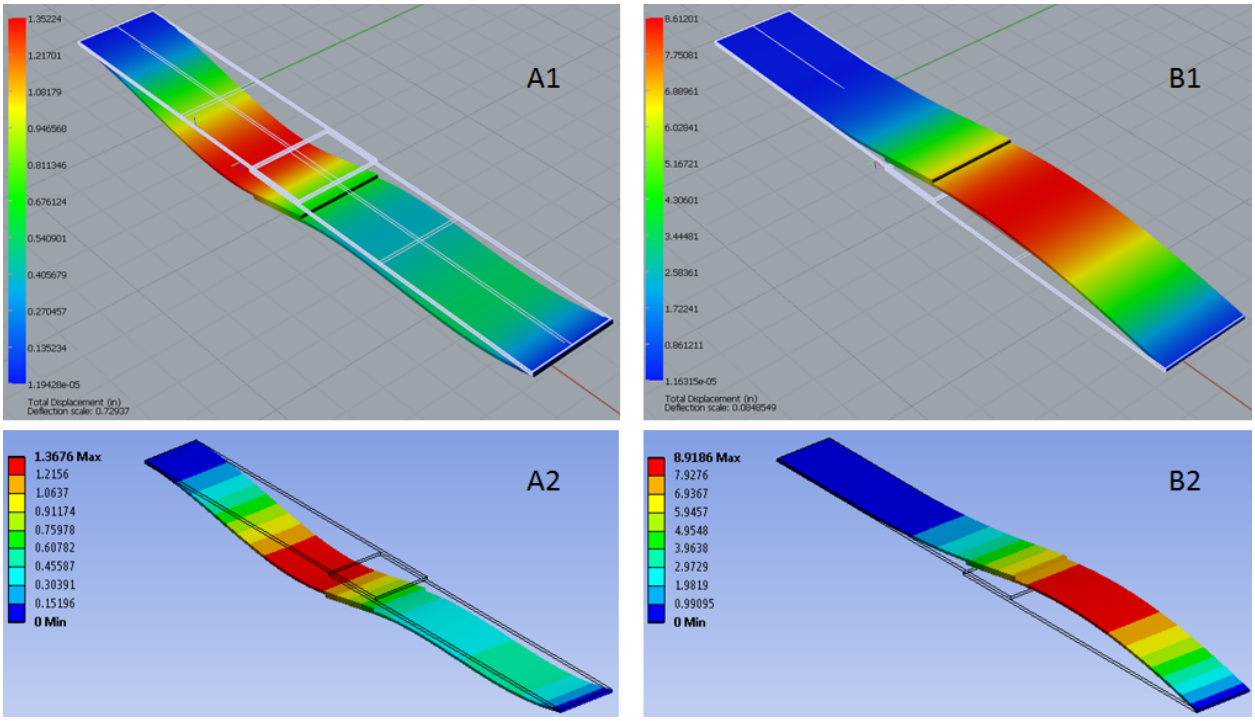

Figure 5.17: Deformation in lap joint made of laminate $[0, 90]$ in 1) SnS, and 2) ANSYS when 0^o plies of the two laminates are bonded. Figure B shows deformation in the lap joint when 90^o plies of the two laminates are bonded.

Observe that the lap joints in Figures 5.17 and 5.18 exhibit significant different deformation patterns, even though the geometry and the boundary conditions are identical. A plausible explanation is as follows. When stretching-bending coupling is not strong, bending due to eccentric forces in the lap joint dominates, and the deformed lap joint looks like Figure 5.16. However, for the lap joint made of [0/90] laminate in Figure 5.17A, stretching-bending coupling is strong and, in Laminate 2, the resultant moment is in the direction opposite to the direction of the moment due to eccentric forces. This causes Laminate 2 to bend in the opposite direction when compared to Figure 5.16. On the other hand, for Laminate 2 of the lap joint in Figures 5.17B, bending due to stretching-bending coupling is in the same direction as bending due to the eccentric forces. Therefore, the out-of-plane deformation pattern is similar, but higher in value when compared to the deformation in Figure 5.16. For the lap joint made of $[-45, 45]$ laminate in Figure 5.18, twisting moment is generated due to coupling in addition to the bending moment due to eccentric forces; therefore, the out-of-plane

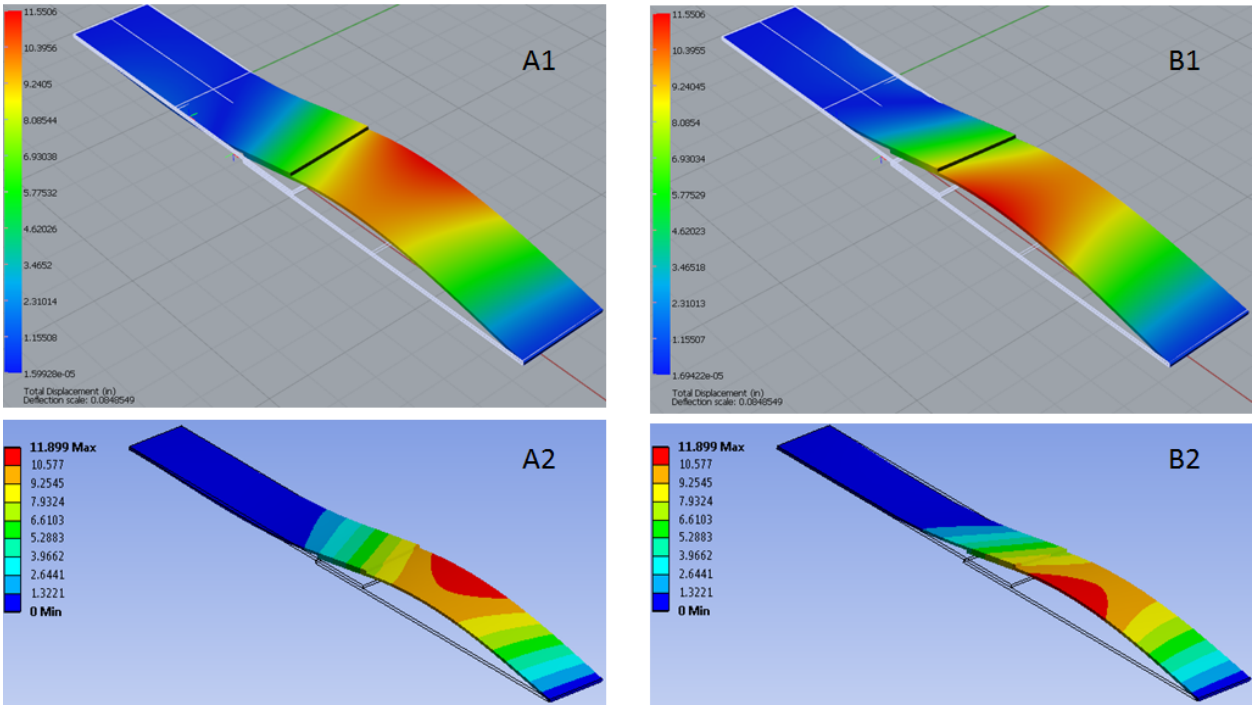

Figure 5.18: A) Deformation in lap joint made of laminate $[-45, 45]$ in 1) SnS, and 2) ANSYS when 45^o plies of the two laminates are bonded. B) Deformation in the lap joint when -45^o plies of the two laminates are bonded.

deformation is not uniform in the width, or y, direction. The direction of the twist reverses when the -45^o plies are bonded together instead of the 45^o plies.

5.4.2 Artifact with Ply Drop-off

Next, I will analyze an artifact with a ply drop-off region that consists of resin pockets. Functionally, the drop-off region serves the purpose of a transition element between a thick panel and a thin panel. The manufacturing and functional structure of the artifact is illustrated in Figures 5.19A and B, respectively. The actual behavior consist of emergent 3D behavior around the transition solid, as shown in Figure 5.19C. The artifact is clamped on two opposite ends and the loaded side (transverse pressure of $1\,psi$) is the thick panel region.

For my method, different virtual materials for different behavior regions were used: HSDT virtual material for thick plate while FSDT virtual material for thin plate behavior. Original material was used in the region with 3D behavior. The results from my method are compared to

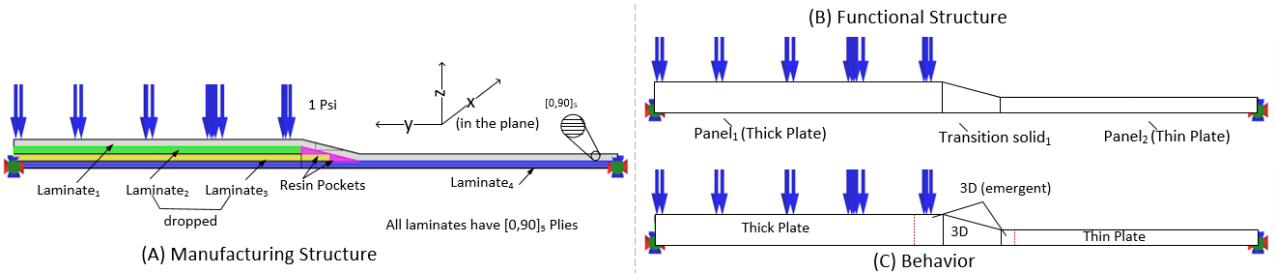

Figure 5.19: Structure and behavior of a composite artifact with a simple ply drop-off.

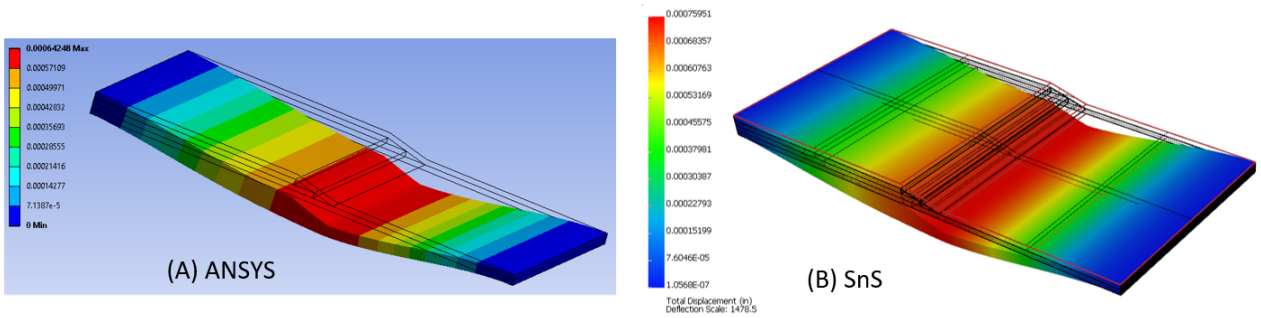

Figure 5.20: Comparison of displacement distribution.

results from ANSYS which used 3D layered element for each laminate and tetrahedral elements for the resin pockets. The displacement fields and Von Mises strain fields are compared in Figure 5.20 and 5.21, respectively. The maximum deformation and strain value are slightly over-predicted using my method in comparison to ANSYS, $6.4E^{-4}$ vs. $7.6E^{-4}$ and $3.1E^{-5}$ vs. $4.7E^{-5}$. However, the deformation and strain distribution are very similar with my method accurately capturing 3D strains in the transition region.

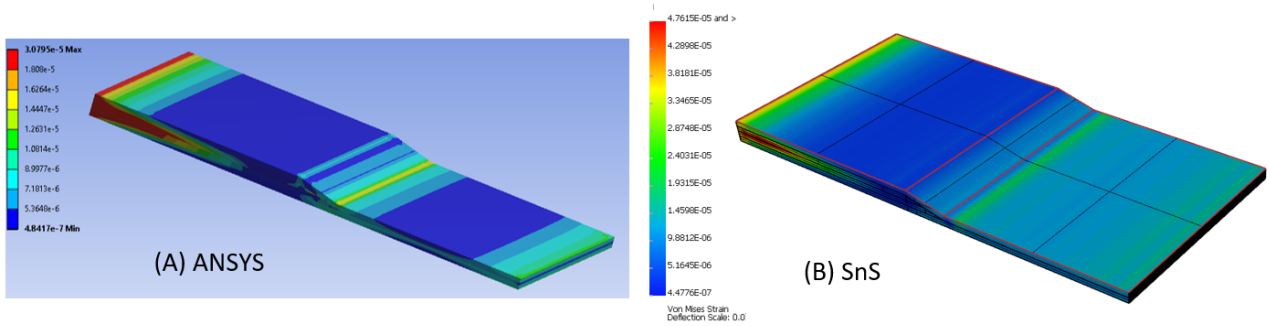

Figure 5.21: Comparison of strain distribution (Von Mises) in drop-off region.

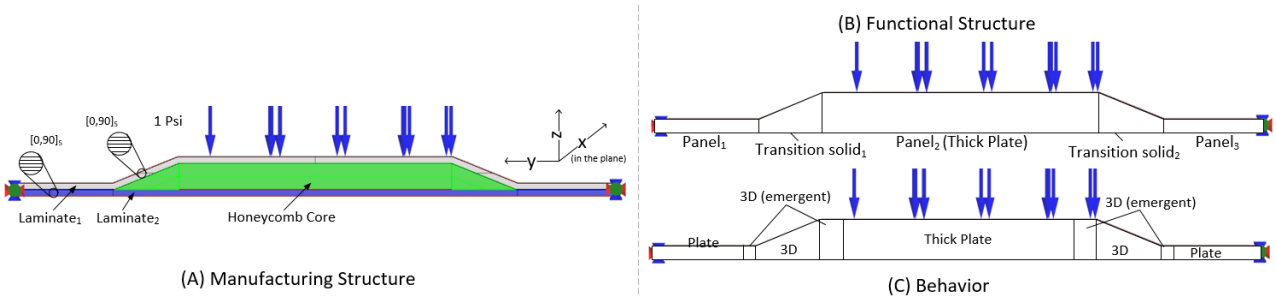

Figure 5.22: Manufacturing structure, functional structure, and behavior of a composite artifact that consists of a tapered core.

5.4.3 Sandwich Composite Artifact with Tapering

As discussed, sandwich structures have thick plate behavior with substantial transverse shear in the core. Moreover, tapered cores have local bending behaviors which result into 3D strains and stresses in the tapering region. To demonstrate that we can capture these effects using my proposed method, I analyze a simple honeycomb sandwich artifact which is illustrated in Figure 5.22. The artifact is made of two laminates with plies $[0, 90]_5$ and honeycomb core that is thicker in the middle and tapers near the ends, as shown in the manufacturing structure in Figure 5.22A. Functionally, the artifact consist of three panels and two transition solids. The thicker panel has a thick plate behavior, while the two thin panel in the ends have thin plate behavior. Moreover, emergent behaviors are present in the region around transition regions, as shown in Figure 5.22C.

For my method, HSDT virtual material for thick plate region while FSDT virtual material for thin plate behavior was used. Original material was used in the region with 3D behavior in the transition and emergent regions. The results from my method are compared to results from ANSYS which used 3D layered element for each laminate and the core except for the tapering regions, for which tetrahedral elements were used. The displacement fields and Von Mises strain fields are compared in Figure 5.23 and 5.24, respectively. This time, the maximum deformation is off by 7% (SnS: $9.1e^{-4}$ and ANSYS: $9.8e^{-4}$), while the maximum Von Mises strain is slightly under-predicted (SnS: $1.71e^{-4}$ and ANSYS: $1.1e^{-4}$) using my method in comparison to ANSYS. However, the deformation and strain distribution are again very similar, and my method accurately capturing 3D strains in the transition region.

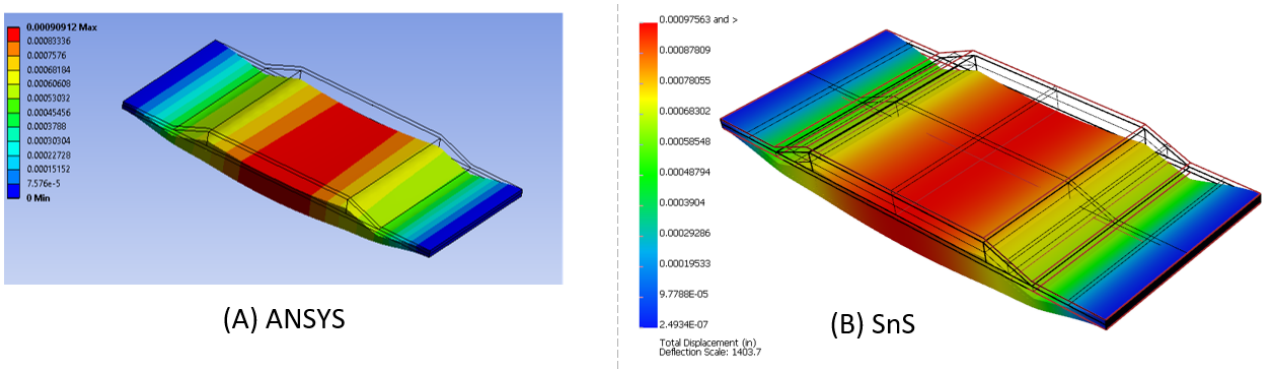

Figure 5.23: Comparison of displacement distribution.

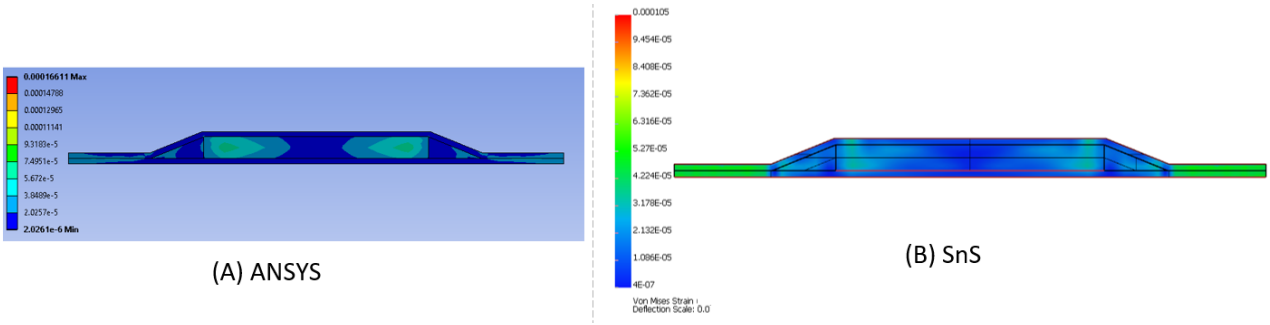

Figure 5.24: Comparison of strain distribution (Von Mises).

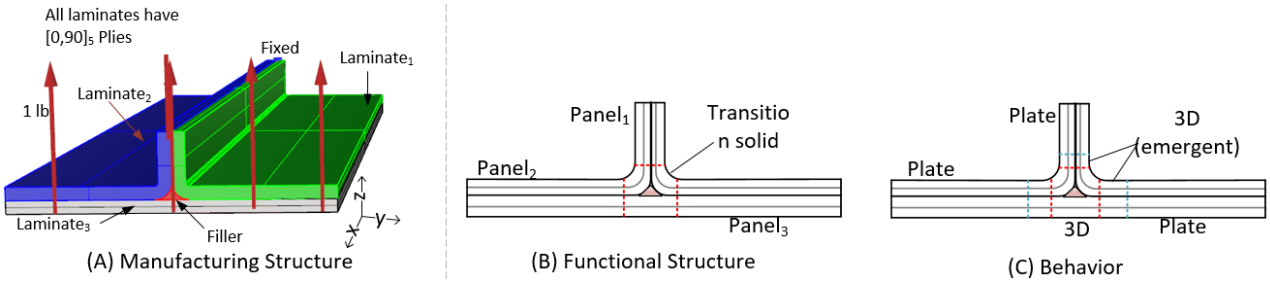

Figure 5.25: Manufacturing structure, functional structure, and behavior of a composite artifact that consists of a T-joint.

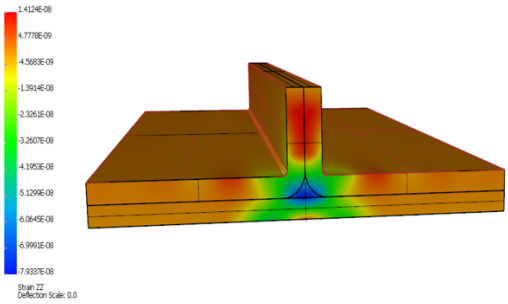

Figure 5.26: Normal strain in the z-direction.

5.4.4 Panels in T-joint with Filler

Finally, I analyze a composite artifact that I was unable to analyze in ANSYS as meshing using layered elements failed due to the sharp curvature in the laminate geometry. The composite artifact is shown in Figure 5.25A: it consist of three laminates with each made of $[0, 90]_5$ plies and a filler in the joint region which could not be reached using plies. One end of the structure is fixed while the other is loaded by a transverse and distributed load of 1 *psi*. Functionally, the artifact is made of three panels with a transition solid connecting them in a 'T' configuration. The three panels have thin plate behavior except in a small region around the transition joint, as shown in Figure 5.25C. Since I don't have results from ANSYS for comparison, I just demonstrate that we can capture 3D strain in the transition region. Figure 5.26 shows the distribution of normal strain in the z-direction. The complex 3D distribution of the stress is evident in the transition region, hence showing that the proposed method can capture 3D deformation while taking advantage of the lower dimensional behavior information.

In the next section, I will describe in detail the implementation of the system that is based on

the proposed virtual material method and used non-conforming finite element analysis.

Chapter 6

System to Analyze Composite Artifacts

In this chapter, I describe the relevant details of the system I implemented based on the FBS framework and the virtual material method. The details are divided into four sections: 1) the first section describes the representation for the structure (manufacturing and functional) and the behaviors in composite artifacts, 2) in the second section, I describe the implementation of the virtual material in a meshfree 3D FEA system, 3) next, I give a quick overview of the system work-flow from the point of view of an analyst, and 4) the final section presents few more complex simulation examples to demonstrate the working of the system.

6.1 Representation for Composite Artifacts

First I describe the representation for the manufacturing structure and then for the functional structure.

6.1.1 Manufacturing Structure

In the definition of manufacturing structure $S^M = \{ s_i^m \}$ for composite artifacts, components s_i^m were laminate solids obtained from the composition of the starting elements in the laminates. First, I present the representation for these laminate solids.

Representation for Laminate

For implementation purposes, I assume that there are three types of laminate solids— ply group, honeycomb core, and filler, for which the representations are as follow:

1. For the ply group type, s^m is a composition of parallel plies, where the plies have identical thickness and material properties (fiber orientations can vary). Such laminate solids, therefore, have a thin-walled shape with uniform thickness everywhere. We can represent a laminate solid $s_i^m = [R, C, L]$ of this type as follows(Figure 6.1A):

   (a) Solid domain R is represented using a boundary-representation.

   (b) Material constitutive relation C is represented using a base surface, a guide curve, and the ply layup information. Base surface and the guide curve are used to specify a curvilinear coordinate system whose 1) x-axis is parallel to the guide curve and is the 0 fiber direction and 2) z-axis is normal to the base surface and is the layup direction. For our case, one of the two lateral[1] faces in the boundary representation of the laminate is chosen to be the base surface, and the layup information is the material distribution along the normal of the base surface. Also, based on the assumption of uniform ply thicknesses, the layup is identical everywhere on the base surface. Base surfaces are smooth with normal defined everywhere, which is a manufacturing constraint as corners cannot be reached by plies.

   (c) Loading L is specified as Dirichlet and Neumann conditions, as typically done in FEA.

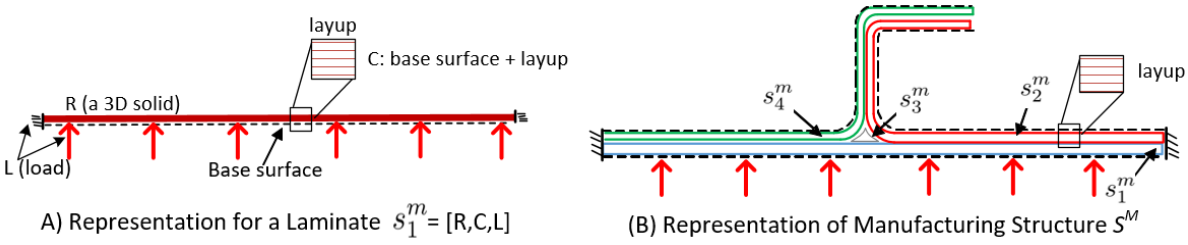

Figure 6.1: Representation for an individual laminate and a manufacturing structure

2. For the second type, s^m is a honeycomb core with a thick wall geometry and optional tapering around the wall edges. The representation for such laminate solids is the same as above except

[1] top and bottom faces for thin-walled solids

there is a restriction to the constitutive relation C: out of the two lateral (top and bottom) faces, only the non-tapering face can be chosen to be the base surface.

3. Finally, filler is the last type of laminate solids. Filler has isotropic material properties and can have arbitrary geometry. Again, R and L of a filler solid $s_i^m = [R, C, L]$ is represented as above. Since C is homogeneous and isotropic, no base surface and guide curve is needed.

Representation For Manufacturing Structure

Representation of manufacturing structure $S^M = \{ s_i^m \}$ is straightforward: it is an assembly of laminate solids, where laminate solids are represented as discussed above. Essentially, the manufacturing structure representation consist of a collection of b-reps (3D solids), base surfaces and layups attached to the b-reps when applicable, and loading, as illustrated in Figure 6.1B.

6.1.2 Functional Structure

Representation For Functional Elements

We saw earlier that given a manufacturing structure for a composite artifact, the functional elements can be specified indirectly by providing (1) a decomposition of the laminate solids (manufacturing elements) into sub-laminate solids and then (2) re-compositions of specific sub-laminate solids to get the functional elements (Figure 4.3). Therefore, given a manufacturing structure as a collection of boundary representations, base surfaces, layups, and loads, the functional structure can be represented procedurally by representing the decomposition and composition operations. I represent the above decompositions and compositions in the system as follows.

1. I represent the decomposition of a laminate solid indirectly through the decomposition of the associated base surface[2] into sub-surfaces. The domain of a laminate solid that consists of parallel plies or a sandwich core has a thin/thick wall geometry, which can be obtained by offsetting the base surface. So, a decomposition of the base surface induces a decomposition of the associated laminate solid, as illustrated in Figure 6.2. The loads and material can be decomposed automatically if the solid domain decomposition is known (by the definition of decomposition).

[2] decomposition of filler is not required.

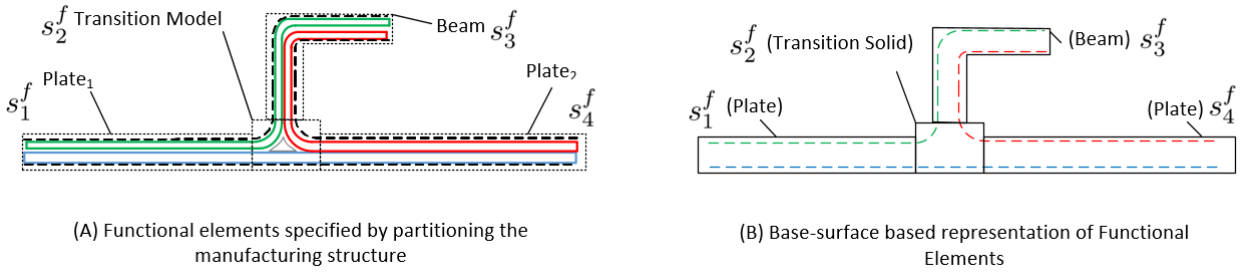

(A) Functional elements specified by partitioning the manufacturing structure

(B) Base-surface based representation of Functional Elements

Figure 6.2: Illustration of how decomposition and re-composition of laminate solids can be indirectly specified through base surfaces.

2. To represent the re-composition, I simply need to identify which sub-laminate solids are to be re-composed. For us, this simply translates into specifying the sub-surfaces of the respective sub-laminate solids, as illustrated in Figure 6.2B.

The details of specifying a panel and a stiffener functional element are illustrated through the examples below.

Laminated and Sandwich Panels To specify a panel, the sub-surfaces whose associated sub-laminate solids form a panel are identified in an arbitrary order. Since we know the layup associated with each sub-surface, we can compute the resulting layup of the panel. One of the sub-surfaces is chosen to be the base-surface of the panel, as illustrated in Figure 6.3. Whether the panel has a thin or thick plate behavior is also specified using a label. This is all the information needed for virtual-material based simplification (a simplified plate model is not needed).

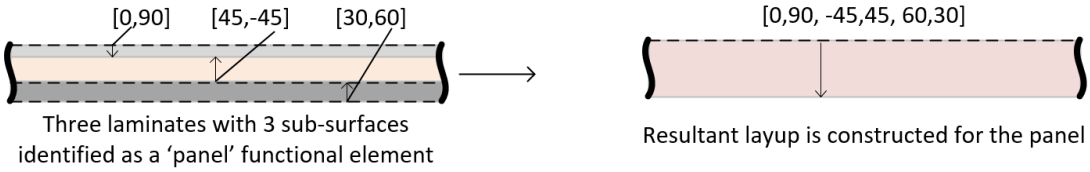

Figure 6.3: Recomposition of the sub-laminate solids that form a panel functional element.

Stiffener To input a stiffener element, first all the sub-surfaces whose sub-laminate solids form the stiffener are specified. Next, the type of the stiffener (I, T, etc.) is specified as a label. Then,

out of the selected sub-surfaces, we further have to specify which sub-surfaces form the web and flange portions of the stiffeners, depending on the stiffer type. Figure 6.4 illustrates this procedure for a T-stiffener.

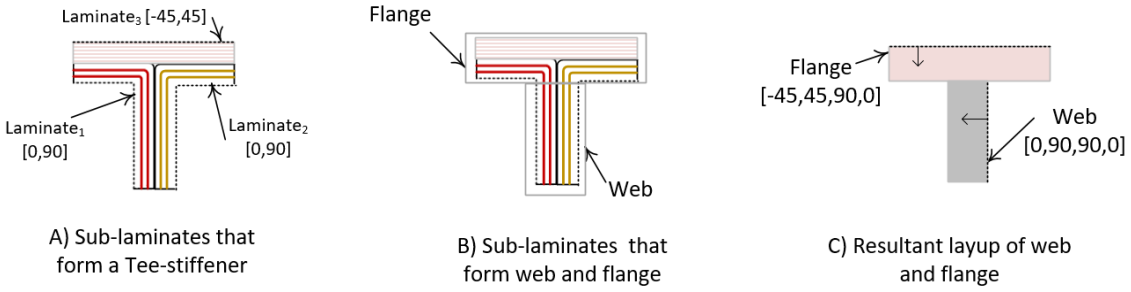

Figure 6.4: Recomposition of the sub-laminate solids that form a T-section beam functional element.

For 3D elements, we have one to one correspondence between the functional and manufacturing elements. Therefore, after identifying the sub-laminate as a 3D element, no further processing is required.

Representation for Joints

Joints are assigned by specifying the two functional elements that share the interface and a label for the type of joint. The exact joint interface is obtained using standard geometric operations including the boolean intersection. The label of the joint could be, for instance, lap, corner, transition, or butt joint.

6.2 Implementation in a Meshfree 3D FEA System

6.2.1 Virtual Material Computation

Once all the functional elements and joints are specified and labeled, virtual material is computed in the following manner (Illustrated in Figure 6.5).

1. For our case, as discussed earlier, all functional elements are essentially a set of plates with a new layup computed as shown in Figures 6.3 and 6.4.

2. So, ultimately, I use two types of virtual materials: virtual material for thin and for thick plate behaviors. For the thin plate behavior, I use virtual material based on the first-order lamination theory and, for the thick plate behavior, I use the higher-order theory based on Touratier's assumption.

3. Virtual material based on the thick plate behavior is used only for 'thick panels', which are generally the regions that consist of sandwich core. Thin plate behavior is used for all other 1D and 2D functional elements. The original material is used for all 3D functional elements.

4. Moreover, I use graded virtual material for both thin and thick plate behaviors, since they are more efficient to analyze when compared to ply-based virtual material.

5. Each graded virtual material is obtained analytically and saved as a set of matrices (A, B, D, etc. matrices). There are as many matrices as the number of coefficients in the virtual material expressions, one matrix for every coefficient.

6. Geometry and loading of the solids require no simplification in virtual material based analysis.

The virtual material information is needed for FEA only during stiffness matrix computation using volume integration. I propose to approximate the volume integration by integrating over a set of surfaces, which I discuss in detail next.

6.2.2 Meshfree Approach

Implementation In Scan And Solve

We implemented the virtual material method in a meshfree FEA system called *Scan and Solve* (SnS) [101]. In SnS, displacements and stresses are approximated using multi-variate B-spline functions that are constructed over a uniform Cartesian grid. This choice of the basis function addresses the concerns of shear locking as well as numerical ill-conditioning of the stiffness matrix for a wide range of laminate thicknesses. More details about Scan and Solve can be found in the reference [101].

During finite element analysis, the material come into picture while computing the element stiffness matrices given in Equation A.1. If the mesh is conforming and the element's z axis is aligned to the laminate's thickness direction (Figure A.1b), computing volume integration for the

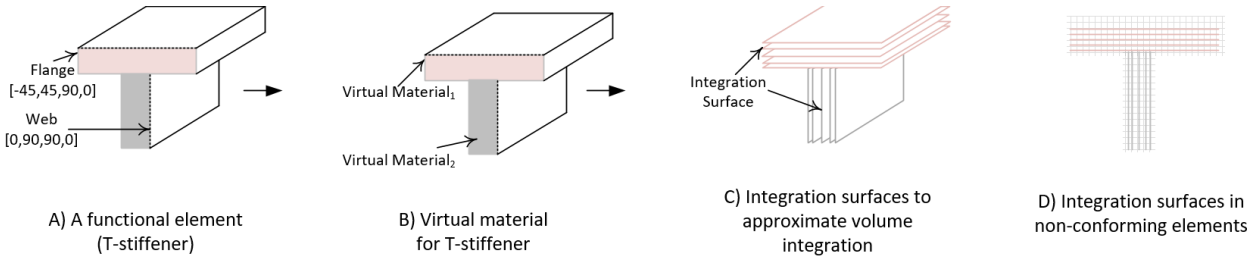

Figure 6.5: Integration surfaces to approximate volume integration.

ply-based virtual material is straightforward. This is because, in a conforming mesh, an individual ply's exact location can be completely determined by its position in the z direction. However volume integration is more involved for the non-conforming mesh. Plies can intersect a grid element at arbitrary angles (Figure A.1c and Figure A.1d), and in artifacts made of multiple laminates, more than one laminate can intersect an element. As a result, computing the intersection of each ply with an element can be both complicated as well as expensive. Therefore, for ease of implementation, I approximate volume integration by integration over surfaces: each laminate is replaced by a set of surfaces parallel to the base surface (Figure 6.5). These surfaces, which we will call *integration surfaces*, can be easily generated as the tooling surface's offsets, a standard geometric operation in a CAD software. The location of these integration surfaces in the laminate's thickness direction can be obtained using one of the quadrature rules, and in the current implementation, I use the Lobatto quadrature rules [104]. In addition to simplifying volume integration, this integration scheme also makes implementation of the quadratically graded layup much easier: since an integration surface is an offset at a constant distance from the laminate's mid-plane, coefficients θ_{ij} of the graded layup (Equations 5.12 and 5.24) are also constant within that integration surface and, therefore, need only be computed once. Integration over each surface is done by first triangulating the surface, and then integrating the obtained triangles using Gauss quadrature rules. The triangles are constrained to conform to the Cartesian grid, or in other words, each triangle lies completely within an element of the Cartesian grid.

While integrating over the triangles, we also need to transform the material matrix $\mathbf{Q}^e$ from its principal coordinate system to the element coordinate system. As explained in Figure 6.6, for every triangle, I transform $\mathbf{Q}^e$ once for the triangle's centroid, and use the transformed properties $\mathbf{Q}^{e'}$ for all the quadrature points of that triangle. The transformation relation is explained in detail in

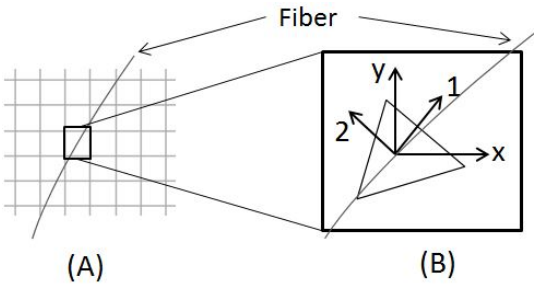

Figure 6.6: A) A xy cross-section of the Cartesian grid and an arbitrary fiber in that cross-section. B) Figure zooms in one of the grid elements and shows a triangle that is being integrated. From the fiber orientation, the material principal directions 1 and 2 are found, which are not aligned to element directions x and y in general.

C.1.1 and in matrix form is given as:

$$\mathbf{Q}^{e'} = \mathbf{G}^T \cdot \mathbf{Q}^e \cdot \mathbf{G}, \tag{6.1}$$

where $\mathbf{G}$ is the transformation matrix. I skip the rest of the implementation details as they are not directly relevant to the contributions in the current work.

6.3 System Workflow

In this section, I briefly describe the workflow of the prototype system from a users perspective. The different steps in the work flow are illustrated with the help of the T-joint assembly (Figure 5.25).

Step 1 User inputs the manufacturing elements of the composite artifact one at a time. For each element, the user first selects the solid domain (b-rep) and then specifies the base surface and the 0 fiber direction (a curve), as illustrated in Figure 6.7. After that, the user has to specify the type of the manufacturing element, the laminate configuration, and the number of plies. The manufacturing element type is either a laminate, a sandwich core, or a filler. This additional information is asked through a command line interface, as illustrated in Figure 6.8.

Once all of the information about a laminate is obtained from the user, the layup information

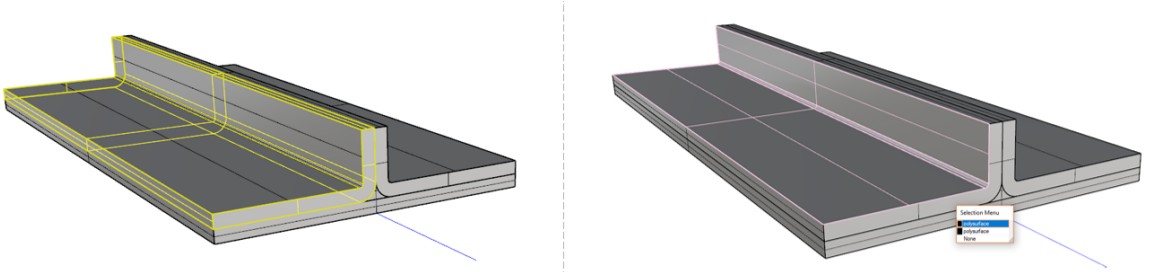

A) Domain(highlighted) of a laminate selected

B) Specify the base-surface(pink) and 0 fiber curve (blue)

Figure 6.7: User inputting the domain and material information (base surface and 0 curve) of a laminate manufacturing element.

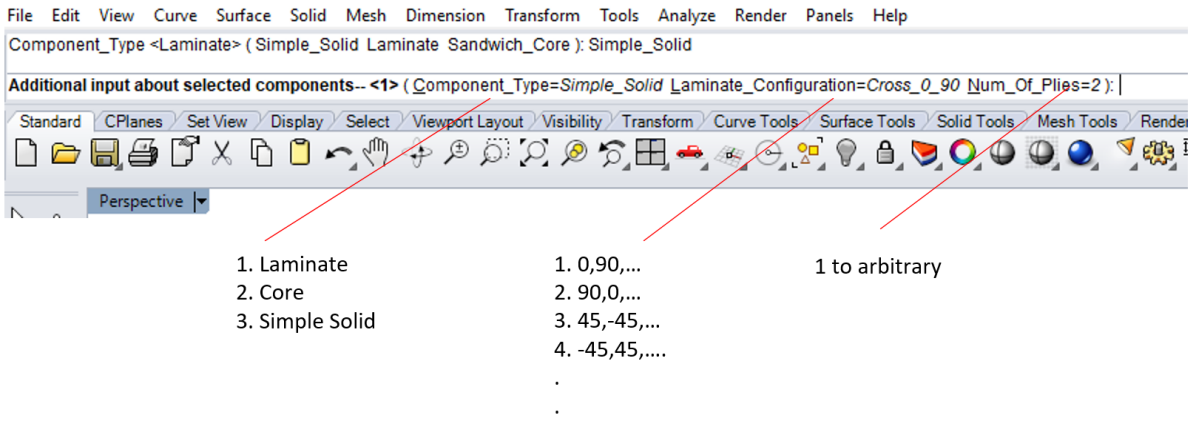

Figure 6.8: User inputting the ply information for a laminate manufacturing element.

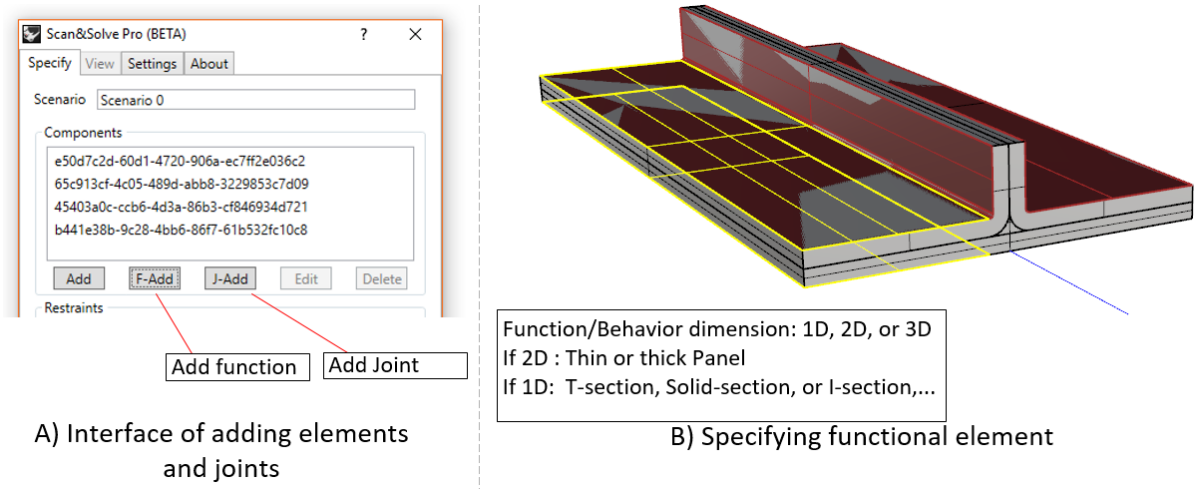

Figure 6.9: User inputting the functional elements in the composite artifact.

is generated automatically. The layup is essentially a list of plies with fiber orientation, thickness, and material. The thickness and material are identical for all of the plies in a laminate.

Step 2 After specifying all of the manufacturing elements, the user must specify the functional elements in the composite artifact. To input a functional element, the sub-surfaces are selected by the user to identify the portions of the manufacturing elements that form the functional element. The interface to add functional elements (also joints) is shown in Figure 6.9A. The selection of the sub-surfaces for a panel functional element is shown in Figure 6.9B. Again, the details of the functional elements are specified using a command line interface. If the functional element has 2D behavior (panel), the user must specify if it is a thin or a thick panel behavior. If the functional element has 1D behavior, the user specifies the cross-section type, as well as which sub-surfaces form the web and the flange portion of the beam. No additional information is needed if the element has 3D behavior.

Once all of the functional elements have been specified, the resulting layups are generated as discussed earlier and illustrated in Figures 6.3 and 6.4.

Step 3 After specifying all the functional elements, user specifies the joint types that produce emergent regions. I have implemented lap-joint, transition, and corner-joint.

Step 4 User, finally, specifies the displacement and force boundary conditions, sets the resolution,

and runs the simulation. There are no 'pre-processing' steps.

Next, I use this prototype system to analyze some complex composite artifacts.

6.4 Numerical Analysis of Complex Composite Artifacts

To demonstrate the system in use, I analyze three example composite artifacts, which are (in increasing order of complexity): 1) a composite chair 2) a panel reinforced with three types of stiffening methods, and 3) a fuselage section. The material properties are the same as earlier: the orthotropic ply material from Equation 5.31, the resin material from Equation 5.34, and the honeycomb core material from Equation 5.35.

6.4.1 Chair Made of Composites

Our first example is a chair that is made of composites. There is a 1:1 correspondence between the functional and manufacturing elements of the chair: each functional element in the chair solid is made of one laminate, as illustrated in the Figure 6.10A. Each laminate consists of 10 plies with configuration $[0/90]_5$. Such a configuration exhibits bending-extension coupling. I use the virtual material method and obtain a quadratically graded material for regions with panel and beam behavior based on the thin plate behavior. The plate behavior is not applicable in the region around joint interfaces due to emergent behavior, as shown in Figure 6.10B. The analysis model for the chair based on the virtual material method and embedded in meshfree finite elements is shown in Figure 6.10C.

The total deformation field of the chair after solving the boundary value problem is shown in Figure 6.11A and the Von Mises strain field is shown in Figure 6.11B. The deflection pattern is as expected: the back of the chair is in bending with maximum deflection at the top tip of the back. The seat and the legs deform very little in comparison. The Von Mises strain has complex 3D distribution in the joint regions. High strains can also be found near the top end of the front legs. The legs have uniform strain away from the ends, signifying they have 1D behavior. This shows the importance of using 3D behavior for joint regions, as the 3D strain distribution would have been completely missed if the leg was assumed to have a lower dimensional behavior everywhere. On

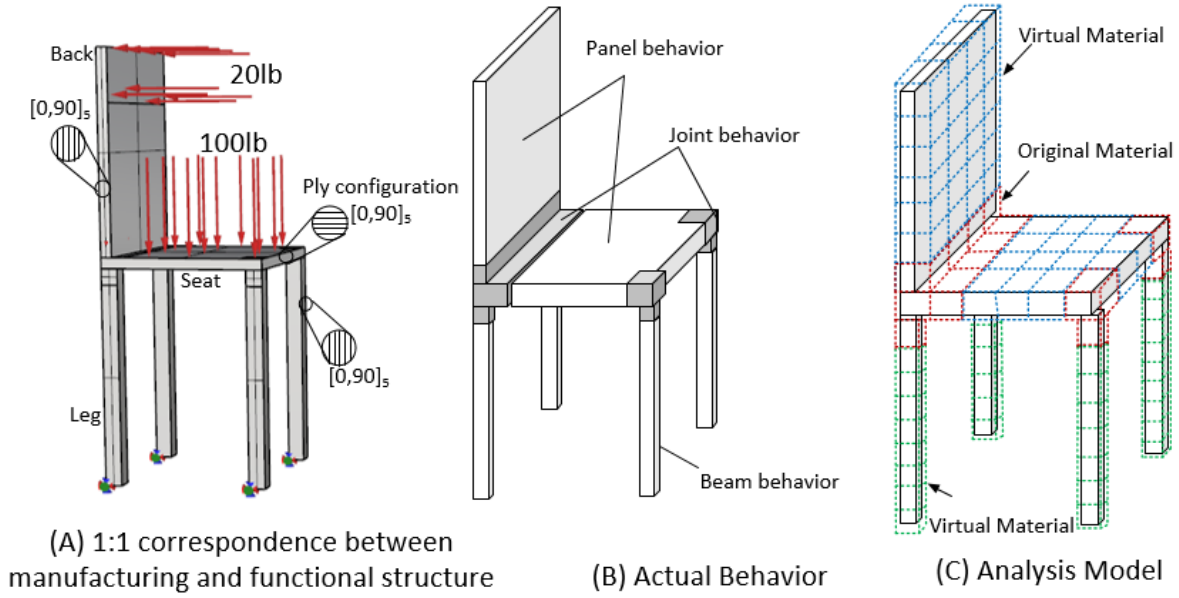

Figure 6.10: Structure, behavior, and analysis model for the chair example.

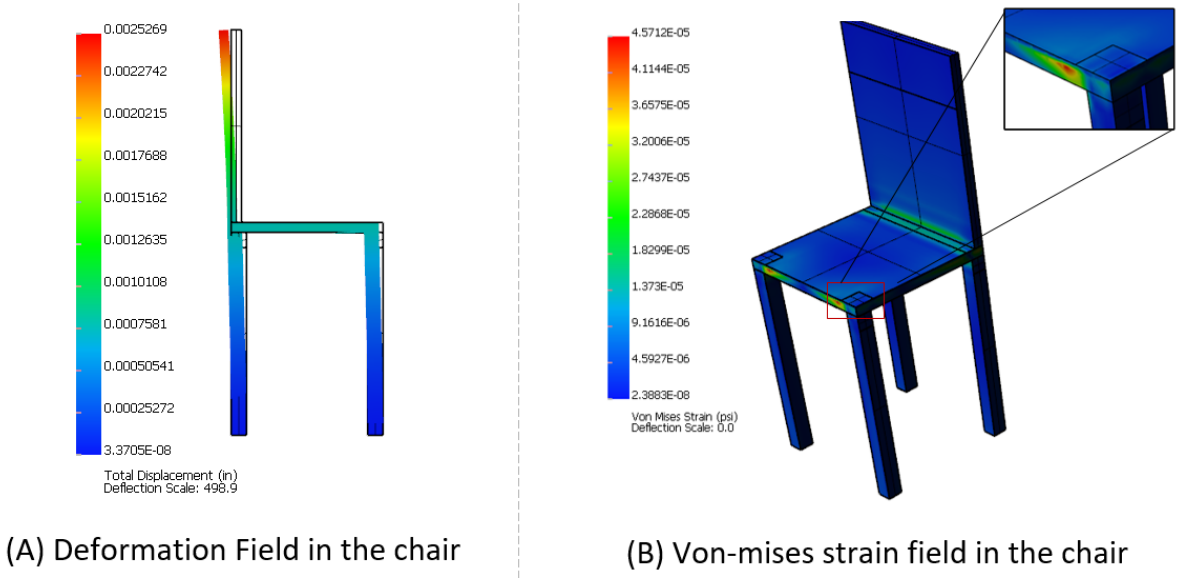

Figure 6.11: Analysis results for the chair problem in Figure 6.10.

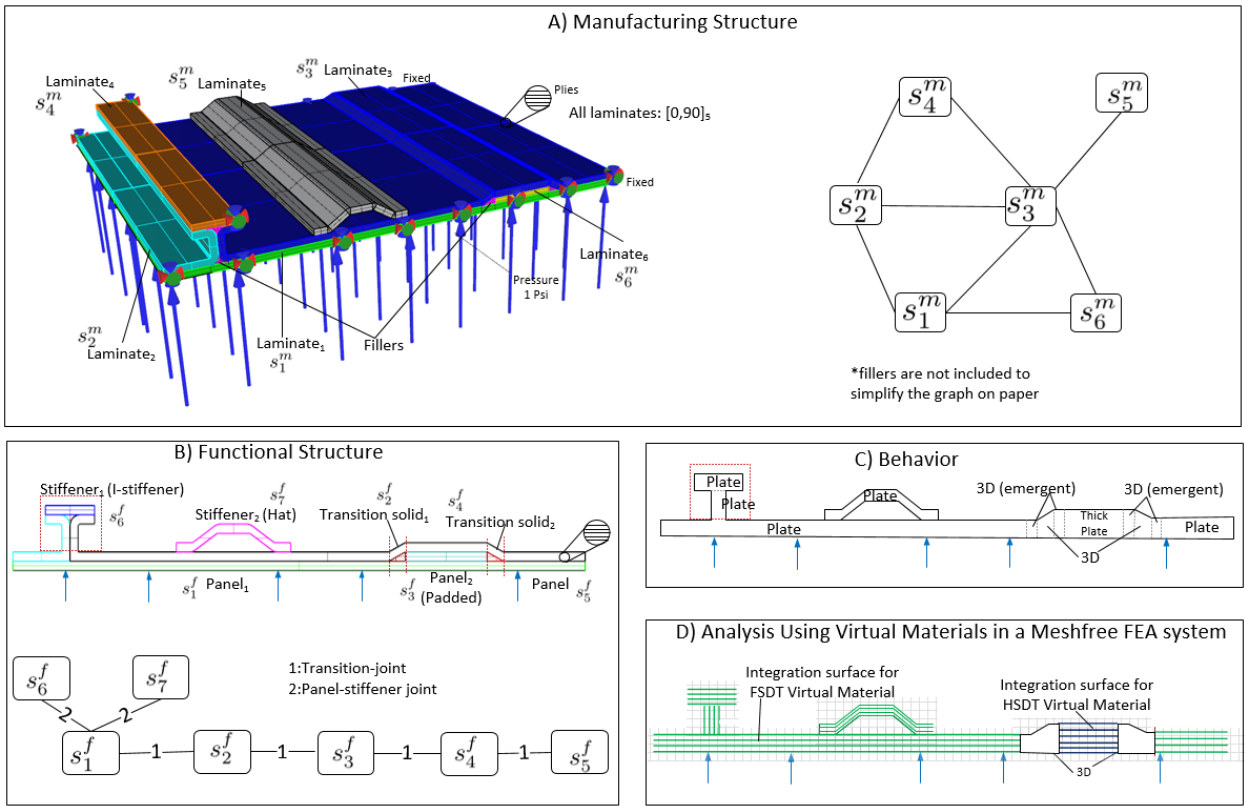

Figure 6.12: A composite solid consisting stiffener-panel joints and ply drop-offs.

the other hand, if the simplified behaviors were not used, each ply would have to be meshed (or integrated) independently, increasing the cost of 3D FEA by several folds.

6.4.2 Panel Stiffened using Different Stiffening Methods

The second example artifact is a complex composite solid with ply drop-offs and integrated stiffeners. The composite artifact (Figure 6.12A) is made of six laminates, with ply configuration $[0, 90]_5$ for each laminate. Functionally, the artifact consist of three panels, two stiffeners, and two transition solids, as shown in Figure 6.12B. Stiffener_1 is an T-section stiffener integrated to the Panel_1 (two laminates are shared between them) and the Stiffener_2 is a hat stiffener made of only one laminate. Both the stiffeners have plate behaviors. Instead of using stiffeners, another way to increase stiffness is by thickening the panel, as done for the Panel_2 by adding Laminate_6. Panel_2 has the behavior of the thick plate. After composing the functional elements, there are emergent behaviors due to transition joints, as shown in Figure 6.12C.

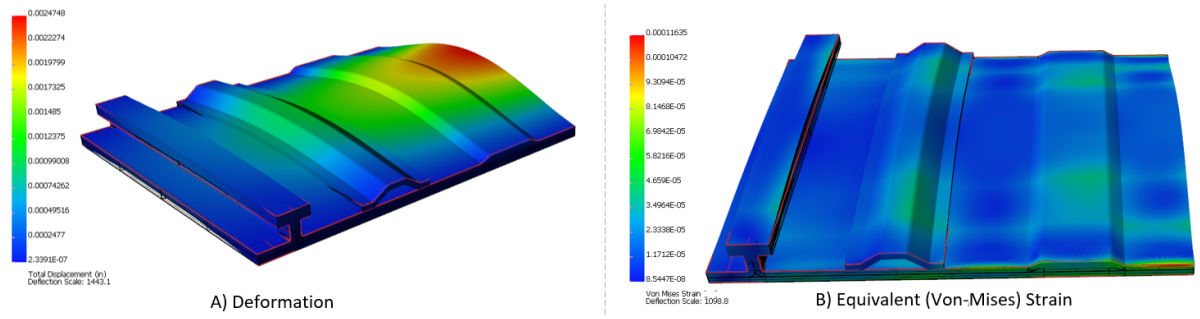

Figure 6.13: Deformation and Von Mises strain of the composite solid in Figure 6.12.

The total deformation field of the stiffened panel after solving the boundary value problem is shown in Figure 6.13A and the Von Mises strain field is shown in Figure 6.13B. The T-section stiffener provides the maximum stiffness, while the maximum deformation is seen in the un-stiffened region at the far end. Similar observation can be made for the Von Mises strain.

6.4.3 Fuselage Section

Our final example is a real world application of composites(Figure 6.14): an airplane fuselage section. The manufacturing and functional structure of the fuselage section is illustrated in the Figure 6.15. The fuselage section, in total, consists of 35 laminates. Each laminate is made of 10 plies that are laid in $[0, 90]_5$ configurations, resulting in a total of 350 individual plies. Functionally, the fuselage is constructed to be an assembly of panels, both flat and curved, and stiffeners 6.15B. The functional structure effectively consists of 2 curved panels, 1 flat panel, 11 T-section stiffeners, and 9 blade-section stiffeners. Through smooth transitions, the panels and stiffeners are integrated together, eliminating the need for fasteners. Due to this integration, several of the laminates are shared between the panels and the stiffeners, as shown in the Figure 6.15B. Both the panels and stiffeners are assumed to have plate behavior. After composing the functional elements, there are emergent behaviors due to the transition joint between the panels.

The results after analyzing the fuselage section are shown in Figure 6.16. The maximum deformation (Figure 6.16A) is seen for the flat panel as it has high pressure that mimics the passenger load. The next higher deflection is in the lower portion of the cylindrical shell which has a higher pressure compared to the rest of the shell to mimic the additional cargo load. The upper portion of the shell has the least pressure and shows the least amount of deflection. The Von Mises strain

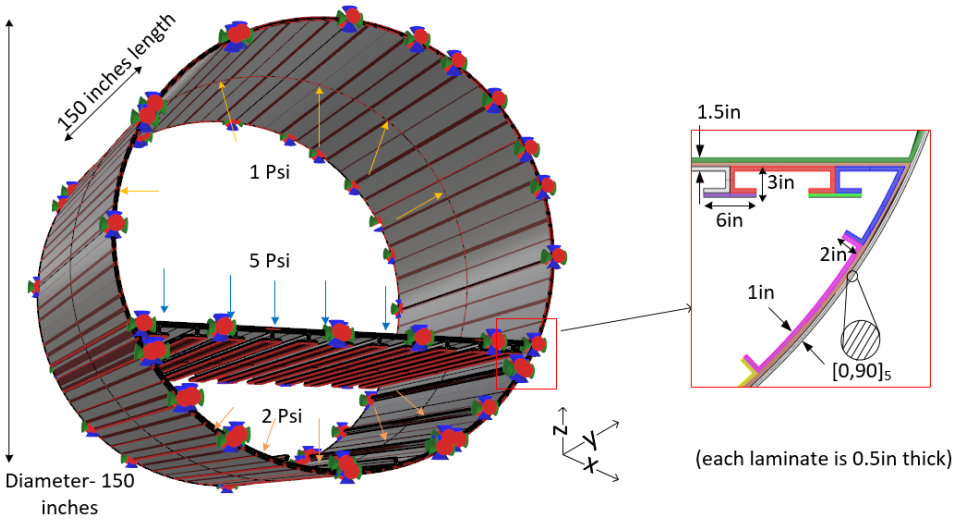

Figure 6.14: Geometry and loading conditions of the fuselage.

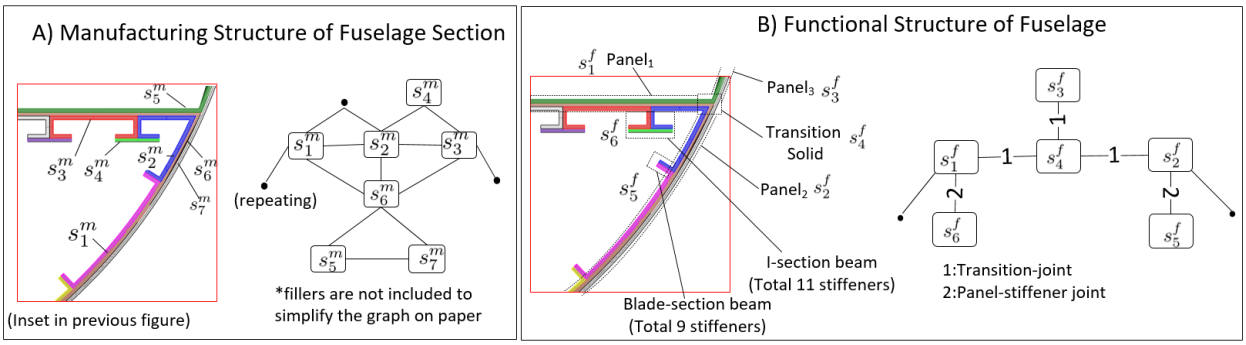

Figure 6.15: Manufacturing and functional structures of the fuselage.

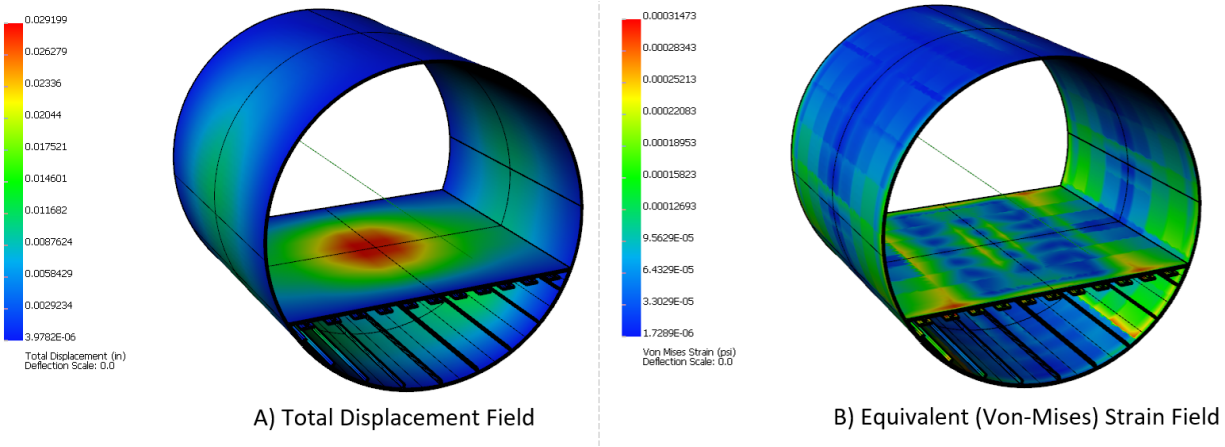

Figure 6.16: Deformation and Von Mises strain of the fuselage section.

field is shown in Figure 6.16B. Overall, higher strains can be seen in the junction region between the flat panel and the cylindrical shell.

The above examples demonstrate the working of the system. The computed displacement and stress fields appear reasonable. With these examples, I conclude the demonstration of the system and continue in the final chapter with the conclusion and discussion of the thesis.

Chapter 7

Conclusion and Open Issues

I proposed and implemented a new framework for design and analysis of composite artifacts. The framework hinges on two key contributions: (1) a formal function-behavior-structure framework for engineering artifacts and (2) the virtual material method to obtain simplified analysis models for the FEA of composite artifacts. The framework resulted into a fully automated yet efficient analysis method for composite artifacts, which I demonstrated with several examples. There are, however, some limitations and open issues to the approach. I discuss them, together with possible extensions, for the two contributions next.

Formal FBS framework for engineering artifacts

The proposed formalization for the FBS framework was based on the extension of the traditional solid modeling to include physics. In physical solid modeling, I defined a physical solid as a boundary value problem whose solution is the state of the solid and the behavior is a mapping between two boundary value problems. Using these definitions, the terminologies of FBS such as manufacturing and functional structures, intended and actual behaviors, and requirements and functions were given a concrete definition for engineering artifacts. The formal FBS framework had at least three major applications for composite artifacts:

1. A way to distinguishing the manufacturing structure from functional structure and showing that the latter should be used for analysis, as they are usually much simpler.
2. A method to predict emergent behaviors from expected behavior for a class of composite

artifacts. The method can be use to systematically store the regions in the artifact with simplified behavior types, which can be used to robustly generate analysis model depending on the type of finite element method being used.

3. A new type of analysis model for efficient 3D FEA of composite artifacts using, so-called, the virtual material method. The method is based on the notion of behavior equivalence, which was obtained for different types of behaviors.

One of the main takeaway messages is that the cost of analyzing an artifact is proportional to the complexity of their functional structure, rather that its manufacturing structure. This has important implications for the analysis of modern engineering artifacts, which are increasingly being manufactured by adding materials in voxels, roads, or layers, and therefore resulting in a complex material structure in the artifact. While laminate composites are essentially manufactured by adding materials in layers, 3D printing methods such as fused deposition modeling, selective laser sintering, and stereolithography adds material in voxels and roads, leading to an even higher complexity of the manufacturing structure. Storing both manufacturing and functional structures, former for manufacturing process and planning and the latter for design and analysis, in the CAD models of such engineering artifacts will also eliminate the pre-processing issues which analysts face because of the current CAD models, which are only based on the manufacturing structure.

One of the open challenges is to define function's purpose-view for engineering artifact which not only formalizes, but also unifies, the informal 'purpose' terminologies used by designers such as 'support', 'transfer', 'brace', and so on. This is needed for high-level conceptual design, from which the design requirements are abstracted. Also, the high-level conceptual definition of the function is usually hierarchical in nature[112], wherein a high-level function is hierarchically decomposed into simpler functions. In the framework, this hierarchy will translate into the hierarchy of the functional structure, which can be defined in the way the hierarchy in the manufacturing structure was defined. For example, the function of an airplane can be decomposed into functions of the fuselage, wings, stabilizers, and so on. Each of these sub-functions can be further hierarchically decomposed, and, at the lowest level, there are functions of panels, stiffeners, etc., in the airplane.

Finally, the proposed method for deterministically obtaining the emergent behavior of an artifact is based on the assumption that the artifact was made of standard functional elements and

joining methods. Although I considered only a limited number of standard functional elements and joints, including additional ones is only a matter of defining the expected behavior for the former and the emergent behaviors for the latter. In case an artifact was not designed by assembling standard elements, the formal FBS framework can still be used as a tool to systematically document the behavior, as obtained using heuristics, geometric analysis, or any other method. The current framework also only covered linear elastic behavior, but it can be extended for dynamics, vibrations, and other types of behaviors of engineering artifacts.

Virtual Material Method

In the thesis, I also proposed a new type of simplified analysis model for efficient 3D analysis of composite artifacts. The essence of the approach is to replace the actual n-ply laminate with a virtual equivalent material model that behaves identically under the assumption of the lamination theory but is much simpler to analyze. This makes 3D FEA of laminated artifacts not only practical but also appealing, as 3D FEA has several advantages over 2D FEA, including no requirement of pre-processing steps such as dimensional reduction. Moreover, the complexity of virtual material for a given behavior remains constant and is independent of the complexity of the actual physical laminate. This implies that the computational efficiency gain grows linearly for 3D FEA: for an n-ply laminate structure with FSDT behavior model, one can expect $O(n/3)$ efficiency gain with the 3-ply model and $O(3n/4)$ for the quadratic graded model using Lobatto quadrature rules for integration. The graded virtual material, as we saw, can be easily implemented in existing FEA systems. Other types of virtual materials, which are more suitable for a particular FEA system, can also be easily derived and implemented. I demonstrated the accuracy of the virtual materials through rigorous numerical testing for benchmark problems in the literature. Virtual materials, however, are based on equivalent single layer theories and cannot be used to predict interlayer stresses between plies. The interlayer stresses, however, can be recovered as a post-processing step using the 3D elasticity theory[14, 34, 35].

We also provided a general scheme to obtain virtual materials for theories based on the unified presentation by Touratier[99]. The scheme elegantly generates a graded virtual material based on the kinematic assumptions made in a particular lamination theory. I showed that the virtual material for plate lamination theories can be used for efficient 3D FEA of one-dimensional functional

elements, instead of using the extremely complex generalized beam theories for composite beams. The virtual material for thin plates captured all the deformation types and coupling in composite beams successfully, which I demonstrated for square and thin-walled I-section beams. Finally, I demonstrated how artifacts consisting of functional features such as bonded-joints, tapered cores, and ply drop-offs can be analyzed using a mix of virtual materials, where applicable, and the original materials for the remaining.

Ultimately, I implemented a system that demonstrated how a complex multi-laminate artifact, which consists of several 1D and 2D functional elements, can be efficiently analyzed using virtual materials and 3D FEA, with minimum pre-processing and manual intervention. I showed that, by using non-conforming 3D finite elements in conjunction with virtual materials, the requirement of mixed-dimensional meshing and multiple types of finite elements including contact and coupling elements can be completely eliminated for the analysis composite artifacts.

Appendix A

Finite Element Methods Summary

Composite laminates can be analyzed using displacement based structural, solid elements, and so-called solid-shell elements. Irrespective of the method used, stiffness matrix for each element must be computed during finite element analysis. Stiffness of each element $\mathbf{K}_e$, in general form, is given as [113]:

$$\mathbf{K}_e = \int_{\Omega_e} \mathbf{B}^T \cdot \mathbf{Q} \cdot \mathbf{B} \; d\Omega, \tag{A.1}$$

where $\mathbf{B}$ is the strain-displacement matrix, $\mathbf{Q}$ is the material constitutive relation matrix, and Ω_e is the element's domain over which integration is done. Different finite element methods differ in how the stiffness matrix is computed. More specifically, they differ in the nature of the element's domain (1D, 2D, or 3D), strain-displacement matrix, and constitutive relation used. The details are discussed in the following subsections.

A.1 Solid Finite Element Methods

Solid elements are general three-dimensional elements which, in theory, can be used to analyze any type of structure. Examples of solid elements are 8 node brick elements and 4 node tetrahedral elements. Each node has 3 displacement degrees of freedom- in x, y, and z directions respectively. Ideally, when analyzing laminated structures, each layer should be meshed independently using solid

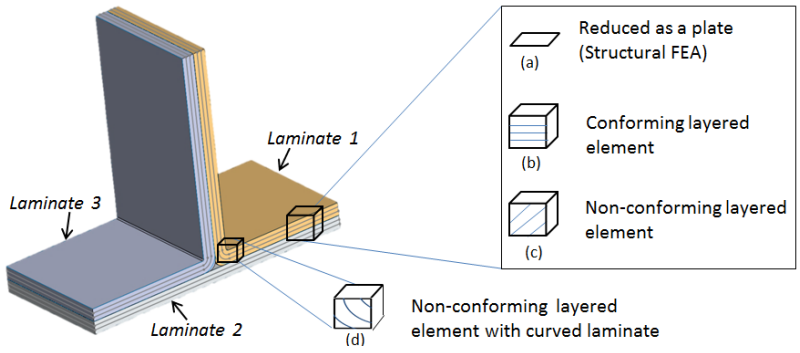

Figure A.1: A structure made of 3 laminates analyzed using different finite element methods (a) Plate structural element (b) Layered solid element of a conforming mesh (c) Layered solid element of a 3D non-conforming mesh (d) Element of a non-conforming mesh with curved laminate inside.

elements, with common nodes at the interface. This would accurately capture different materials in the composite, as well as stress-strain field within the layers and at the interface. However, for practical composite artifacts, FEA using solid elements, or 3D FEA, will require a prohibitively large number of elements.

A much smaller number of elements is required if the so-called *layered-solid* elements[65, 66, 114] are used. Layered elements model multiple layers of material at the same time, as shown in Figure A.1b, c and d. If a layered element is oriented to be aligned to the layers, it is called a conforming layered element (Figure A.1b), otherwise are simply non-conforming layered elements (Figure A.1c and d).

However, although using layered element method reduces the number of solid elements required, it is, nonetheless, computationally expensive for practical composite artifacts. Integration for stiffness matrix computation (Equation A.1) has to be carried out over large number of plies (tens or even hundreds). Integration is performed using quadrature rules that depend on the geometry of the element as well as the degree of the integrand, and amounts to sampling the integrand at a number of quadrature points [113]. To get an idea of the high cost of integration for laminates, let us consider the layered element used in reference [65] to analyze a laminate made of 100 plies. The element used is an eight-node brick element with tri-linear basis functions, which, for a homogeneous material, is fully integrated using 2 integration points in each direction, or 8 integration points in total [65]. However, in a laminate, 8 integration points are needed for each ply, which

results in a 100 fold increase for the 100-ply laminate. Since integration cost represents a significant portion of the overall solution procedure, analysis of composite laminates using layered elements is an expensive proposition.

Solid elements, moreover, can exhibit numerical problems like locking, as well as ill-conditioning of stiffness matrix when used for thin structures such as laminated composites[113, 115]. These problems, however, can be alleviated or eliminated by using higher order *hierarchical*[1] basis functions [102, 103].

Finally, in non-conforming elements (Figure A.1 c and d), plies can intersect elements at arbitrary angles and require computation of intersections between individual plies and elements, which is both non-trivial and computationally expensive. Therefore, 3D FEA of laminates using non-conforming mesh becomes less attractive, despite its advantages over using conforming mesh [101].

A.2 Lower Dimensional Finite Element Methods

Structural elements, such as beams, plates, and shells, are lower dimensional elements (1D or 2D) designed to capture particular responses such as bending and membrane-stretching in structures. These elements have degrees of freedom such as rotation in addition to displacement. Since macro-scale behavior is inbuilt in the basis functions of the element itself, considerably small number of elements are required for accurate results, reducing the computation cost.

However, the same fact that structural elements are build to capture a particular type of response becomes unfavorable for them. In practical structures, which can show different responses in different regions of the structure, multiple different types of structural elements are required. Moreover, responses in some regions of a structure, such as edges, cut-outs and near joints (Figure A.1), cannot be idealized, rendering structural elements unsuitable. Structural elements, like solid elements, can also be sensitive to aspect ratio of a structure's dimensions. An element for thick beam (or plate/shell) can show ill-conditioning and numerical locking when used for thin beam (or plate/shell), thus giving inaccurate results[117]. In addition, structural elements, being 1D or 2D, also require error-prone step of dimension reduction of the 3D structure to be analyzed[95]. Even if the structure is successfully reduced, modeling an assembly of multiple plates and shells can be

[1] A basis function is called *hierarchical* when a higher order basis function contains all the lower order basis functions; for example, B-splines are hierarchical basis functions.

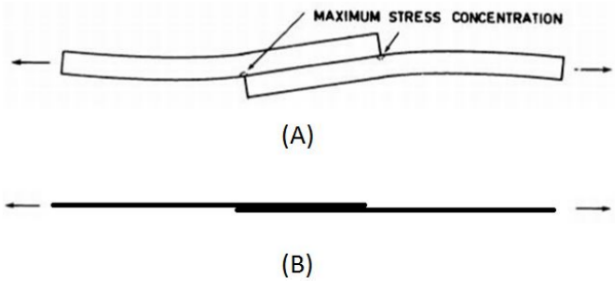

Figure A.2: A) A lap joint bending under in-plane loading, which leads to high stress concentration near the joint [53, 116] B) When analyzed as a 2D structure, bending in lap joint is not captured at all.

problematic [10]. In addition, due to dimensional reduction, 2D FEA can sometimes completely miss a 3D phenomenon. For example, in the lap joint problem shown in Figure A.2, 2D FEA misses the moments due to eccentric forces when the lap joint is reduced to a surface.

Problems of different methods for plates, cylindrical shells, doubly curved shells, etc.

A.3 Hybrid Finite Element Methods

Due to limitations of both solid elements and structural elements, several hybrid methods that incorporate structural responses in solid elements have been proposed. For example, *Solid-shell elements* are solid elements that use Assumed Natural Strain method to deform like plates and shells[10, 64]. Their three-dimensional nature is well suited for interfacing with other solid elements in assemblies. These elements, however, still require mid-surface extraction and also cannot simulate behaviors other than plate and shell.

Continuum solid-shell elements, unlike solid-shell elements, are standard displacement based elements, but use advanced finite element techniques like Assumed Strain Method and Enhanced Strain Method to improve their performance for thin structures [65, 66]. The higher the number of assumed and enhanced parameters, the better is the element's performance, but is at the expense of the generality of the element [65, 67]. Although these elements do not require mid-surfaces explicitly, they must conform to the geometry of the laminate, with their z direction aligned to the transversal direction of structure's offset thickness, because the in-plane and out-of-plane behaviors are assumed

or enhanced differently. These elements fall in the category of conforming layered elements (Figure A.1b), and, like solid layer elements, are still very expensive for laminated structures.

Appendix B

Definition for 1D and 2D Elements and Their Behaviors

B.1 1D Elements

A one-dimension (1D) element is illustrated with the help of Figure B.1a. Region R is a slender solid (a generalized cylinder, to be formal) obtained by sweeping a 2D cross-section along an axis. The axis passes through the cross-sections' centroids and is assumed to be aligned to a generalized z coordinate. The cross-section is allowed to change gradually but they always lie in the xy-plane. The end cross-sections are called *end-faces* of the 1D element. Load L consists of fixed displacement or distributed stress loads on the end-faces, denoted as T^1 and T^2, and uniform or slowly varying

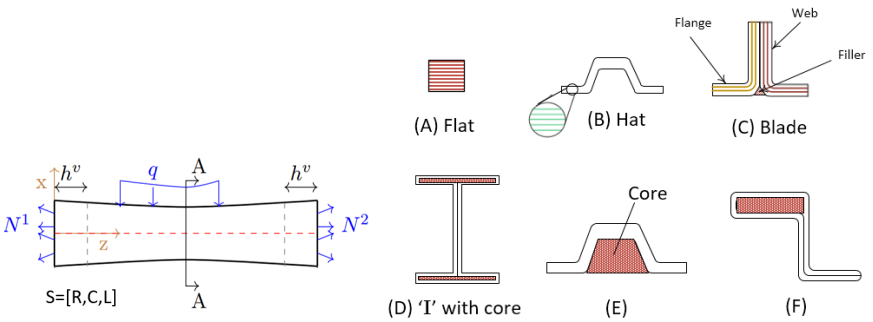

(a) Nomenclature of 1D Element. **(b)** Example configurations of cross-section AA.

Figure B.1: A general 1D element and typical cross-sections.

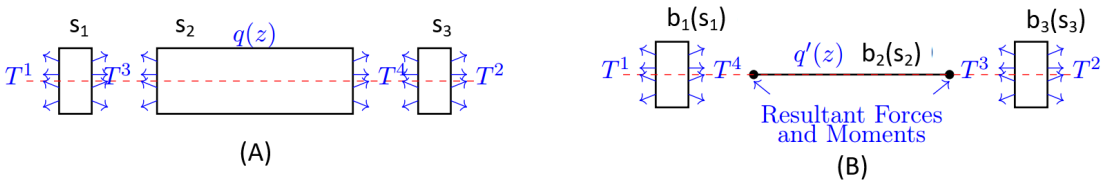

Figure B.2: (A) Sub-solids in 1D element in Figure B.1a. (B) Simplified solids of the sub-solids

distributed stress load q on the lateral face(s). Finally, constitutive relation C can be arbitrary within a cross-section, but it is either constant or varies slowly from cross-section to cross-section. Some example cross-sections made of composite plies and cores are shown in Figure B.1b[9]

Behavior of a 1D element S is illustrated in Figure B.2 where $\{ s_i \}$ is the structure of S into two end-solids s_1 and s_3 and interior-solid s_2. The regions of the end-solids extend h^v distance from the end-faces, where h^v is the characteristic decay length[118]. Behavior map b_2 maps s_2 to a simplified 1D solid s_2^s, while b_1 and b_3 are identity maps because end-solids cannot be simplified. For composites, h^v depends on h^o, the charactersitic thickness of 1D element, as well as ply layup in the cross-section[118]. If performing only global analysis, h^v can be assumed to be zero.

Beam, bar, and shaft elements are subclasses of 1D elements with additional properties. For example, in bar elements, the axis is a line segment, forces on the end-faces have resultants along the z direction, and lateral force $q = 0$. As a result, the simplified solid s_2^d has additional properties as well: resultant force N is normal point load in the z direction, constitutive matrix C includes only stretching stiffness, and resultant strain E is an axial normal strain. The different subclasses of 1D elements are given in Table B.1.

B.2 2D Elements

A 2D element is illustrated with the help of Figure B.3A. Region R of a 2D element is an offset solid obtained by offsetting a smooth mid-surface Ψ equally on both sides. The top and bottom faces of R which are offsets of Ψ are the *base-faces*, while rest of faces are called the *end-faces*. Load L consists of fixed displacements or distributed stress loads (T_1 and T_2) on portions of the end-faces and uniform or slowly varying distributed load $q(x, y)$ on the base faces. Finally, constitutive relation C is restricted to be uniform or vary slowly along any direction parallel to the mid-surface.

Table B.1: Subclasses of 1D elements.

Subclass	Axis geometry	Restrictions on Applied loads	Resultant Forces	Resultant Constitutive
Bar	Line	Resultant of T_1 and T_2 is normal force along z axis. $q = 0$	Normal axial force	Stretching stiffness
Shaft	Line	Resultant of T_1 and T_2 is torque along z axis	Torque along z	Twisting stiffness
Beam	Line	Resultant of T_1 and T_2 is not a force or torque along z	Bending moments and transverse shears	Bending and Shear stiffness
Beam-bar	Smooth curve	Resultant of T_1 and T_2 has no torque along z axis	Bending moments, axial force, and Transverse shears	Bending, stretching and shear stiffness
General	Smooth curve	-	Bending moments, axial force, torque, and Transverse shears	Bending, stretching, twisting, and shear stiffness

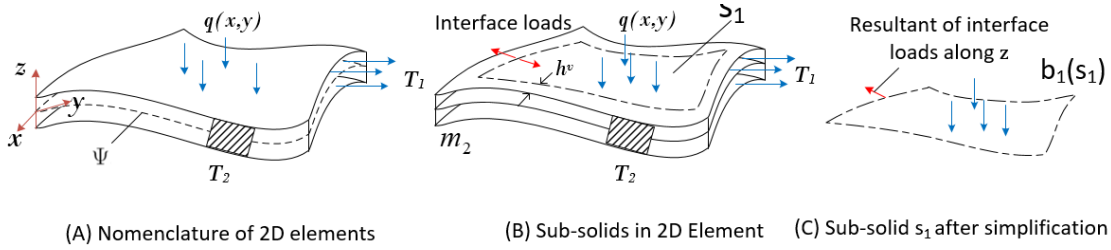

Figure B.3: Nomenclature of 2D element and its simplified solids.

Behavior of a 2D element S whose region has no holes is illustrated in Figures B.3B and C) where $\{ s_i \}$ is decomposition of S into end-solid s_2 and interior-solid s_1. Region of end-solid s_2 extend from the end-faces to h^v, the characteristic decay length, distance away the end-faces. Behavior map b_1 maps s_1 to a simplified 2D solid s_1^d, while b_2 is an identity behavior map.

Plates, shells, and membranes are subclasses of 2D elements with additional properties. For example, in membrane elements, the mid-surface is planar, forces on the end-faces have resultants which are parallel to mid-surface, and lateral force $q = 0$. The simplified solid m_1^s has additional properties too: resultant force vector N consists of normal and shear forces per unit length whose line-of-actions are in the plane of the mid-surface, constitutive matrix C is a 3×3 matrix which

Table B.2: Subclasses of 1D elements.

Subclass	Mid-surface	Restrictions on applied loads	Resultant Forces	Resultant Constitutive
Membrane	Plane	Resultant of T_1 is and T_2 forces along x and y axis. $q = 0$	Normal axial force	Stretching stiffness
Plate	Plane	Resultant of T_1 and T_2 is no torque along z axis	Torque along z	Stretching, bending, and shear stiffness
Shell	Smooth Surface	Resultant of T_1 and T_2 is no torque or torque along z	Bending moments and transverse shears	Stretching, bending, and shear stiffness

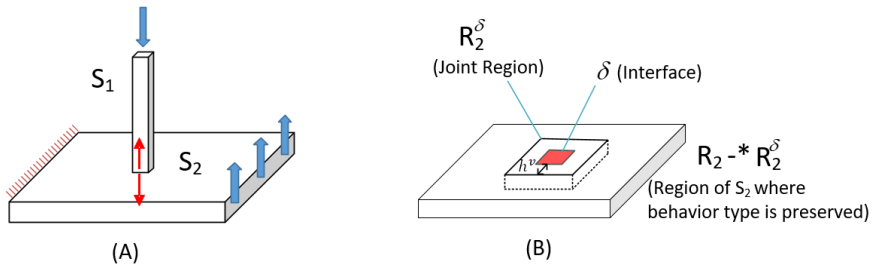

Figure B.4: A) Composition between a plate element (S_1) and a beam element (S_2) B) Joint-region for such composition.

includes normal and shear stretching stiffnesses in x and y directions, and resultant strain E is normal and shear strain vector in x and y directions. Details of the subclasses are discussed in Table B.2.

B.3 Obtaining Emergent Behavior in a Functional Element

Based on St. Venant's principle, the region of the emergent behavior is found h^v distance away from the interface of the joint, where h^v is the characteristic decay length. For solids with 3D behavior, emergent behavior is not an issue. The region of the emergent 3D behavior, is present, can be formally obtained as follows. Consider the plate and beam assembly in Figure B.4). The region of emergent behavior in each functional element is obtained independently. I show how to obtain the region for the plate element (S_2).

- Let δ denote the interface.
- Region of emergent behavior is given as $R_2^{\delta} = (ball(h^v) \oplus \delta) \cap R$, where $ball(h^v)$ is a solid sphere with radius radius h^v and $\oplus$ denotes Minkowski sum operation.
- The region of S_2 where the original behavior type is preserved is given as $R_2 -^* R_2^{\delta}$, where $-^*$ is regularized Boolean subtraction.

Appendix C

Supplementary Material for Virtual Material Method

C.1 Constitutive Relationships

C.1.1 Full Constitutive Relationships for Orthotropic Plies

For an orthotropic material, constitutive relationship relating stresses and strains in material principal direction is given as:

$$\begin{bmatrix} \sigma_x \\ \sigma_y \\ \sigma_z \\ \tau_{yz} \\ \tau_{xz} \\ \tau_{xy} \end{bmatrix} = \begin{bmatrix} C_{11} & C_{12} & C_{13} & 0 & 0 & 0 \\ C_{12} & C_{22} & C_{23} & 0 & 0 & 0 \\ C_{13} & C_{23} & C_{33} & 0 & 0 & 0 \\ 0 & 0 & 0 & C_{44} & 0 & 0 \\ 0 & 0 & 0 & 0 & C_{55} & 0 \\ 0 & 0 & 0 & 0 & 0 & C_{66} \end{bmatrix} \cdot \begin{bmatrix} \epsilon_x \\ \epsilon_y \\ \epsilon_z \\ \gamma_{yz} \\ \gamma_{xz} \\ \gamma_{xy} \end{bmatrix}.$$

In a coordinate system different from material coordinate system, the constitutive matrix has to be transformed and is given as:

$$\mathbf{C}' = \mathbf{G}^T \cdot \mathbf{C} \cdot \mathbf{G},$$

where G is the transformation matrix. G in terms of direction cosines of material directions

l, r, t with respect to general coordinate directions x, y, z is given as:

$$G = \begin{bmatrix} l_x^2 & l_y^2 & l_z^2 & l_y l_z & l_x l_z & l_x l_y \\ r_x^2 & r_y^2 & r_z^2 & r_y r_z & r_x r_z & r_x r_y \\ t_x^2 & t_y^2 & t_z^2 & t_y t_z & t_x t_z & t_x t_y \\ 2r_x t_x & 2r_y t_y & 2r_z t_z & r_y t_z + r_z t_y & r_z t_x + r_x t_z & r_x t_y + r_y t_x \\ 2l_x t_x & 2l_y t_y & 2l_z tz & l_y t_z + l_z t_y & l_z t_x + l_x t_z & l_x t_y + l_y t_x \\ 2l_x r_x & 2l_y r_y & 2l_z r_z & l_y r_z + l_z r_y & l_z r_x + l_x r_z & l_x r_y + l_y r_x \end{bmatrix}.$$

C.1.2 Plane-stress Constitutive Relationship for Orthotropic Materials

For thin structures, stresses in z direction are negligible, and plane-stress assumptions result in a 2D constitutive model, which in arbitrary coordinate system is given as:

$$\begin{bmatrix} \sigma_x \\ \sigma_y \\ \tau_{xy} \end{bmatrix} = \begin{bmatrix} Q_{11} & Q_{12} & Q_{13} \\ Q_{12} & Q_{22} & Q_{23} \\ Q_{13} & Q_{23} & Q_{33} \end{bmatrix} \cdot \begin{bmatrix} \epsilon_x \\ \epsilon_y \\ \gamma_{xy} \end{bmatrix}.$$

C.2 Classical Lamination Plate Theory

When a structure is in stretching and pure bending, strains ϵ_i are assumed to vary linearly in the laminate's thickness direction. In terms of strains ϵ_i^o and curvatures κ_i at the mid-plane, ϵ_i are given as:

$$\epsilon_i = \epsilon_i^o + z \cdot \kappa_i \qquad \text{i} = 1,2,3.$$

The stresses in the thickness direction of the structure can be integrated and reduced to forces and moments respectively [4]. Stresses summed along the thickness result in forces per unit length N_i [4]:

$$\begin{aligned} N_i = & \int_{-\frac{t}{2}}^{\frac{t}{2}} \sigma_i \, dz = \int_{-\frac{t}{2}}^{\frac{t}{2}} Q_{ij} \cdot \epsilon_j \, dz \\ = & \int_{-\frac{t}{2}}^{\frac{t}{2}} Q_{ij} (\epsilon_j^o + z \cdot \kappa_j) \, dz. \end{aligned}$$

Since ϵ^o and κ are constant across thickness, above equation can be further reduced:

$$N_i = (\int_{-\frac{t}{2}}^{\frac{t}{2}} Q_{ij}\, dz) \cdot \epsilon_j^o + (\int_{-\frac{t}{2}}^{\frac{t}{2}} Q_{ij}\, z dz) \cdot \kappa_j,$$

which can be rewritten in matrix forms as:

$$\mathbf{N} = \mathbf{A} \cdot \epsilon^o + \mathbf{B} \cdot \kappa.$$

Using the fact that a laminate is made of plies and material properties Q_{ij}^k of the k^{th} ply is constant within that ply, matrices $\mathbf{A}$ and $\mathbf{B}$ can be further simplified:

$$\begin{aligned} A_{ij} = &\quad \int_{-\frac{t}{2}}^{\frac{t}{2}} Q_{ij}\, dz = \sum_{k=1}^{n} \int_{h_k-1}^{h_k} Q_{ij}^k\, dz \\ = &\quad \sum_{k=1}^{n} Q_{ij}^k (h_k - h_{k-1}), \end{aligned}$$

and

$$\begin{aligned} B_{ij} = &\quad \int_{-\frac{t}{2}}^{\frac{t}{2}} Q_{ij}\, z dz = \sum_{k=1}^{n} \int_{h_k-1}^{h_k} Q_{ij}^k\, z dz \\ = &\quad \sum_{k=1}^{n} Q_{ij}^k (h_k^2 - h_{k-1}^2), \end{aligned}$$

where k^{th} ply lies between heights h_{k-1} and h_k.

Similarly, resultant moments per unit length M_i can also be obtained:

$$\begin{aligned} M_i = &\quad \int_{-\frac{t}{2}}^{\frac{t}{2}} \sigma_i\, z dz = \int_{-\frac{t}{2}}^{\frac{t}{2}} Q_{ij} \cdot \epsilon_j\, z dz \\ = &\quad \int_{-\frac{t}{2}}^{\frac{t}{2}} Q_{ij} (\epsilon_j^o + z \cdot \kappa_j)\, z dz. \end{aligned}$$

Again, since ϵ^o and κ are constant across the thickness, moments M_i reduce to

$$M_i = (\int_{-\frac{t}{2}}^{\frac{t}{2}} Q_{ij}\, z dz) \cdot \epsilon_j^o + (\int_{-\frac{t}{2}}^{\frac{t}{2}} Q_{ij}\, z^2 dz) \cdot \kappa_j$$

which, in matrix form, is given as:

$$\mathbf{M} = \mathbf{B} \cdot \epsilon^o + \mathbf{D} \cdot \kappa.$$

Matrices **B** is same as above, while **D** is given as:

$$D_{ij} = \int_{-\frac{t}{2}}^{\frac{t}{2}} Q_{ij}\, z^2 dz = \sum_{k=1}^{n} \int_{h_k-1}^{h_k} Q_{ij}^k\, z^2 dz$$
$$= \sum_{k=1}^{n} Q_{ij}^k (h_k^3 - h_{k-1}^3).$$

C.3 Derivation of *ABD-equivalent* Models

C.3.1 3-Ply Model

The three plies have material properties Q_{ij}^{*k} for $k = 1, 2, 3$. Also assume the first ply lies between h_0 and h_1, the second between h_1 and h_2, and the third between h_2 and h_3.

Since the 3-ply model must result in ABD matrices identical to the given ABD matrices, Q_{ij}^{*k} will satisfy the following equations:

$$A_{ij}^o = \sum_{k=1}^{3} \int_{h_k-1}^{h_k} Q_{ij}^{*k}\, dz$$
$$= Q_{ij}^{*1}(h_1 - h_0) + Q_{ij}^{*2}(h_2 - h_1) + Q_{ij}^{*3}(h_3 - h_2)$$

$$B_{ij}^o = \sum_{k=1}^{3} \int_{h_k-1}^{h_k} Q_{ij}^{*k}\, z dz$$
$$= \tfrac{1}{2}\{Q_{ij}^{*1}(h_1^2 - h_0^2) + Q_{ij}^{*2}(h_2^2 - h_1^2) + Q_{ij}^{*3}(h_3^2 - h_2^2)\}$$
$$= \tfrac{1}{2}\{Q_{ij}^{*1}(h_1^2 - h_0^2) + Q_{ij}^{*3}(h_3^2 - h_2^2)\}$$

$$D_{ij}^o = \sum_{k=1}^{3} \int_{h_k-1}^{h_k} Q_{ij}^{*k}\, z^2 dz$$
$$= \tfrac{1}{3}\{Q_{ij}^{*1}(h_1^3 - h_0^3) + Q_{ij}^{*2}(h_2^3 - h_1^3) + Q_{ij}^{*3}(h_3^3 - h_2^3)\}.$$

Assuming that the three plies are of equal thickness, and the total laminate thickness is t, above equations can be solved for Q_{ij}^{*k} and is given in Equation 5.11.

C.3.2 Graded Material Model

The quadratically graded material $Q^*_{ij} = z^2\,\Lambda^2_{ij} + z\,\Lambda^1_{ij} + \Lambda^0_{ij}$ also must result in ABD matrices identical to the given ABD matrices. Therefore, Q^*_{ij} must satisfy the following equations:

$$
\begin{aligned}
A^o_{ij} = \int_{-\frac{t}{2}}^{\frac{t}{2}} Q^*_{ij}\,dz &= \int_{-\frac{t}{2}}^{\frac{t}{2}} (z^2\,\Lambda^2_{ij} + z\,\Lambda^1_{ij} + \Lambda^0_{ij})\,dz \\
&= \left[\tfrac{z^3}{3}\,\Lambda^2_{ij} + \tfrac{z^2}{2}\,\Lambda^1_{ij} + z\,\Lambda^0_{ij}\right]_{-\frac{t}{2}}^{\frac{t}{2}} \\
&= \tfrac{t^3}{12}\,\Lambda^2_{ij} + t\,\Lambda^0_{ij} \\
B^o_{ij} = \int_{-\frac{t}{2}}^{\frac{t}{2}} Q^*_{ij}\,z dz &= \int_{-\frac{t}{2}}^{\frac{t}{2}} (z^2\,\Lambda^2_{ij} + z\,\Lambda^1_{ij} + \Lambda^0_{ij})\,z dz \\
&= \left[\tfrac{z^4}{4}\,\Lambda^2_{ij} + \tfrac{z^3}{3}\,\Lambda^1_{ij} + \tfrac{z^2}{2}\,\Lambda^0_{ij}\right]_{-\frac{t}{2}}^{\frac{t}{2}} \\
&= \tfrac{t^3}{12}\,\Lambda^1_{ij} \\
D^o_{ij} = \int_{-\frac{t}{2}}^{\frac{t}{2}} Q^*_{ij}\,z^2 dz &= \int_{-\frac{t}{2}}^{\frac{t}{2}} (z^2\,\Lambda^2_{ij} + z\,\Lambda^1_{ij} + \Lambda^0_{ij})\,z^2 dz \\
&= \left[\tfrac{z^5}{5}\,\Lambda^2_{ij} + \tfrac{z^4}{4}\,\Lambda^1_{ij} + \tfrac{z^3}{3}\,\Lambda^0_{ij}\right]_{-\frac{t}{2}}^{\frac{t}{2}} \\
&= \tfrac{t^5}{80}\,\Lambda^2_{ij} + \tfrac{t^3}{12}\,\Lambda^0_{ij}.
\end{aligned}
$$

Above equations can be solved for Λ^k_{ij} for $k = 1, 2, 3$ and is given in Equation 5.13.

Bibliography

[1] R. F. Gibson, Principles of composite material mechanics, CRC Press, 2011.

[2] F. C. Campbell Jr, Manufacturing processes for advanced composites, Access Online via Elsevier, 2003.

[3] A. Handbook, Vol. 21, Composites 380.

[4] I. M. Daniel, O. Ishai, I. M. Daniel, I. Daniel, Engineering mechanics of composite materials, Vol. 3, Oxford university press New York, 1994.

[5] W. J. Renton, D. Olcott, W. Roeseler, R. Batzer, W. Baron, A. Velicki, Future of flight vehicle structures (2000 to 2023), J Aircraft 41 (5) (2012) 986–998. doi:10.2514/1.4039.

[6] [link].
URL http://www.compositesworld.com/articles/integrated-optimized-aircraft-door

[7] J. R. Vinson, R. L. Sierakowski, The behavior of structures composed of composite materials, Vol. 105, Springer Science & Business Media, 2006.

[8] C. Arya, Design of structural elements: Concrete, steelwork, masonry and timber designs to British standards and Eurocodes, CRC Press, 2009.

[9] R. M. Jones, Mechanics of composite materials, Vol. 193, Scripta Book Company Washington, DC, 1975.

[10] F. L. Matthews, Finite element modelling of composite materials and structures, CRC Press, 2000.

[11] C. G. Armstrong, Modelling requirements for finite-element analysis, Computer-aided design 26 (7) (1994) 573–578.

[12] A. K. Noor, W. S. Burton, J. M. Peters, Hierarchical adaptive modeling of structural sandwiches and multilayered composite panels, Applied Numerical Mathematics 14 (1) (1994) 69–90.

[13] J. Reddy, Mechanics of laminated composite plates and shells: theory and analysis, CRC press, 2004.

[14] E. Carrera, Theories and finite elements for multilayered, anisotropic, composite plates and shells, Archives of Computational Methods in Engineering 9 (2) (2002) 87–140.

[15] ASME, Asme y14.37-2012 composite part drawings.

[16] R. E. Murrish, Methods and systems for explicit representation of composite structures, uS Patent 7,809,531 (Oct. 5 2010).

[17] L. F. da Silva, P. J. das Neves, R. Adams, J. Spelt, Analytical models of adhesively bonded joints—part i: Literature survey, International Journal of Adhesion and Adhesives 29 (3) (2009) 319–330.

[18] A. Bogdanovich, I. Kizhakkethara, Three-dimensional finite element analysis of double-lap composite adhesive bonded joint using submodeling approach, Composites Part B: Engineering 30 (6) (1999) 537–551.

[19] D. C. Nolan, C. M. Tierney, C. G. Armstrong, T. T. Robinson, Defining simulation intent, Computer-Aided Design 59 (2015) 50–63.

[20] C. G. Dávila, Solid-to-shell transition elements for the computation of interlaminar stresses, Computing Systems in Engineering 5 (2) (1994) 193–202.

[21] K. W. Shim, D. J. Monaghan, C. G. Armstrong, Mixed dimensional coupling in finite element stress analysis, Engineering with Computers 18 (3) (2002) 241–252.

[22] J. S. Gero, Design prototypes: a knowledge representation schema for design, AI magazine 11 (4) (1990) 26.
URL https://scholar.google.com/scholar?cluster=6095751141762195739

[23] W. Zhang, Y. Lin, N. Sinha, On the function-behavior-structure model for design, Proceedings of the Canadian Engineering Education Association.
URL https://scholar.google.com/scholar?cluster=700337699260519634

[24] L. Qian, J. S. Gero, Function–behavior–structure paths and their role in analogy-based design, Artificial Intelligence for Engineering, Design, Analysis and Manufacturing 10 (04) (1996) 289. doi:10.1017/s0890060400001633.
URL http://dx.doi.org/10.1017/s0890060400001633

[25] Y. Umeda, H. Takeda, T. Tomiyana, H. Yoshikawa, Function, behavior, and structure.

[26] Composite part drawings- engineering drawing and related documentation practices (2012).

[27] Z. Hashin, Analysis of composite materials—a survey, Journal of Applied Mechanics 50 (3) (1983) 481–505.

[28] V. Premkumar, S. Krishnamurty, J. Wileden, A semantic knowledge management system for laminated composites.

[29] K. A. Hunten, A. B. Feeney, V. Srinivasan, Recent advances in sharing standardized step composite structure design and manufacturing information, Computer-Aided Design 45 (10) (2013) 1215–1221.

[30] E. J. Barbero, Introduction to composite materials design, CRC press, 2010.

[31] O. K. Bedair, A contribution to the stability of stiffened plates under uniform compression, Computers & structures 66 (5) (1998) 535–570.

[32] U. Icardi, F. Sola, Analysis of bonded joints with laminated adherends by a variable kinematics layerwise model, International Journal of Adhesion and Adhesives 50 (2014) 244–254.

[33] H. T. Hahn, Composite Materials: Fatigue and Fracture: a Symposium Sponsored by ASTM Committee D-30 on High Modulus Fibers and Their Composites, Dallas, TX, 24-25 Oct. 1984, Vol. 1230, ASTM International, 1995.

[34] I. Kreja, A literature review on computational models for laminated composite and sandwich panels, Open Engineering 1 (1) (2011) 59–80.

[35] A. K. Noor, W. S. Burton, Assessment of shear deformation theories for multilayered composite plates, Applied Mechanics Reviews 42 (1) (1989) 1–13.

[36] J. Reddy, An evaluation of equivalent-single-layer and layerwise theories of composite laminates, Composite Structures 25 (1) (1993) 21–35.

[37] A. K. Noor, W. S. Burton, C. W. Bert, Computational models for sandwich panels and shells, Applied Mechanics Reviews 49 (3) (1996) 155–199.

[38] W. Burton, A. Noor, Assessment of continuum models for sandwich panel honeycomb cores, Computer methods in applied mechanics and engineering 145 (3) (1997) 341–360.

[39] J. Hohe, W. Becker, Effective stress-strain relations for two-dimensional cellular sandwich cores: Homogenization, material models, and properties, Applied Mechanics Reviews 55 (1) (2002) 61–87.

[40] S. S. Vel, V. Caccese, H. Zhao, Elastic coupling effects in tapered sandwich panels with laminated anisotropic composite facings, Journal of composite materials 39 (24) (2005) 2161–2183.

[41] N. Paydar, C. Libove, Stress analysis of sandwich plates with unidirectional thickness variation, Journal of applied mechanics 53 (3) (1986) 609–613.

[42] D. Graesser, Z. Zabinsky, M. Tuttle, G. Kim, Optimal design of a composite structure, Composite structures 24 (4) (1993) 273–281.

[43] J.-S. Wang, T.-M. Hsu, Discrete analysis of stiffened composite cylindrical shells, AIAA journal 23 (11) (1985) 1753–1761.

[44] S. Kidane, G. Li, J. Helms, S.-S. Pang, E. Woldesenbet, Buckling load analysis of grid stiffened composite cylinders, Composites Part B: Engineering 34 (1) (2003) 1–9.

[45] N. Jaunky, N. F. Knight, D. R. Ambur, Formulation of an improved smeared stiffener theory for buckling analysis of grid-stiffened composite panels, Composites Part B: Engineering 27 (5) (1996) 519–526.

[46] E. A. Sadek, S. A. Tawfik, A finite element model for the analysis of stiffened laminated plates, Computers & Structures 75 (4) (2000) 369–383.

[47] R. Rikards, A. Chate, O. Ozolinsh, Analysis for buckling and vibrations of composite stiffened shells and plates, Composite Structures 51 (4) (2001) 361–370.

[48] R. Chandra, I. Chopra, Experimental and theoretical analysis of composite i-beams with elastic couplings, AIAA journal 29 (12) (1991) 2197–2206.

[49] X.-X. Wu, C. Sun, Simplified theory for composite thin-walled beams, Aiaa Journal 30 (12) (1992) 2945–2951.

[50] C. Kim, S. R. White, Thick-walled composite beam theory including 3-d elastic effects and torsional warping, International journal of solids and Structures 34 (31-32) (1997) 4237–4259.

[51] D. Li, G. Qing, Y. Liu, A layerwise/solid-element method for the composite stiffened laminated cylindrical shell structures, Composite Structures 98 (2013) 215–227.

[52] L. F. da Silva, P. J. das Neves, R. Adams, A. Wang, J. Spelt, Analytical models of adhesively bonded joints—part ii: Comparative study, International Journal of Adhesion and Adhesives 29 (3) (2009) 331–341.

[53] G. Kumar, V. Shapiro, Analysis of multi-material bonded assemblies on a non-conforming mesh, in: ASME 2012 International Design Engineering Technical Conferences and Computers and Information in Engineering Conference, American Society of Mechanical Engineers, 2012, pp. 111–123.

[54] F. Mortensen, O. T. Thomsen, A simple approach for the analysis of embedded ply drops in

composite and sandwich laminates, Composites science and technology 59 (8) (1999) 1213–1226.

[55] B. Vidyashankar, A. K. Murty, Analysis of laminates with ply drops, Composites science and technology 61 (5) (2001) 749–758.

[56] K. He, S. Hoa, R. Ganesan, The study of tapered laminated composite structures: a review, Composites Science and Technology 60 (14) (2000) 2643–2657.

[57] B. Varughese, A. Mukherjee, A ply drop-off element for analysis of tapered laminated composites, Composite structures 39 (1) (1997) 123–144.

[58] K. J. Saeger, P. A. Lagace, D. J. Shim, Interlaminar stresses due to in-plane gradient stress fields, Journal of composite materials 36 (2) (2002) 211–227.

[59] V. Shapiro, I. Tsukanov, A. Grishin, Geometric issues in computer aided design/computer aided engineering integration, Journal of Computing and Information Science in Engineering 11 (2) (2011) 021005.

[60] S. Arabshahi, D. Barton, N. Shaw, Towards integrated design and analysis, Finite Elements in Analysis and Design 9 (4) (1991) 271–293.

[61] D. T. Ross, Applications and extensions of sadt, Computer 4 (18) (1985) 25–34.

[62] O. Hamri, J.-C. Léon, F. Giannini, B. Falcidieno, Software environment for cad/cae integration, Advances in Engineering Software 41 (10) (2010) 1211–1222.

[63] O. Hamri, J. C. Léon, F. Giannini, B. Falcidieno, Computer aided design and finite element simulation consistency, Strojniški vestnik-Journal of Mechanical Engineering 56 (11) (2010) 728–743.

[64] K.-J. Bathe, E. N. Dvorkin, A formulation of general shell elements—the use of mixed interpolation of tensorial components, International Journal for Numerical Methods in Engineering 22 (3) (1986) 697–722.

[65] S. Klinkel, F. Gruttmann, W. Wagner, A continuum based three-dimensional shell element for laminated structures, Computers & Structures 71 (1) (1999) 43–62.

[66] K. Dorninger, F. G. Rammerstorfer, A layered composite shell element for elastic and thermoelastic stress and stability analysis at large deformations, International Journal for Numerical Methods in Engineering 30 (4) (1990) 833–858.

[67] S. Hossain, P. Sinha, A. H. Sheikh, A finite element formulation for the analysis of laminated composite shells, Computers & structures 82 (20) (2004) 1623–1638.

[68] K. Jorabchi, J. Danczyk, K. Suresh, Algebraic reduction of beams for cad-integrated analysis, Computer-Aided Design 42 (9) (2010) 808–816.

[69] K. Jorabchi, J. Danczyk, K. Suresh, Efficient and automated analysis of potentially slender structures, Journal of Computing and Information Science in Engineering 9 (4) (2009) 041001.

[70] B. Chandrasekaran, J. R. Josephson, Function in device representation, Engineering with Computers 16 (3-4) (2000) 162–177. doi:10.1007/s003660070003.
URL http://dx.doi.org/10.1007/s003660070003

[71] B. CHANDRASEKARAN, Representing function: Relating functional representation and functional modeling research streams, AI EDAM 19 (02). doi:10.1017/s0890060405050079.
URL http://dx.doi.org/10.1017/s0890060405050079

[72] M. S. Erden, H. Komoto, T. J. van Beek, V. D'Amelio, E. Echavarria, T. Tomiyama, A review of function modeling: approaches and applications, Artificial Intelligence for Engineering Design, Analysis and Manufacturing 22 (02) (2008) 147–169.

[73] J. J. Shah, M. Mäntylä, Parametric and feature-based CAD/CAM: concepts, techniques, and applications, John Wiley & Sons, 1995.

[74] W. Regli, J. Rossignac, V. Shapiro, V. Srinivasan, The new frontiers in computational modeling of material structures, Computer-Aided Design 77 (2016) 73–85.

[75] M. Y. DENG, Function and behavior representation in conceptual mechanical design, AI EDAM 16 (05). doi:10.1017/s0890060402165024.
URL http://dx.doi.org/10.1017/s0890060402165024

[76] A. Chakrabarti, Supporting two views of function in mechanical designs 98 (1998) 26–30.
URL https://scholar.google.com/scholar?cluster=2840847459098328322

[77] D. C. Nolan, C. M. Tierney, C. G. Armstrong, T. T. Robinson, J. E. Makem, Automatic dimensional reduction and meshing of stiffened thin-wall structures, Engineering with Computers (2013) 1–13doi:10.1007/s00366-013-0317-y.

[78] T. T. Robinson, C. G. Armstrong, G. McSparron, a. Quenardel, H. Ou, R. M. McKeag, Automated mixed dimensional modelling for the finite element analysis of swept and revolved CAD features, Proceedings of the 2006 ACM symposium on Solid and physical modeling 1 (June) (2006) 117–128. doi:10.1145/1128888.1128905.

[79] S. H. Lee, A cad–cae integration approach using feature-based multi-resolution and multi-abstraction modelling techniques, Computer-Aided Design 37 (9) (2005) 941–955. doi:10.1016/j.cad.2004.09.021.
URL http://dx.doi.org/10.1016/j.cad.2004.09.021

[80] M. A. Price, T. T. Robinson, D. Soban, A. Murphy, C. G. Armstrong, R. McConnell, R. Roy, Maintaining design intent for aircraft manufacture, CIRP Annals - Manufacturing Technology 62 (1) (2013) 99–102. doi:10.1016/j.cirp.2013.03.124.
URL http://dx.doi.org/10.1016/j.cirp.2013.03.124

[81] R. Courant, D. Hilbert, Methods of mathematical physics, Vol. 1, CUP Archive, 1965.

[82] J. M. Zagajac, Engineering Analysis Over Subdomains, Cornell University, May, 1997, phD Thesis.

[83] V. Kumar, D. Burns, D. Dutta, C. Hoffmann, A framework for object modeling, Computer-Aided Design 31 (9) (1999) 541–556.

[84] R. S. Palmer, V. Shapiro, Chain models of physical behavior for engineering analysis and design, Research in Engineering Design 5 (3-4) (1993) 161–184.

[85] A. DiCarlo, F. Milicchio, A. Paoluzzi, V. Shapiro, Solid and physical modeling with chain complexes, in: Proceedings of the 2007 ACM symposium on Solid and physical modeling, ACM, 2007, pp. 73–84.

[86] V. Shapiro, Solid modeling, Handbook of computer aided geometric design 20 (2002) 473–518.

[87] A. A. Requicha, Representations of rigid solid objects, Springer, 1980.

[88] C. M. Hoffmann, Geometric and solid modeling.

[89] M. Mäntylä, An introduction to solid modeling.

[90] M. E. Gurtin, The linear theory of elasticity, in: Linear Theories of Elasticity and Thermoelasticity, Springer, 1973, pp. 1–295.

[91] B. D. Coleman, M. E. Gurtin, Thermodynamics with internal state variables, The Journal of Chemical Physics 47 (2) (1967) 597–613.

[92] L. D. Landau, E. M. Lifsic, L. Pitaevskii, A. Kosevich, Course of Theoretical Physics: Volume 7, Theory of Elasticity, Pergamon Press, 1986.

[93] S. P. Timoshenko, J. Goodier, Theory of elasticity.

[94] K. T. Ventsel E., Thin Plates and Shells - Theory, Analysis, and Applications .pdf, 2001.

[95] K. Suresh, Automating the cad/cae dimensional reduction process, in: Proceedings of the eighth ACM symposium on Solid modeling and applications, ACM, 2003, pp. 76–85.

[96] B. P. Kristinsdottir, Z. B. Zabinsky, M. E. Tuttle, S. Neogi, Optimal design of large composite panels with varying loads, Composite Structures 51 (1) (2001) 93–102.

[97] M. D. Banea, L. F. M. da Silva, Adhesively bonded joints in composite materials: an overview, Proceedings of the Institution of Mechanical Engineers, Part L: Journal of Materials: Design and Applications 223 (1) (2009) 1–18. doi:10.1243/14644207JMDA219.
URL http://pil.sagepub.com/lookup/doi/10.1243/14644207JMDA219

[98] C. Sun, S. Li, Three-dimensional effective elastic constants for thick laminates, Journal of Composite Materials 22 (7) (1988) 629–639.

[99] A. Idlbi, M. Karama, M. Touratier, Comparison of various laminated plate theories, Composite Structures 37 (2) (1997) 173–184.

[100] J. N. Reddy, A simple higher-order theory for laminated composite plates, Journal of applied mechanics 51 (4) (1984) 745–752.

[101] M. Freytag, V. Shapiro, I. Tsukanov, Finite element analysis in situ, Finite Elements in Analysis and Design 47 (9) (2011) 957–972.

[102] A. Düster, H. Bröker, E. Rank, The p-version of the finite element method for three-dimensional curved thin walled structures, International Journal for Numerical Methods in Engineering 52 (7) (2001) 673–703.

[103] M. Suri, Analytical and computational assessment of locking in the< i> hp</i> finite element method, Computer Methods in Applied Mechanics and Engineering 133 (3) (1996) 347–371.

[104] A. R. Krommer, Numerical Integration: On Advanced Computer Systems, Vol. 848, Springer, 1994.

[105] A. U. Manual, Ansys inc, Canonsburg, PA.

[106] I. SolidWorks, Solidworks corporation, Concord, MA.

[107] N. J. Pagano, Exact solutions for rectangular bidirectional composites and sandwich plates, Journal of composite materials 4 (1) (1970) 20–34.

[108] N. Pagano, H. J. Hatfield, Elastic behavior of multilayered bidirectional composites, AIAA journal 10 (7) (1972) 931–933.

[109] A. M. Zenkour, Three-dimensional elasticity solution for uniformly loaded cross-ply laminates and sandwich plates, Journal of Sandwich Structures and Materials 9 (3) (2007) 213–238.

[110] J. Reddy, C. Liu, A higher-order shear deformation theory of laminated elastic shells, International Journal of Engineering Science 23 (3) (1985) 319–330.

[111] A. Khdeir, J. Reddy, An exact solution for the bending of thin and thick cross-ply laminated beams, Composite Structures 37 (2) (1997) 195–203.

[112] Erden, H. Komoto, T. v. Beek, A review of function modeling: approaches and applications. URL https://scholar.google.com/scholar?cluster=17109055237284481575

[113] R. D. Cook, et al., Concepts and applications of finite element analysis, Wiley. com, 2007.

[114] M. Chatiri, T. Güll, A. Matzenmiller, An assessment of the new ls-dyna layered solid element: basics, patch simulation and its potential for thick composite structure analysis, in: 7th European LS-DYNA Conference, Salzburg, 2009.

[115] J. O. Dow, D. E. Byrd, The identification and elimination of artificial stiffening errors in finite elements, International Journal for Numerical Methods in Engineering 26 (3) (1988) 743–762.

[116] L. J. Hart-Smith, Adhesive-bonded single-lap joints, Langley Research Center Hampton, VA, 1973.

[117] O. C. Zienkiewicz, R. L. Taylor, The finite element method for solid and structural mechanics, Butterworth-Heinemann, 2005.

[118] C. Horgan, Saint-Venant end effects in composites, J Compos Mater 16 (5) (1982) 411–422. doi:10.1177/002199838201600506.